HADRON PHYSICS IN THE 200 - 2000 GeV ENERGY RANGE*

by

M. Jacob
CERN, Geneva

Abstract

This paper reviews hadron physics, as first explored at the CERN ISR, over the first six years of operation of the machine. It therefore surveys proton-proton interactions in the 250 - 2000 GeV range. Related results from Fermilab are also presented. The key features of hadron physics, as now ascertained are considered in turn. New knowledge and new questions serve as a basis for a discussion of physics with proton and anti-proton in the ISR and of physics with the new generation of colliders, with center-of-mass energies one order of magnitude above those reached with the present ISR, as they are presently proposed or developing at different laboratories.

* This paper is based on a series of lectures given at the University of California, Riverside, in the spring of 1976. It is updated for the CERN, ISR Workshop, in the fall of 1977.

Introduction

The intersecting storage ring (ISR) facility at CERN is the only proton storage ring machine in the world[1]. It is limited in the type of experiments which it allows to perform, since proton-proton collisions only can be studied. Yet it opened up for experimentation a new and wide range of energies where fragmentary pieces of information only were hitherto available from Cosmic Ray research[2]. Experimentation with deuterons has recently been possible and, in the future, one may consider proton-anti-proton collisions with a reasonable luminosity. Nevertheless, one is far from the versatility of a fixed target machine. It remains that in a very few years (1972 and 1973 were particularly fruitful in new findings) research at the ISR has defined, through a series of important discoveries, the topical fields of hadron physics which have since represented the main lines of research in this field, at the ISR, but also at Fermilab and now at the CERN-SPS. These main new findings were as follows:

(i) The rising total cross-sections

(ii) Short range order in particle production

(iii) Large mass diffractive excitation

(iv) Important production at large transverse momentum

(v) Prompt lepton production.

They are actually used to define the physics topics which are studied in turn in this review. They are all of important significance. One should also mention at this stage a very important, even if negative, finding, namely the non-observation of quarks in collisions where the center-of-mass energy reaches 60 times the rest mass of the incident particles! The same applies to magnetic monopole particles. Present limits for the production cross-sections are at the picobarn level (10^{-36} cm^2). Particle search is always an important activity and in particular at a new machine. The ISR has not yet been very successful along that line[3].

While the ISR was definitely first with the discoveries referred to as (i), (ii), (iii) and (iv), it should be stressed that they all correspond to phenomena which already show up rather well as the equivalent laboratory energy exceeds 200 GeV. The pertinent effects were therefore also later found at Fermilab. Evidence for prompt lepton production was reported at about the same time at Fermilab and at the ISR. Furthermore, it may be considered a disappointment that, once these key new features are ascertained beyond 200 GeV, reaching 2000 GeV has not brought so far anything radically new[4]. Changes occur but they are not often very important. This is particularly the case for topics (i), (ii)

and (iii) which globally correspond to what is referred to as "ln s physics". What set the pace for changes is indeed the logarithm of the energy, or the available rapidity range ΔY[5], rather than the center-of-mass energy proper. In the case of (iv) and (v) one however still observes important changes (well over one order of magnitude for yields). This is where present research at the ISR has been specializing. This is where the ISR main advantage of reaching higher energies may still compensate for the wide variety of beams, higher luminosities and experimental flexibility available at Fermilab and at the SPS. Indeed, it is the somewhat complementary role which the ISR and the SPS (Fermilab) are called to play over the coming few years which motivates to a large extent this new review of physics in the 200 - 2000 GeV energy range[6].

This paper is organized as follows. In section 2 we present the key features of research at the ISR as they now stand. We first describe the machine from a user's point of view. We define and list key parameter values as met in typical runs. We next come back to the list of specific physics topics already considered, discussing very briefly in each case what are the main corresponding features and what are their present significances. Such statements are supported by specific reviews of each topic, which are the object of sections 3 to 7, respectively. Discussed in turn are total cross-section and elastic scattering (section 3), particle production (section 4), diffractive excitation (section 5), large transverse momentum phenomena (section 6) and lepton and lepton pair production (section 7). Though focussing primarily on ISR results, this part of the review borrows a great deal from recent results from Fermilab, trying to globally summarize present knowledge and present problems in the study of hadronic interactions at very high energy. Even though this paper tries to be self-contained and somewhat complete in its coverage of the main lines of research at the ISR, it strongly emphasizes relatively recent results and present problems[6]. It does not attempt to describe research activities as they gradually developed since the first proton-proton collisions were observed in the spring of 1971, but rather dwell on their actual outcome when now compared with that obtained over the same period at Fermilab. At the same time, in its global coverage of physics at the ISR, this paper cannot be complete in its discussion of any specific physics topics. Some of them have already been the object of specialized reviews. They should be consulted for a more detailed discussion[7]. Section 8 is a status report on particle searches. Section 9 considers the physics potential which one associates with the availability of an intense anti-proton source. Recent developments in cooling techniques could allow for a very reasonable luminosity ($L \sim 10^{29}$ say). In two years time this could lead to very interesting experiments on the ISR. Section 10 leads us a little further into the future and that in a more tentative way. It reviews the physics potential of the new generation of

colliders. The emphasis is put on the use of the Fermilab Tevatron and that of the SPS as a proton-anti-proton storage ring. The physics potentials of the most extensive present project, Isabelle, have been discussed already in detail[8].

Trying to summarize in a few words physics at the ISR one may say that its aim is "to understand the proton structure". At present, the proton structure in terms of quarks is supported by a tremendous array of evidence, from hadronic spectroscopy to deep inelastic neutrino collisions and the level structure of charmonium. In hadronic physics, as studied at the ISR, the overall proton shape, the importance of diffractive excitation and, more specifically, the properties of large transverse momentum reactions and lepton pair formation, point at a structure with internal degrees of freedom which can be most fruitfully associated with the presence of quarks. Yet, the proton does not break up into such constituents. At present quark confinement is at the origin of a revival in field theory models which may provide a new and more fundamental look at strong interactions than Regge theory could in the sixties. All physics topics discussed in sections 3 to 8 contribute to the analysis of the proton structure in a variety of ways. Some appear to do it at a more superficial level (testing for global coherent effects among constituents) and some at a deeper level (testing almost directly the interaction at the constituent level). It is however much too early to assess the importance which each pertinent present contribution should eventually take when more is understood about hadronic structure.

2. Research at the ISR, an overall view

a) The machine from a user's point of view

Coasting protons stacked in two rings can collide in almost head on collisions. Figure 2-1 shows the general lay-out of the two rings, with their respective beam transport lines connecting them to the PS. The ISR is made of two slightly distorted concentric rings, 300 m in diameter, which intersect in eight different zones. The two beams then cross each other at an angle of 14.7°. Figure 2-2 is an aerial view of part of the CERN site. The ISR ring is in the upper right corner. Also seen, at center left, is the PS ring.

A key parameter is the luminosity L which determines the number of reactions which take place at each intersection. The counting rate R associated with a particular reaction with cross-section σ is given by

$$R = L\sigma \qquad (2.1)$$

The machine luminosity is proportional to the product of the two beam intensities I_1 and I_2. It also depends on specific geometrical factors. It is instructive to show how it depends on the machine parameters and how it is usually

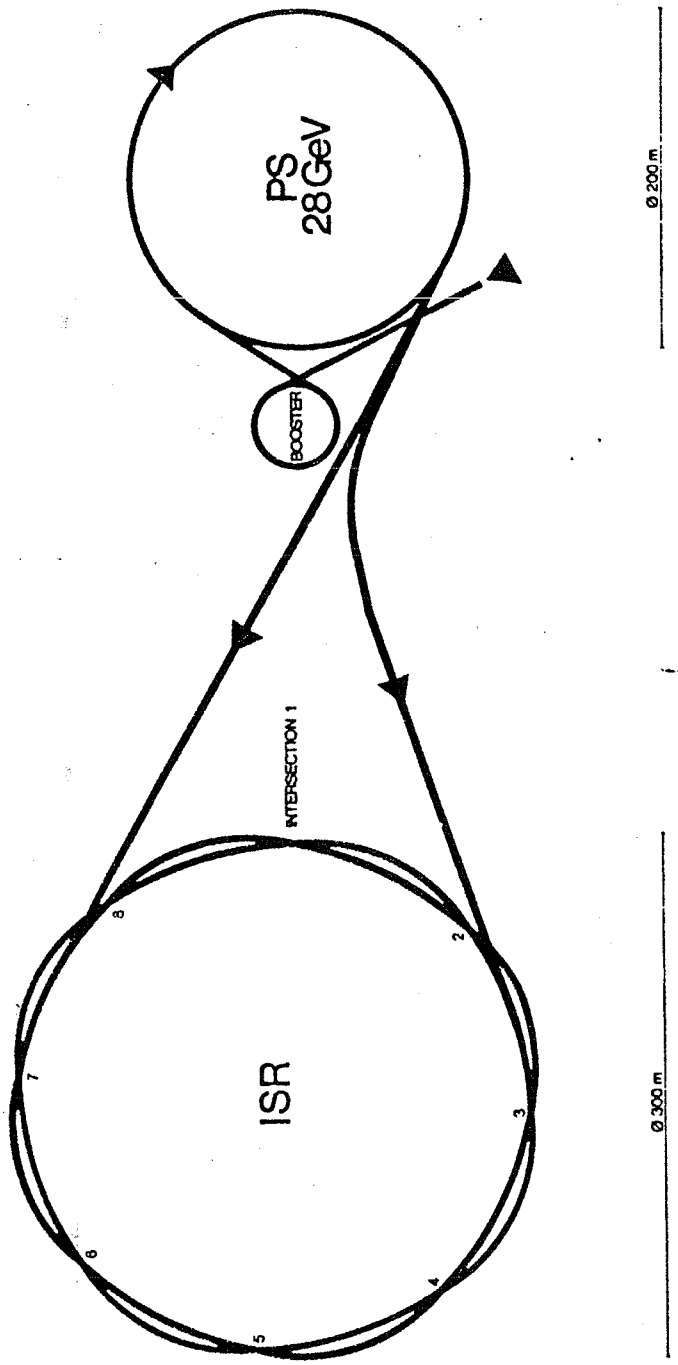

Figure 2-1 : Schematic View of the PS and ISR Rings

measured in practice. An accurate way to measure it with a physics experiment is to observe Coulomb scattering. This however requires measuring very small angle scattering ($|t| < 0{,}001$ say) which is very difficult. Such measurements actually show the reliability of the Van der Meer method which is currently applied and which we now briefly describe.

The two proton beams, with intensities I_1 and I_2 respectively, intersect each other in an intersection volume, the projection of which on the beam plane is a diamond, as shown in figure 2-3. Figure 2-4 shows such an intersection zone. The two beams intersect each other in a bicone vacuum chamber.

The two beams have a roughly rectangular cross-section, with an horizontal spread d of 3 to 5 cm, and a vertical spread H of 0,5 cm. The two beams intersect with an angle α (14.7^o at the ISR).

The volume of the intersection region, where the two beams overlap is

$$V = \frac{Hhh'}{2} \tag{2.2}$$

where

$$h = \frac{d}{\cos \alpha/2} \qquad h' = \frac{d}{\sin \alpha/2} \tag{2.3}$$

The interaction rate is proportional to the interaction volume V and to the densities $\rho_1(\rho_2)$ of the two beams. They are not bunched and, for the sake of argument, we shall assume them to be uniformly distributed. This implies

$$\rho_1 = \frac{I_1}{dHec} \qquad \rho_2 = \frac{I_2}{dHec} \tag{2.4}$$

The reaction rate is also proportional to the cross-section σ and to the invariant flux factor written as

$$u = \frac{\vec{P_1} \cdot \vec{P_2}}{E_1 E_2} c^3 \approx (1 + \cos\alpha)\, c \tag{2.5}$$

where $\vec{p}(E)$ are the momentum (energy) of the colliding protons. The total reaction rate therefore reads:

$$R = L\sigma = \frac{I_1 I_2}{d^2 H^2 e^2 c^2} \; H \frac{d^2}{\sin\alpha} \; (1 + \cos\alpha)\, c\sigma \tag{2.6}$$

thus clearly separating the different factors previously itemized. This gives

$$L = \frac{I_1 I_2}{e^2 c H \operatorname{tg} \alpha/2} \tag{2.7}$$

Relation (2.7) shows the role of the geometrical factors entering the luminosity.

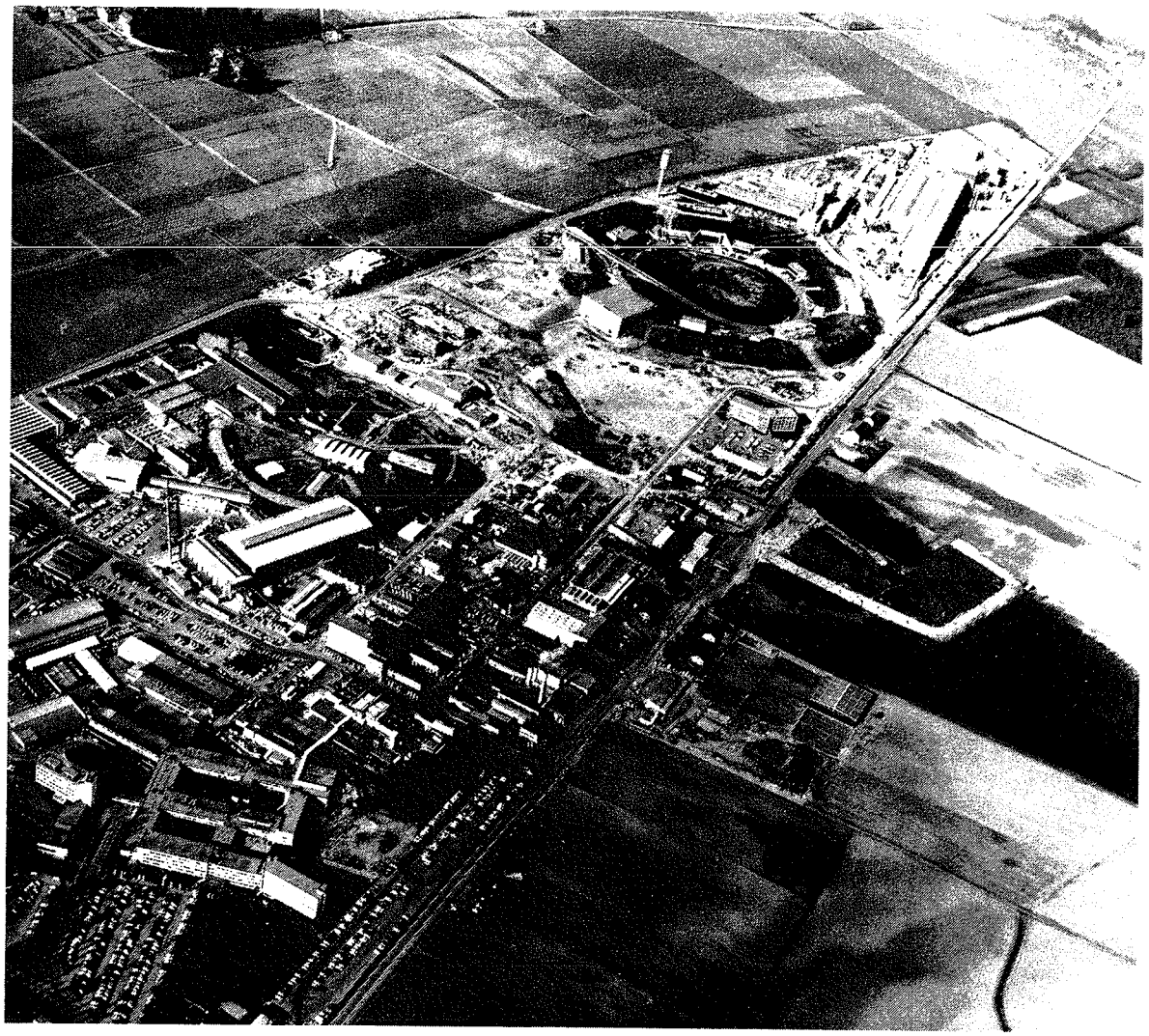

Figure 2-2 : Aerial view of part of the CERN site (previously called Lab I) showing the relative location of the PS (centre left) and the ISR (upper right)

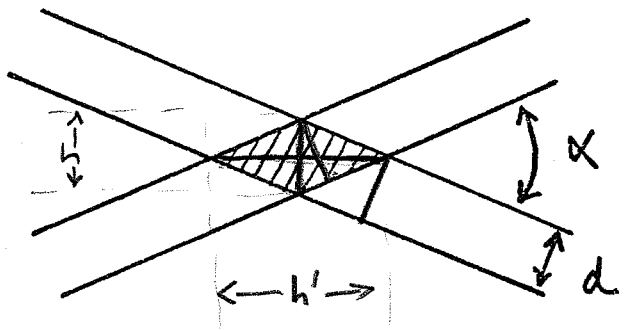

Figure 2-3 : The intersection diamond - a projection on the beam plane

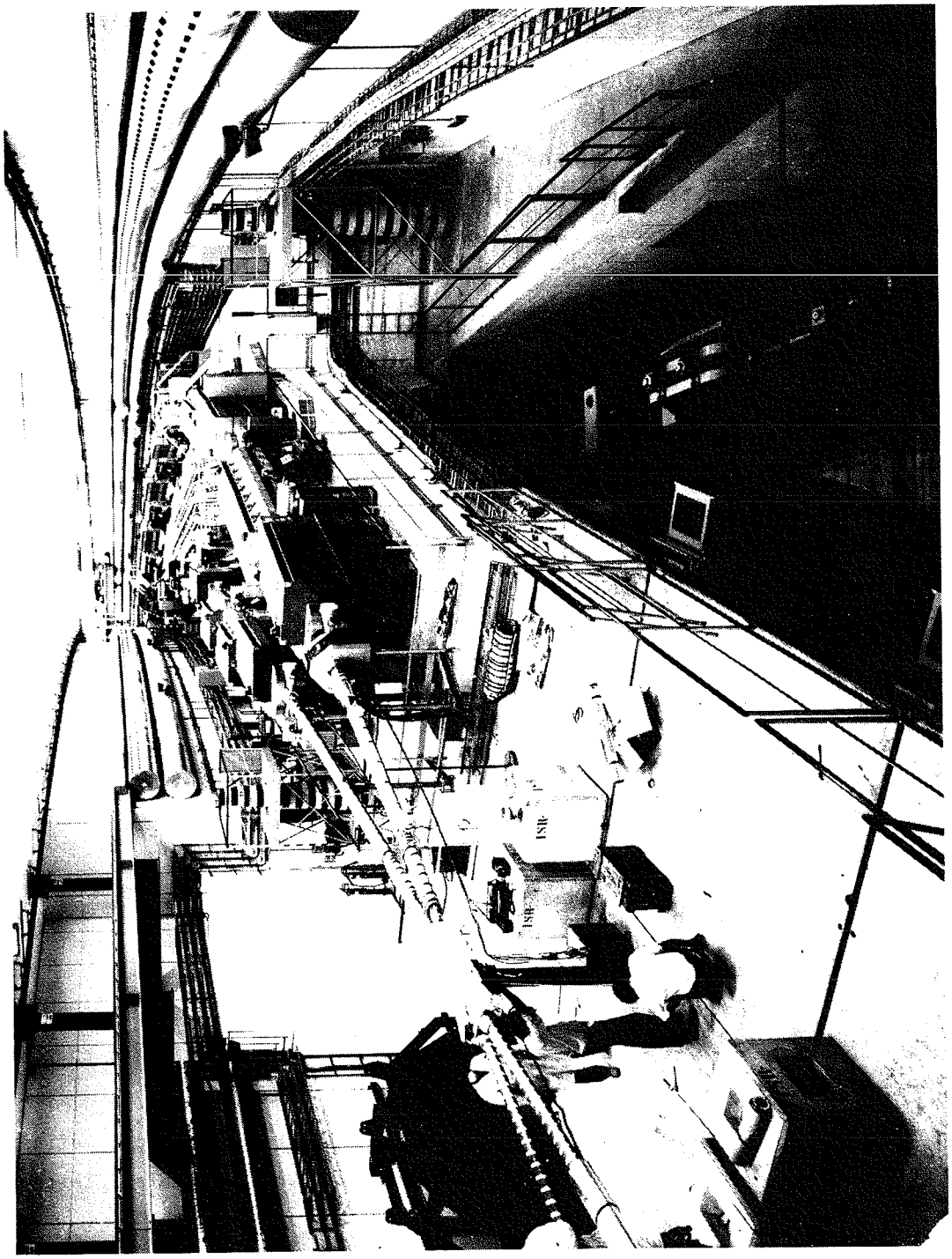

Figure 2-4 : An Intersection Area. The intersection bicone vacuum chamber is here being degassed. One also sees (lower right) one of the transport beams from the PS.

In practice however, one cannot expect the two beam densities to be uniform over the intersection region. Relation (2.7) is however still valid provided that one replaces H by an effective overlap height <H>.

The standard method used to measure the luminosity is the Van der Meer method. One considers a global type of process (observing forward and backward particles over a rather wide monitor detector (beam-beam trigger) which does not practically depend on the exact location of the interaction within the vacuum chamber. One, thus observes a rate R_M associated with the corresponding type of process which relates to a particular cross section σ_M. By definition $L = R_M/\sigma_M$.

The factor $I_1 I_2/H$ in (2.7) should more generally be replaced by

$$\frac{I_1 I_2}{\langle H \rangle} = \int_{-\infty}^{+\infty} I_1(z)\, I_2(z)\, dz \tag{2.8}$$

which gives the actual vertical (z axis) overlap between the two beams. On the other hand density fluctuations in the horizontal direction can be neglected to a good approximation in view of the relatively large width of the beams. The measured rate, as given by (2.7) and (2.8) is therefore

$$R_M = \frac{\sigma_M}{e^2 c \operatorname{tg} \alpha/2} \int_{-\infty}^{+\infty} I_1(z)\, I_2(z)\, dz \tag{2.9}$$

The Van der Meer method is now as follows. One shifts vertically one beam with respect to the other by an amount δ. The rate in the monitor then changes to

$$R_M(\delta) = \frac{\sigma_M}{e^2 c \operatorname{tg} \alpha/2} \int_{-\infty}^{+\infty} I_1(z)\, I_2(z+\delta)\, dz \tag{2.10}$$

As already mentioned the process used by the monitor is chosen so that the observed rate does not depend appreciably on where in the diamond the interaction has occurred.

One now integrates (2.10) over δ and uses the rather sharply defined limits of the two beams to justify infinite limits on the integrals. This gives

$$\int_{-\infty}^{+\infty} R_M(\delta)\, d\delta = \frac{\sigma_M\, I_1 I_2}{e^2 c \operatorname{tg} \alpha/2} \tag{2.11}$$

One can thus obtain σ_M and hence L from R_M. The luminosity measurement which can thus be made has a precision of 1 to 2%. Beam stability over a run may increase the overall uncertainty by 1%. This gives a 3% precision which is satisfactory in most cases.

The achieved luminosity depends on the momentum of the coasting beams.

Table 2-1 puts together the standard coasting momenta, the corresponding center-of-mass energy, the equivalent laboratory momentum for a fixed target accelerator and the average luminosity, as available at the end of '75. At 26 GeV/c the achieved luminosity is the best. Its value is typically $L = 1.6 \times 10^{31}$ cm^{-2} s^{-1}. For a cross-section of 40 mb, this corresponds to 6.4×10^{5} interaction per second in each intersection zone. The luminosity thus compares well with that available on an hydrogen target with a typical secondary beam at Fermilab (SPS) even if it is about a million times less than that available from the full proton beam.

Table 2-1

Coasting beam momenta p(GeV/c), center-of-mass energy $\sqrt{s}$(GeV), equivalent laboratory momentum for a fixed target machine P lab (GeV/c) and luminosity L (10^{30} cm^{-2} s^{-1}). The center-of-mass energy corresponds to symmetric conditions. The machine can also run with asymmetric momenta. The highest momentum used requires acceleration within the ISR. Under standard conditions the colliding beams have a momentum spread of 2%.

P	$\sqrt{s}$	P_{lab}	L
11.8	23.4	291	2
15.3	30.4	691	4
22.4	44.4	1053	10
26.5	52.6	1474	16
31.4	62.3	2062	3

One of the ISR intersections (the so-called low-β section) is now specially equipped to provide an extra increase of the luminosity by a factor of two.

A special superconducting high luminosity insertion, which is presently considered, would allow a gain in luminosity by an order of magnitude. The geometry of the intersection zone would be spherical rather than diamond-shaped. This may be advantageous for some experiments.

The beam intensity is an important factor in the luminosity. The beam intensity is rather severely limited by the rate of beam gas collisions with secondary ion formation on the walls of the vacuum pipe. Indeed the extreme vacuum reached at the ISR turned out to be an important asset for machine performance. The vacuum is at the level of 10^{-11} torr over the whole of the rings and reaches 10^{-12} in some intersection regions. The decay of the beam, once stacked in a matter of minutes, is mainly through beam gas collisions but it is limited to 10^{-6} min^{-1}. Proton storage for experimentation may easily extend over 40h. The typical beam intensity at 26 GeV/c is 24 A. This results in the quoted luminosity of 1.6×10^{31}.

This concludes our machine survey.

a) An historical outlook

The number of experiments which has been on the machine floor at any given instant has remained essentially constant over the first five years of experimentation, averaging 10. Six out of the eight intersection regions are continuously used for physics experimentation. At present, as experimentation looks at much more subtle effects than first exploration did, detectors have increased in sophistication and size and 7 experiments is a maximum. This would include two using the Split Field Magnet facility and one on each of the other 5 intersections.

Trends in research have changed much in time for reasons which have been mentioned already. In 1972 there was a wide front approach using relatively simple detectors. Measurements included angular distribution only in the many particle case and inclusive distribution only when a particle was analyzed (nature and momentum). In July 1975, almost all experiments involved correlations among particles and the research programme was already much specialized. In 1977, the specialization is even stronger with lepton pair production and large transverse momentum phenomena only being primarily studied. This involves new large sophisticated detectors capable of momentum measurement and particle identification over wide solid angles. This is illustrated in Table 2-2, which lists the experiments then going on at different times in each of the intersection areas[9]. It shows how experimentation at the ISR specialized itself in order to best compete with experimentation at Fermilab and now also at SPS.

Experimentation at the ISR has some advantages over experimentation at a fixed target machine. The only key advantage of the ISR as compared to the SPS (Fermilab) is however and of course the available gain in energy which, at present, corresponds to a factor two in the center-of-mass system. Working in the center-of-mass system has also some advantages. Secondary particles are

widely separated in angle. This may however turn into disadvantages when particle identification is required with accordingly large solid angle detectors. On the other hand, the ISR main weak points are the following

(i) Great difficulties in reaching very low momentum transfers where a large fraction of certain cross-sections is to be found.

(ii) Weak momentum resolution when precision measurements would be needed.

(iii) Low luminosity when one wishes to study process much below the μb level.

(iv) Inaccessibility of the actual reaction vertex and spurious secondaries associated with the wall of the vacuum chamber.

(v) Lack of variety in the types of reactions which can be studied.

These different points should be kept in mind when deciding on the comparative merits of the ISR and SPS for the further analysis of the physics questions discussed through Sections 3 to 8. Nevertheless, when comparing a future super ISR to the potentiality of a still larger fixed target accelerator, only point (v) is actually relevant. The other four can always be at least partly overcome with appropriate equipment.

Table 2-2

A tour around the ring in 1972, 1975 and 1977

	1972	1975	1977
I1	Electron and photon at large angle (102,103) large p_t phenomena discovered	Search for multigamma events (monopoles) (107	Electrons and large p_t hadron production with a Solenoid detector (108)
I2	Inclusive production small angle (201), medium angle (202) and large angle (203)	Correlation studies of diffractive excitation (double arm spectrometer) (207)	Muon pair production with a toroid detector (804)
I4	Quark search (402) neutron production (405) SFM tests	Correlation studies of large p_t reactions (407/408) (410/413) Diffractive studies part of the time (401-411) also Particle search (406)	Correlation involving large p_t particles with the SFM (407/408), and with the SFM and a wide angle spectrometer (410/413)
I6	Elastic scattering (601) (602)	Search for charmed particles electron production at small angles (605)	Electron pair production using the Lamp Shade magnet detector (606)
I7	-	Search for charmed particle electron production at wide angles (702)	Electron pair and large p_t hadron production using a double arm spectrometer (702)
I8	Total cross-section (801) Correlation, short range order discovered	Elastic scattering at very small angle (805) Electron and photon production calorimeter study (806)	Electron pair production using a transition radiation detector and an argon calorimeter (806)

c) Physics at ISR energies

Present information on hadron interactions in the 200 - 2000 GeV energy range readily leads one to separate so far observed phenomena into two main categories. On the one hand, one finds processes which correspond to rather important cross-sections. They all show but a very slow change with increasing energy. As already mentioned, the most relevant variable appears to be the available rapidity range ΔY, which increases as $\ell n\ s$[10]. One may therefore refer globally to all these phenomena as "ℓn s physics". Going from PS to ISR energies increases the rapidity range by a factor two. It goes from four to eight, a gain of 4 units. From 400 to 2000 GeV, one merely gains 1.6 units in the available rapidity range. Figure 2-5 gives a typical example of a ℓn s physics feature. It shows rapidity (a rather pseudo rapidity[11]) correlations among charged particles at 250 and 2000 GeV equivalent laboratory momentum respectively, thus spanning the full ISR energy range.

The correlation is defined as

$$R(\eta_1,\eta_2) = \sigma_{in}\ \frac{d^2\sigma/d\eta_1 d\eta_2}{d\sigma/d\eta_1\ d\sigma/d\eta_2} - 1 \qquad (2.12)$$

where σ_{in} is the total inelastic cross-section. The cross-sections are integrated over the transverse momentum distribution which does not change with energy. The key feature is the ridge which extends along the main diagonal. As discussed later in section 4, it stands for the short range nature (rapidity wise) of the correlations. What matters is more the rapidity distance of the two observed particles than their actual rapidities, provided that they remain relatively small. If a particle is observed, there is an enhanced probability that a second one will be found in the same region of phase space (similar rapidity) and this, to a first approximation, whatever the energy of the first one is. Furthermore, the observed correlation is practically independent of the reaction energy when it varies by almost an order of magnitude. As the energy increases, the rapidity range extends (but only logarithmically), the ridge extends, the effect becomes clearer. Nevertheless, the effect, with its qualitative and quantitative features, is already present at 250 GeV. It actually appears in an unambiguous way between 100 and 200 GeV. At lower energies, the available rapidity range is too small as compared to the range which is proper to the correlation and there is only a maximum at $\eta_1 = \eta_2 = 0$. Observing the effect requires SPS (Fermilab) energies. Once there however, there is but a little gain using the full ISR energy range. One should then compare the advantages of track chamber analysis at a fixed target machine with actual momentum measurement and particle identification over a wide solid angle at the ISR. Competition is very hard and, as shown by table 2-2, it was not taken up.

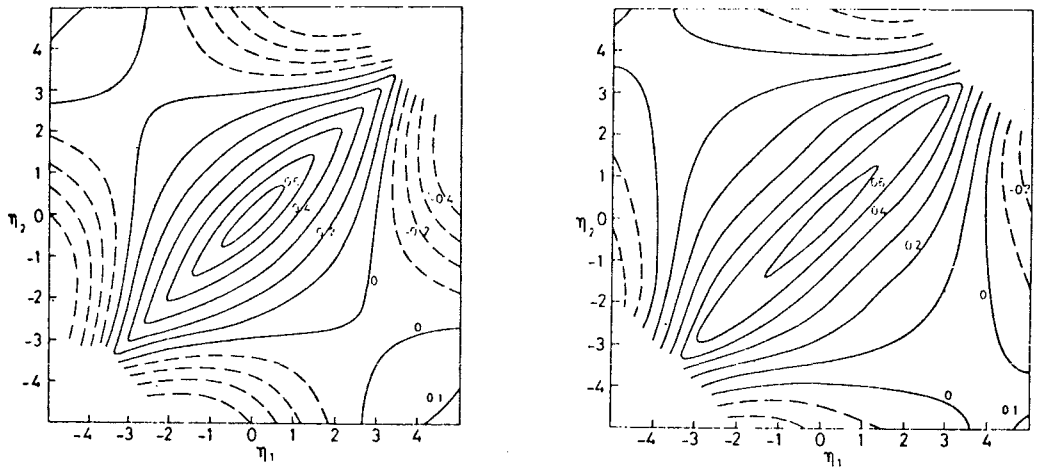

Figure 2-5 : Rapidity Correlations at $\sqrt{s}$ = 22 GeV and 62 GeV. Data from the Pisa-Stony Brook Collaboration

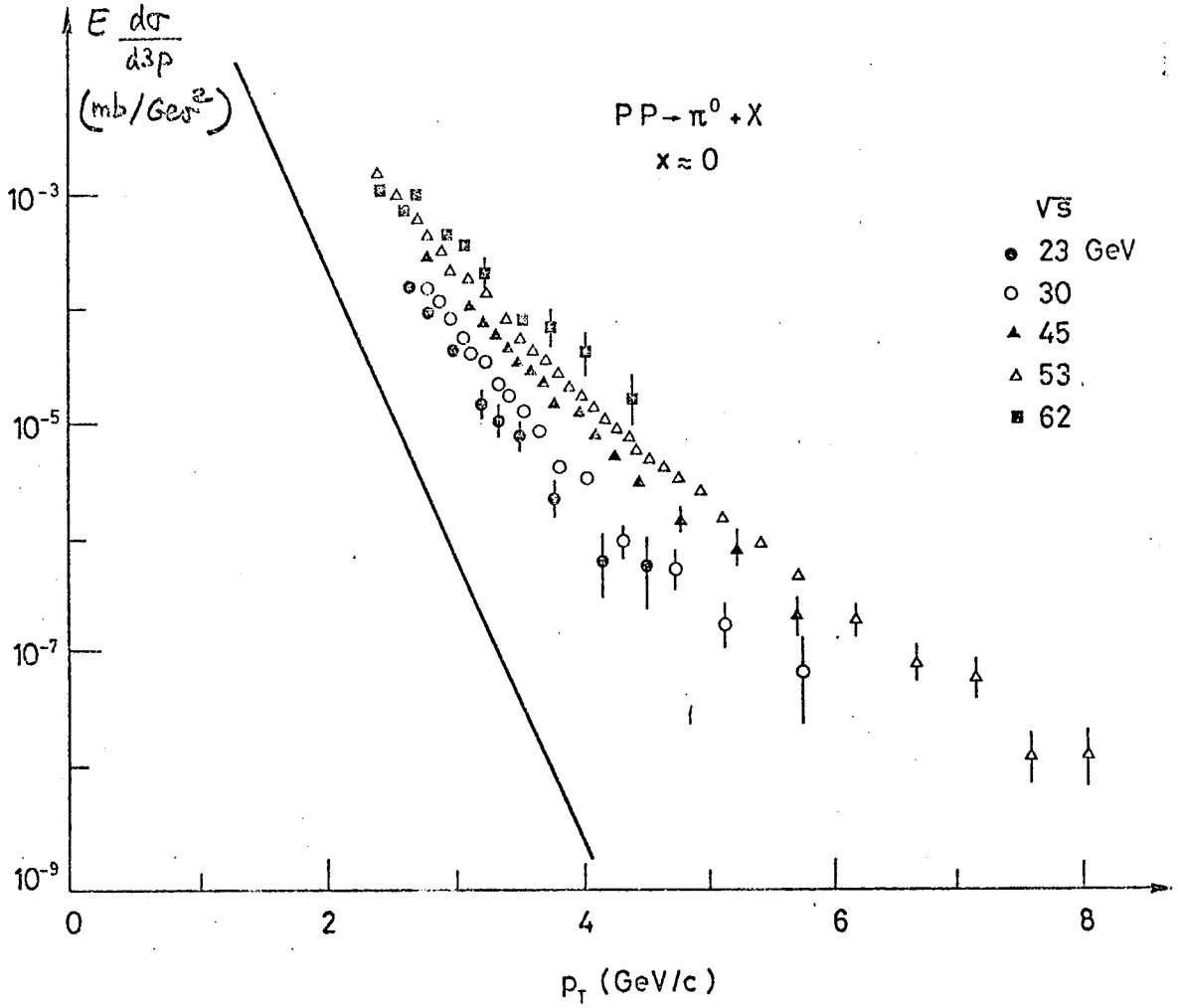

Figure 2-6 : Large p_t π^0 yield at wide angle. Data from the CERN-Columbia-Rockefeller Collaboration. The solid line is the simple extrapolation of the low p_t data (p_t < 1 GeV/c)

On the other hand, figure 2-6 shows a very different type of behaviour. The π^o yield at wide angle (90^o in the center-of-mass) and large transverse momentum ($p_t > 2$ GeV/c), still sharply increases with energy over the ISR range, and the more so the larger p_t is. At $p_t = 4$ GeV/c one gets an order of magnitude increase between 250 and 2000 GeV. The pertinent cross-section remains small (10^{-6} to 10^{-5} mb/GeV^2). Nevertheless, the phenomenon shows such an important change that research at the ISR is likely to reveal interesting features which might not be accessible at the SPS (Fermilab). As shown in table 2-2, the study of large p_t production has thus remained an important topic at the ISR.

Even if it may to a large extent belong now to the past, "ℓn s physics" research has been very successful at the ISR. It will be reviewed in sections 3, 4 and 5.

Within ℓn s physics one may conveniently distinguish different topics which we shall separately review.

The rising total cross-section has been an important surprise[12]. It was generally accepted that, at very large energy ($s >> m^2$), some simple asymptotic diffractive behaviour, with a constant total cross-section, would eventually set in. The discovery that total cross-sections eventually do rise with energy, if only logarithmically, has destroyed the idea of an accessible asymptotic domain[13]. Figure 2-7 shows the total proton-proton cross-section as now measured with high precision over the ISR energy range. The observed rise is well within the limits of what theoretical models may predict, with a $\ell n^2 s$ behaviour corresponding to the Froissart bound. Yet theoretical models which allow for a rising cross-section may now lead to a simple asymphotic behaviour only for $\ell n \frac{s}{m^2} \gg 1$, as opposed to $\frac{s}{m^2} \gg 1$, which was formerly expected to be enough! Asymptopia has become but an elusive concept. The observed rise is actually much less than one could expect were the proton to become opaque. Even if the total cross-section rises the proton remains fairly transparent. This is also an important result which could be deduced from elastic scattering measurements at the ISR. This is also discussed in section 3.

While the total cross-section, when measured over a new and extensive energy range, has shown a surprising behaviour, cross-section differences for particle and antiparticle scattering and charge exchange cross-sections have been found in beautiful agreement with what could be expected from Regge behaviour. In this case most of the experimental information comes from Fermilab. This is also discussed in section 3.

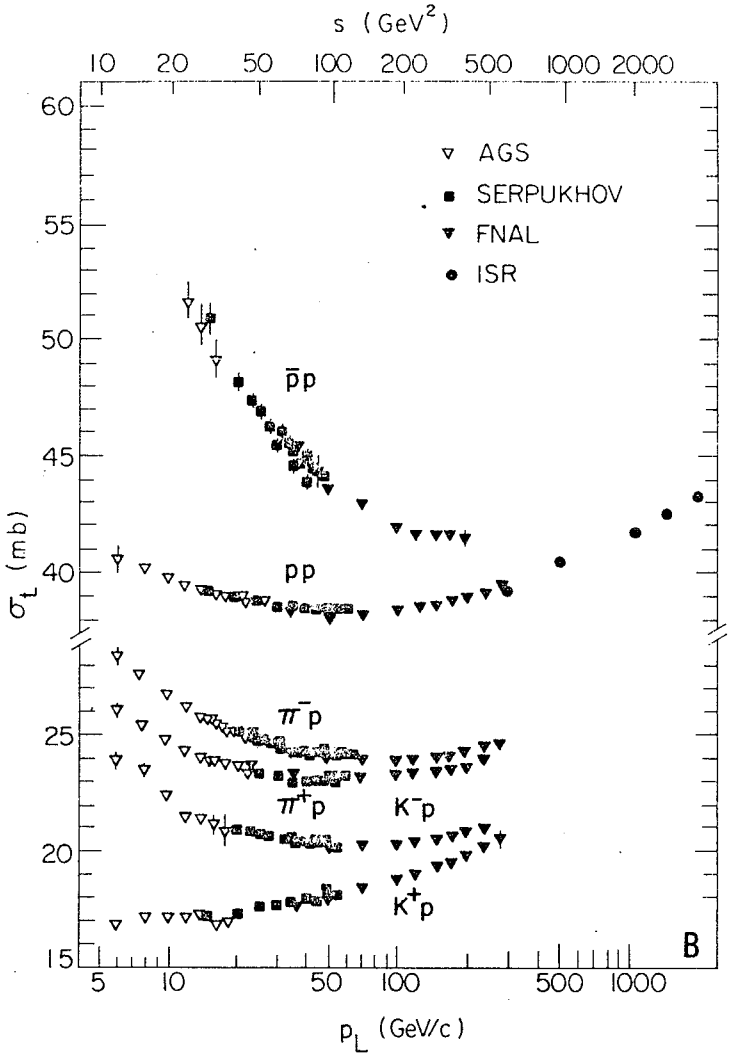

Figure 2-7 : pp total cross-section at ISR energies. Data from the CERN-Rome Collaboration. Normalization to the Coulomb peak allows a precise measurement of σ_{tot}. Also shown are total cross-sections measured at Fermilab at lower energies.

Another important topic in ℓn s physics, which is discussed in section 4 is that of particle production. The key feature here is the stability of the density in longitudinal phase space. Considering non-diffractive processes, which correspond to about 0.7 of the inelastic cross-section, one may identify six important general features which are now ascertained:

(i) limited transverse momentum of the secondaries (typically an exponential decrease with $\langle p_t \rangle = 0.35$ GeV/c)

(ii) leading particle effect (the incident proton retains on the average half of its energy)

(iii) slow increase with energy of the multiplicity of the produced particle, consisting mainly of pions (roughly a logarithmic increase, with 85% of pions)

(iv) scaling behaviour of the inclusive cross-sections (the longitudinal momentum distribution of each type of secondaries is independent of energy when measured (scaled) in terms of the incident momentum)

(v) independence from incident particles (the multiplicity depends practically only on the center-of-mass energy)

(vi) short range order or clustering (correlations are positive and depend mainly on rapidity differences, as shown in figure 2-5, as if particles would originate from independent clusters).

Properties (iii) to (vi) can be globally summarized saying that, while the rapidity range extends, the rapidity density (and density fluctuations), hardly changes. This is stability in longitudinal phase space. Properties (i) to (iii) were known before the ISR started. Properties (iv) to (vi) resulted from experimentation, at the ISR, and at Fermilab (v). This will be discussed in section 4 where, while giving examples of these new properties which have contributed a great deal to present understanding of particle production, we shall indicate some important remaining questions.

The last item in ℓn s physics is that of diffractive excitation. It was well known that in a high energy collision a particle could be excited to a new state, with the same internal quantum numbers, while retaining most of its incident energy. In most cases the other incident particle is merely quasi-elastically scattered. Such processes are referred to as diffractive excitation.

For reasons discussed later such a process can be kinematically separated from others provided that the diffractively excited mass M is such that

$M^2 \lesssim 5 \times 10^{-2} s$. At ISR energies it is indeed possible to follow diffractive excitation well above 10 GeV. It was then found that the excitation cross-section is important, decreasing only as $d\sigma/dM^2 \sim (M^2)^{-1}$ [14]. The existence of high mass diffraction with such properties is of great interest. Diffraction can be described in terms of an exchange process, where the exchanged object is referred to as the Pomeron. Phrased in terms of pomeron-hadron interaction, high mass diffraction stands for a great similarity between such a new process and typical hadronic reactions. This is discussed in section 5.

Turning now to processes with a rapid change with energy, one meets large p_t production, as previously mentioned (figure 2-6). Secondary hadrons are practically all produced with low p_t values ($\langle p_t \rangle \simeq 0.35$ GeV/c) and are mainly pions. This is most generally expected for a process which is coherent over the interaction zone, the transverse dimensions of which (typically 1 fermi) are not modified by the Lorentz contraction. The p_t distribution is exponentially falling with a slope of $6(\text{GeV})^{-1}$ and practically energy independent. It was an important discovery at the ISR to find that this behaviour no longer applies beyond $p_t \sim 1.5$ GeV/c [15]. The large p_t yield is much above what the simple extrapolation of the low p_t behaviour would lead to expect (figure 2-6). Furthermore, the large p_t yield increases with energy in contradistinction with what the low p_t distribution does, and it includes relatively many heavy particles. To the extent that a structure in the p_t distribution is most generally tentatively associated with incoherent production localized within the protons, the study of large p_t phenomena has quickly become very topical. At present, their association with scattering among proton constituents has met with an impressive array of results obtained at the ISR, and at Fermilab. The key feature is the production of jets of hadrons at wide angle. The analysis of such jets, with similarities and differences with those observed in lepton induced processes is of great topical interest. This is discussed in section 6.

Large p_t hadrons hid for some time the lepton yields initially searched for past the overwhelming hadron production at low p_t. Eventually prompt leptons (not associated with the weak decay of known hadrons) have been ascertained among large p_t particles [16]. They were discovered in 1974 at Fermilab and at the ISR. The lepton yield (electron and muon are comparable) is proportional to the pion yield (at a level of 10^{-4}) over a wide range of p_t values ($1 < p_t < 4$ GeV/c), and over the whole ISR energy range. The origin of these prompt leptons now raises many interesting questions. Some (if not most) of those observed at rather large p_t ($p_t > 1.5$ GeV/c say) could come from high mass lepton pairs which are at present associated with collisions at the proton constituent level through the Drell-Yan process. Some should come from the known

new particles, or signal still new ones. At lower p_t ($1 < p_t < 1.5$ GeV/c say) they come from production and decay of well known vector mesons but could also originate from the weak decay of charmed particles. As is clear from table 2-2, the study of prompt leptons is of great topical interest. The ISR benefits from yields increasing sharply with energy. Its competing role, with respect to Fermilab (SPS) is however suffering from luminosity and background problems. The recent discovery of the 9.5 GeV peaks in muon pair production at Fermilab[17] stands for the edge which fixed target machines actually have. Experimentation with leptons, while of great promise, is very difficult. This has triggered much effort at the ISR (table 2-2). The present (and fast moving) status of prompt lepton physics is discussed in section 7. Lepton pair production and large p_t hadron production share a high topical interest in view of their relation with reactions at the constituent level. Their study is also of great value at exploring the potentials of the coming generation of colliders, considered as machines on which the weak bosons could be discovered. This is discussed in section 10.

3. Total cross-sections and elastic scattering

This global title stems from the fact that the measurement of the elastic differential cross-section at small momentum transfer t is used to determine the imaginary part of the forward amplitude, which, through the optical theorem, gives the total cross-section.

$$\mathrm{Im}\ F(s,0) = s\,\sigma_{tot}(s) \tag{3.1}$$

$$\frac{d\sigma}{dt} = \frac{1}{16\pi s^2}\,|F(s,t)|^2 \tag{3.2}$$

The $t = 0$ extrapolation is usually achieved in practice from measurements of elastic scattering in the range $0.01 < |t| < 0.1$ $(\mathrm{GeV/c})^2$. A determination of the real part (and therefore a precise determination of the imaginary part) implies the study of interferences with the Coulomb contribution. It requires cross-section measurements down to $0.001 < |t| < 0.1$ $(\mathrm{GeV/c})^2$. From (3.1) and (3.2), one gets

$$\sigma_{tot}^2 = \frac{16\pi\ d\sigma/dt\,|_{t=0}}{1+\rho^2} \tag{3.3}$$

where

$$\rho(s) = \frac{\mathrm{Re}\ F(s,0)}{\mathrm{Im}\ F(s,0)} \tag{3.4}$$

is the ratio of the Real to the Imaginary part of the forward amplitude.

More generally speaking, if one thinks of very high energy scattering as a diffractive (shadow) effect, elastic scattering gives the shape of the absorbing area globally associated with the total cross-section. Measurements of the proton-proton total cross-section at the ISR have actually followed different lines. An experiment by the Pisa Stony-Brook Collaboration (1973) relied on the separate measurement of the luminosity (Van der Meer method) and of the total number of interactions measured per unit time using an almost 4π scintillation counter detector. The method is of course reminiscent of the standard transmission method used at conventional machines.

At the same time an experiment by the CERN-Rome Collaboration (1973) determined the elastic scattering amplitude and used the Optical theorem.

These two approaches were later combined by both collaborations in a joint measurement of the total rate and of elastic scattering, thus eliminating the luminosity. If N stands for the counting rate (2-1) one has

$$\sigma_{tot} = \frac{16\pi \, dN/db \,|_{t=0}}{N(1+\rho^2)} \qquad (3.5)$$

Systematic error in σ_{tot} could thus be reduced to 0.6%. Eventually, normalization to the Coulomb peak could be achieved throughout the ISR energy range. The total cross-section, as now known, is shown in figure 2-7[12]. Also shown are results from Fermilab[7]. All total cross-sections eventually rise with energy. Even though the reported rate of rise is well within accepted bounds, this phenomenon has profoundly affected theoretical approaches to hadronic interactions. A simple parameterization from 100 to 2000 GeV is:

$$\sigma_{tot} = 38.4 + 0.49 \ln^2\left(\frac{s}{122}\right)$$

when σ is in mb and s in GeV^2.

The rise of the total cross-sections is not yet well understood. It is however known to be associated with the diffractive component of hadron scattering. Whenever Quantum numbers are exchanged between the two colliding particles, Regge behaviour, with a trajectory intercept of the order $\alpha(o) \leq 0.5$ and a slope of the order of $\alpha' = 0.9$ $(GeV/c)^{-2}$, is found to apply surprisingly well. This calls for a parenthesis which borrows much from Fermilab results. While total cross-sections for particle and antiparticle eventually rise, their difference falls as an inverse power, as expected from Regge behaviour. This has been verified to be a general property in experiments at Fermilab. Figure 3-1 shows the corresponding effect in the case of K^+p and K^-p scattering. One has

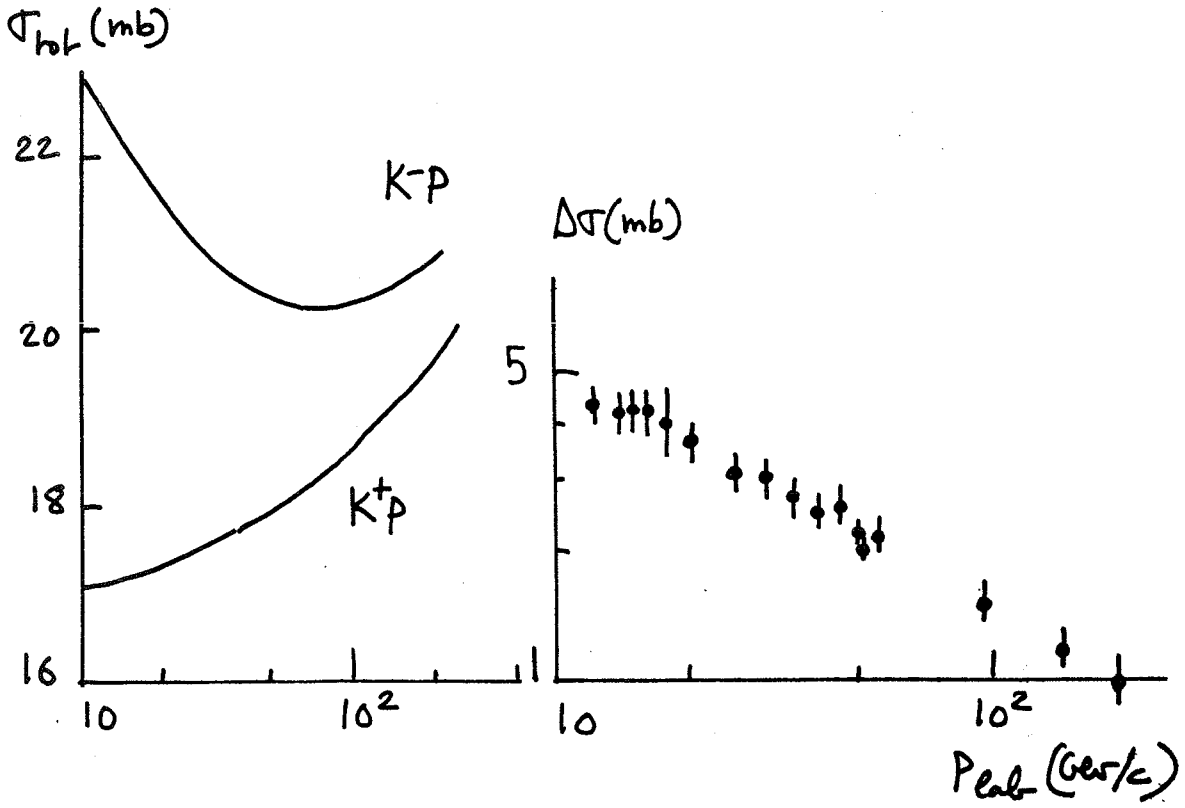

Figure 3-1 : Total cross-sections and total cross-section difference for $K^{\pm}p$ scattering. The Regge behaviour corresponds mainly to ω exchange

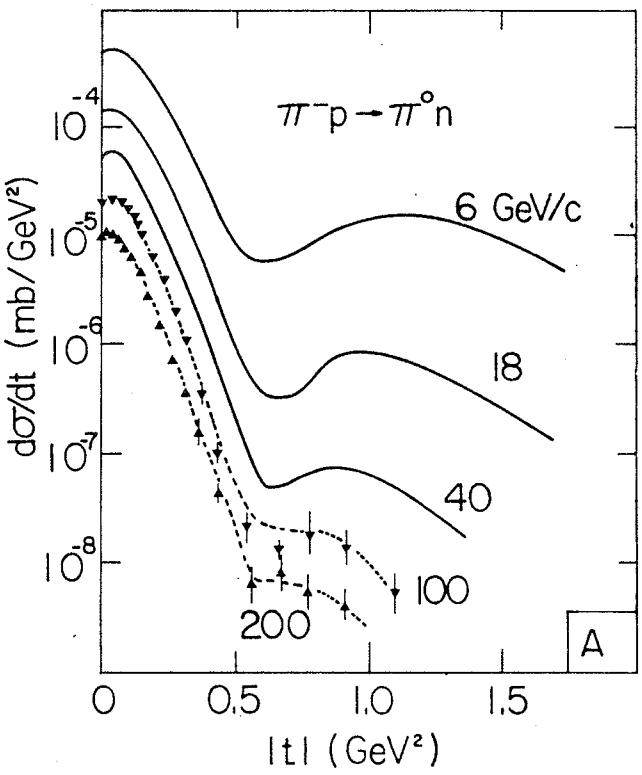

Figure 3-2 : πp charge exchange differential cross-section at Fermilab. The data agree very well with what is expected from Regge behaviour, which corresponds to ρ exchange

indeed $$\Delta\sigma \sim s^{-\alpha(0)}$$

with $$\alpha(0) = 0.40 \pm 0.04 \qquad (3.6)$$

and this over the whole energy range. Charge exchange scattering cross-sections are also found to be in very good agreement with Regge behaviour. Figure 3-2 shows the differential cross-sections observed for πp charge exchange at Fermilab. This agrees very well with ρ exchange. Such a beautiful check of a Regge phenomenology, adjusted to the 5 to 20 GeV/c range, and found to apply up to 400 GeV/c would have been a great success of particle physics. It was of course completely overshadowed by the discovery of the new particles! Figure 3-3 shows a very interesting effect of Regge behaviour. It corresponds to recent ISR results obtained by the CHOV (CERN-Hamburg-Orsay-Vienna) Collaboration for the charge exchange reaction $pp \rightarrow n\Delta^{++}$. Up to 500 GeV the process appears to be dominated by π exchange (sharp forward peak and s^{-2} behaviour of $d\sigma/dt$). Beyond 500 GeV, one sees ρ exchange taking over (forward dip and s^{-1} behaviour for $d\sigma/dt$). In view of the higher intercept of the ρ trajectory, ρ exchange was expected to eventually dominate. Nevertheless, this does require an extremely high energy. This is a very clear and beautiful illustration of Regge behaviour in high energy scattering. This closes our discussion of quantum number exchange.

Connecting the rise of the total cross-section with the diffractive part of the scattering amplitude is an hypothesis which was actually immediately considered. An important consequence was that $\rho(s)$ (3.4) had eventually to become positive while slowly decreasing as $(\ell n\ s)^{-1}$. This was a particularly interesting consequence in view of the fact that, at lower energies ($E \sim 20$ - 60 GeV say) ρ is negative. The parameter ρ is related to the total cross-section for pp and $\bar{p}p$ scattering through a dispersion relation. The observed behaviour for σ (figure 2-7) then implies that ρ vanishes through the Fermilab energy range. As shown in figure 3-4-a, this was indeed observed. Most recent measurements of ρ at the ISR, which are shown in figure 3-4-b, allow for a prediction of the behaviour of σ_{tot} at much higher energies. A dispersion calculation shows that the pp (and $\bar{p}p$) total cross-sections should keep rising, up to at least $\sqrt{s} \sim 300$ GeV, reaching there a common value of about 55 mb. The behaviour beyond that is no longer controlled by the measured values of ρ which extend up to $\sqrt{s} \sim 60$ GeV.

The asymptotic behaviour of ρ follows from analyticity and crossing symmetry.

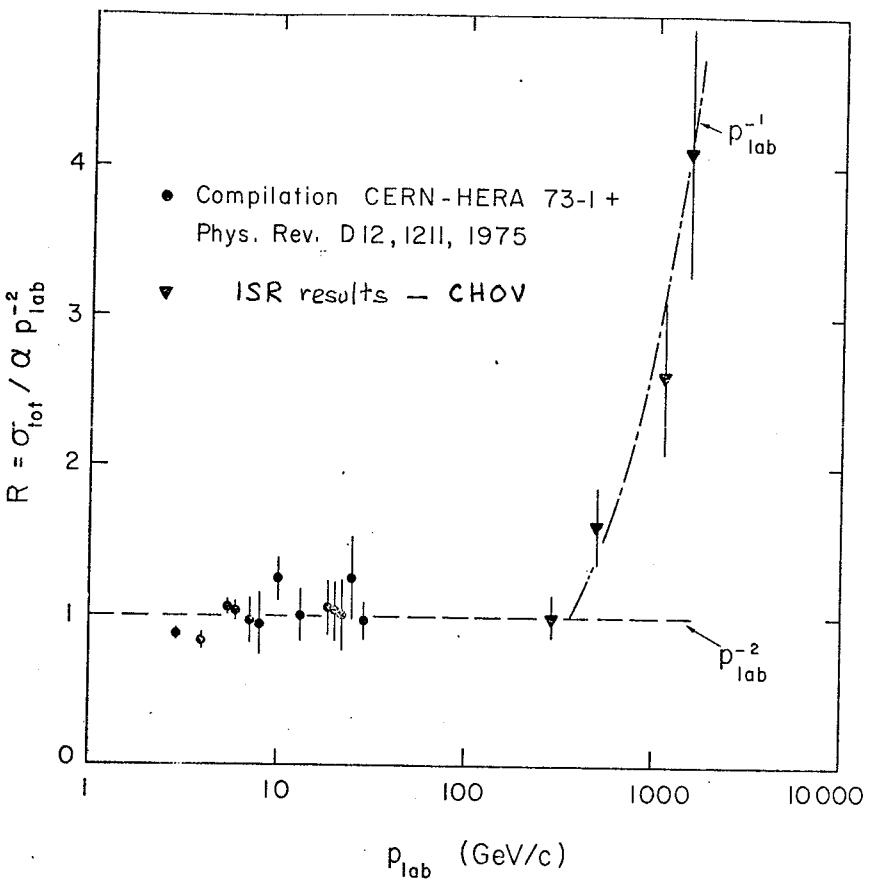

Figure 3-3-a) : The energy dependence of the $pp \to n\Delta^{++}$ cross-section. One switches from π dominance (s^{-2}) to ρ dominance (s^{-1})

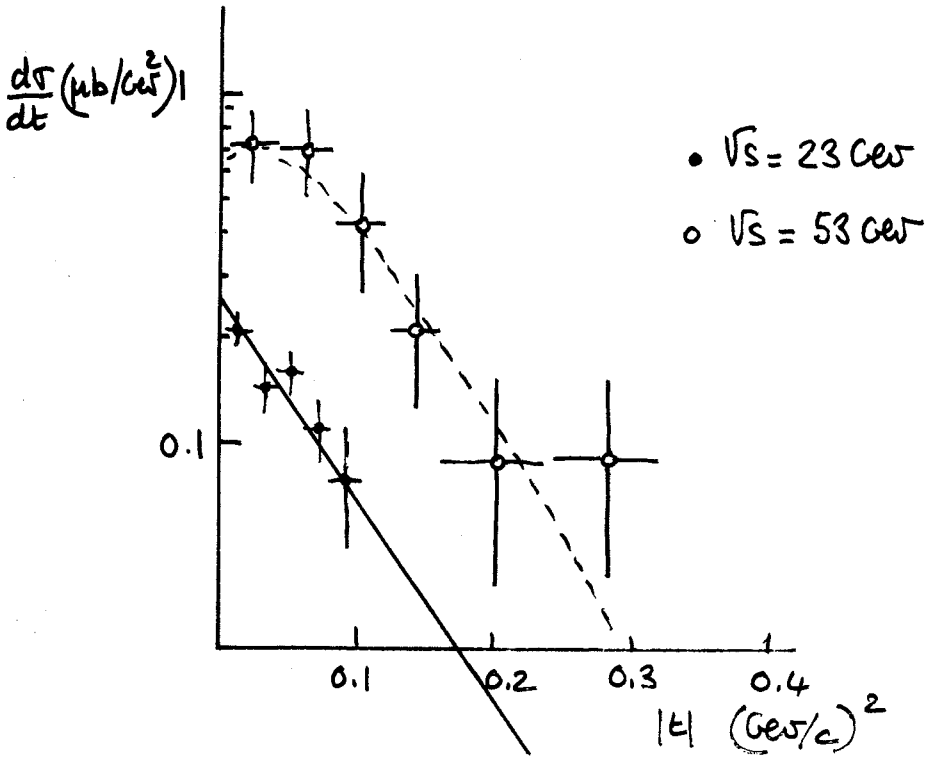

Figure 3-3-b) : Differential cross-section for $pp \to n\Delta^{++}$ over the ISR energy range. The 23 GeV data are reduced by a factor 50 as compared to the 53 GeV data (vertical scale). One goes from pion exchange (forward peak) to ρ exchange (forward dip). The Data are from the CERN-Hamburg-Orsay-Vienna Collaboration

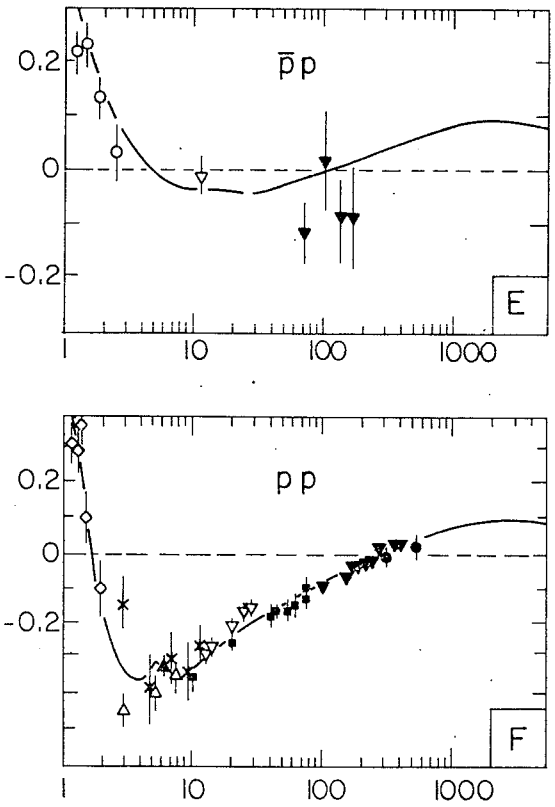

Figure 3-4-a) : The ρ parameter for pp and $\bar{p}p$ scattering. The vanishing of ρ through the Fermilab energy range was a predicted consequence of the rising cross-section. Data (on pp) from the US-Soviet gas jet Collaboration at Fermilab. The solid lines correspond to dispersion relation calculations

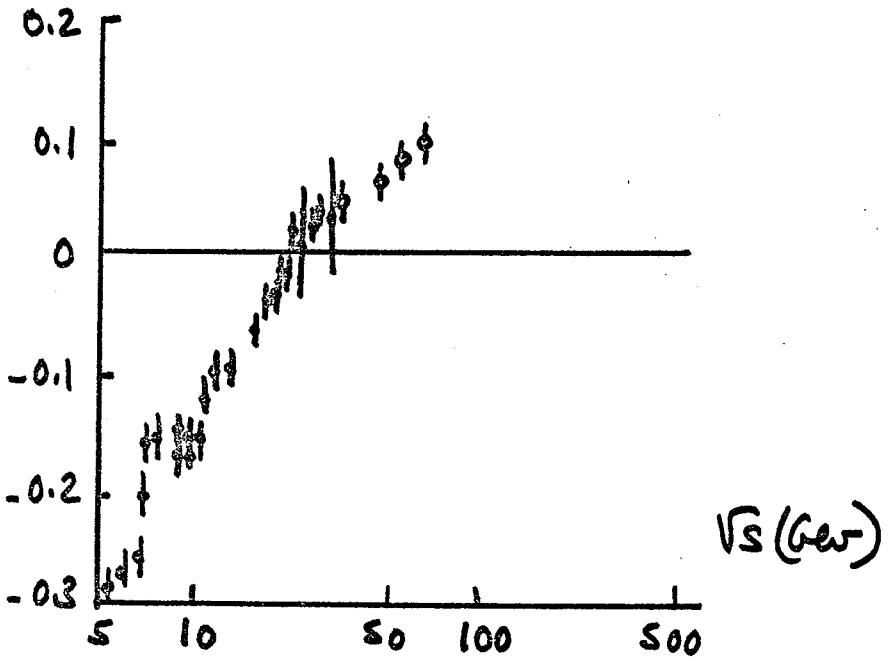

Figure 3-4-b) : Recent ISR measurements of ρ (open dots). Data from the CERN-Rome Collaboration

The scattering amplitude is an analytic function of s defined in a cut plane (figure 3-5). If the amplitude is asymptotically even under crossing, with the pp and $\bar{p}p$ amplitude approaching the same behaviour, its value at $-s-i\varepsilon$ is the same as that at $s + i\varepsilon$, which defines the physical value. Its value at $-s+i\varepsilon$ is the complex conjugate of its value at $s + i\varepsilon$. Rotating counterclockwise in the s complex plane (figure 3-5) by π one thus replaces F by F*. This imposes drastic restriction on the mathematical form of F. In particular, whenever including a $\ell n\ s$ term in F, in order to find it eventually in the expression for the cross-section (3-1), one has to actually include a $(\ell n\ s - \frac{i\pi}{2})$ term, which indeed transforms into its complex conjugate through the π rotation. A suitable asymptotic behaviour for a logarithmically rising cross-section is therefore $(0 < \alpha \leq 2)$

$$F(s,0) = is\left(\ell n s - \frac{i\pi}{2}\right)^{\alpha} \tag{3.7}$$

which implies

$$\rho(s) \sim \frac{\alpha\pi}{2}(\ell n s)^{-1} \tag{3.8}$$

more generally, imposing even crossing property and analyticity gives an operational relation between ReF(s) and ImF(s). It is as follows

$$\mathrm{Re}\,F(s) = \left(\tan\frac{\pi}{2}\frac{\partial}{\partial \ell n s}\right)\mathrm{Im}\,F(s) \tag{3.9}$$

which in practice reads, as a series expansion

$$\mathrm{Re}\,F(s) = \left(\frac{\pi}{2}\frac{\partial}{\partial \ell n s} + \frac{1}{3}\left(\frac{\pi}{2}\right)^3\frac{\partial^3}{\partial \ell n s^3} + \ldots\right)\mathrm{Im}\,F(s) \tag{3.10}$$

A rising cross-section (a rising ImF(s) through the optical theorem) eventually imposes a positive real part.

At present energy one has to combine the expected asymptotic even behaviour with Regge contributions with even and odd parts. One may also use a dispersion relation. This gives the curves drawn on figure 3-4-a).

Checking for the expected behaviour of ρ (figure 3-4) and $\Delta\sigma$ (figure 3-1) were important points. Associating the rising cross-section with the diffractive part of the amplitude is now secured. Yet even at ISR energies, ρ and σ are still far from showing the correlated behaviour (3.8) which is expected asymptotically.

A similar conclusion is drawn for the shape of the diffraction peak. A striking feature in the differential cross-section is obviously the dip at a $|t|$ value of the order of 1.4 $(\mathrm{GeV/c})^2$. This was first observed at the ISR[18]. The differential cross-section in the dip region is shown in figure 3-6. The dip becomes more pronounced with increasing energy and then recedes. It moves inwards as the forward peak shrinks. We focus on the peak first.

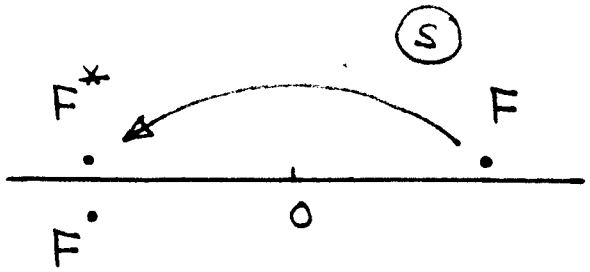

Figure 3-5 : The forward amplitude as defined in the complex s plane

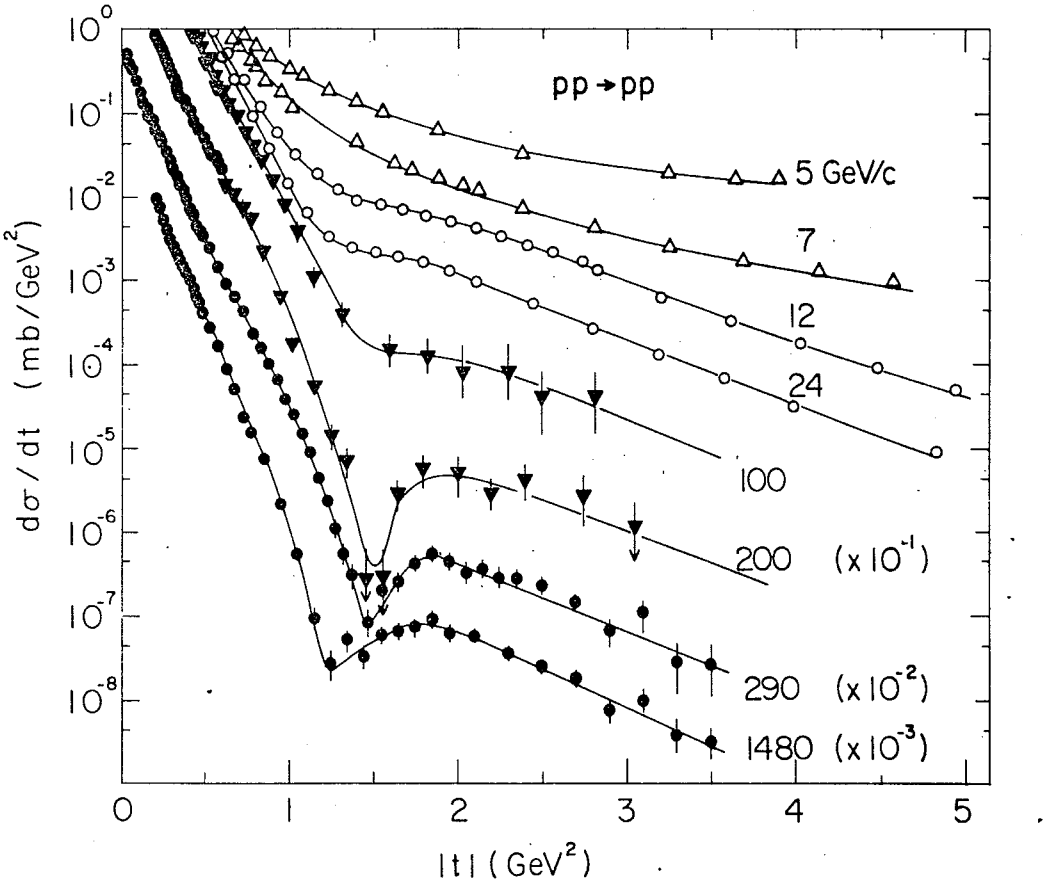

Figure 3-6 : A compilation of pp differential cross-sections in the dip region

The forward peak ($|t| < 0.1$ (Gev/c)^2 is well parametized in terms of a simple exponential with a slope b(s) which increases logarithmically with energy

$$b(s) = 8 + 0.55 \ln s \tag{3.11}$$

with b in (GeV/c)$^{-2}$ and s in (GeV)^2.

This corresponds to an effective Regge slope for the Pomeron $\alpha' \approx 0.25$. With $\rho \approx 0$ (figure 3-4) and a purely exponential dependence one easily gets

$$b(s) = \frac{\sigma_{tot}^2(s)}{16\pi\,\sigma_{el}(s)} \tag{3.12}$$

Despite different best fits this is found to be rather well satisfied with b, σ_{tot} and σ_{el} practically proportional to one another from 200 to 2000 GeV[19]. This is referred to as geometrical scaling. The proton increases in size with energy (σ_{tot} increases) but its shape does not change appreciably. Actually an exponential shape is also a very good approximation for the diffraction peak all the way from $|t| = 0.1$ to $|t| = 1.4$ (GeV/c)^2. However the slope aprameter is 2 units below what it is at lower $|t|$. The corresponding kink is not yet well understood. Figure 3-7 gives the σ_{el}/σ_{tot} ratio as measured at the ISR and at Fermilab for $\bar{p}$. The values do merge together with increasing energy as it should for a diffractive effect. The constant value corresponds to an energy independent shape.

Neglecting the real part (or assuming it to be proportional to the imaginary part) one can calculate the scattering amplitude at impact parameter r through a Fourier transform.

$$f(r,s) = \frac{1}{2\pi}\int \frac{|F(s,t)|}{8\pi s}\, e^{-i\vec{q}\cdot\vec{r}}\, d^2\vec{q} \tag{3.13}$$

where $\vec{q}$ is the 2 dimensional momentum transfer ($t = -\vec{q}^2$). This gives the profile function shown in figure 3-8.

The profile function (figure 3-8) and the value of σ_{el}/σ_{tot} (figure 3-7) show that, even at ISR energies, one is very far from a full absorption limit where the proton would behave as a black disc with a grey edge. Even at zero impact parameter the proton remains not fully absorbent. It rapidly becomes rather transparent as one moves away in impact parameter. The resulting absorption factor has a Gaussian shape with a width of about 0.9 f. As the energy increases the width increases (logarithmically). The overall shape stays however the same. The proton remains very grey[20].

The relative transparency of the proton at extremely high energy is still a very puzzling question. One is far from the standard hypothesis of a few years ago whereby the many open channels would result in full absorption.

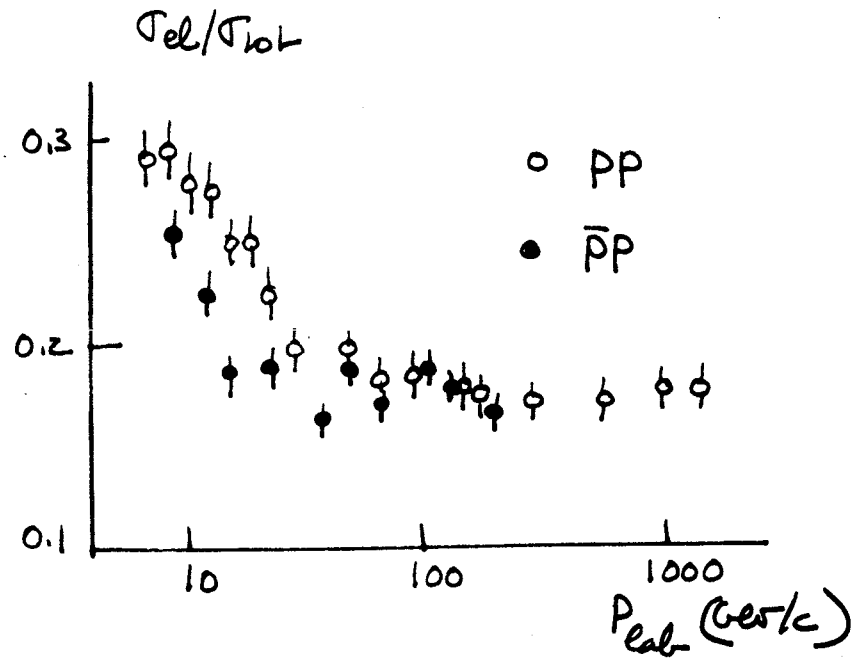

Figure 3-7 : The proportionality between σ_{el} and σ_{tot} at ISR energies

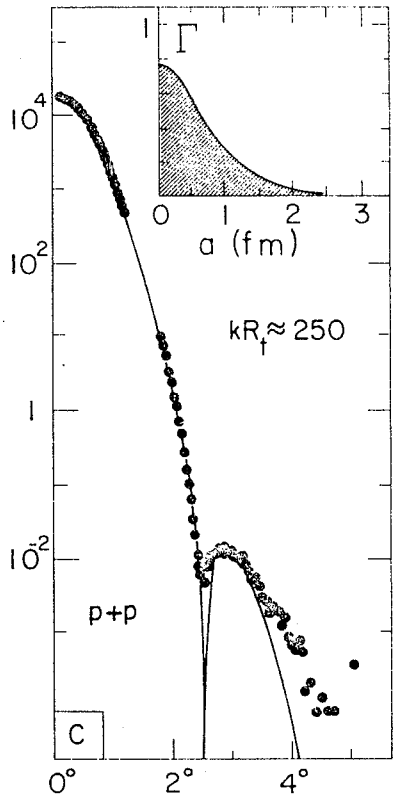

Figure 3-8 : pp elastic scattering angular distribution at p_t = 1500 GeV/c and the corresponding profile function Γ, corresponding to $2|f(r)|$. Full absorption would correspond to $|f(r)| = 0.5$. The proton is therefore rather transparent. For full absorption one would also have $\sigma_{el} = 0.5\ \sigma_{tot}$. It is much less.

Present theoretical models may reach, through a very elegant field theoretic approach, asymptotic forms which are (to leading ℓn s) of the type[21]

$$F(s,t) = s^{\alpha(t)} (\ell n s)^{\kappa} g\left(-t(\ell n s)^{\nu}\right) \qquad (3.14)$$

with $\alpha(o) = 1$. Such model amplitudes have a structure which may match all features now observed. Nevertheless, they are expected to apply when $\ell n\, s \gg 1$ only, and their relevance to the ISR energy range is still unclear.

The rising total cross-section came as a surprise. Even if now well understood phenomenologically, such a behaviour still raises very important and challenging theoretical questions, the key one being "Why do cross-sections rise so little since they rise at all?".

The dip structure has no visible effect on the profile function of figure 3-8 since the second maximum is 6 orders of magnitude below the forward peak value. Its presence shows in any case that the scattering amplitude is almost purely imaginary since a sizeable real part would otherwise smear away any effect of that type. This is indeed what probably occurs at much larger $|t|$ values as shown by figure 3-9. A second zero in the imaginary part at $|t| \approx 8 (GeV/c)^2$ could be smeared by a relatively important real part for which one theoretically expects an increasingly important (relative) role at wider angles[22].

Diffractive scattering should lead to a predominantly imaginary amplitude. Indeed, this seems to prevail up to rather large $|t|$ values as the marked dip structure and the rather stable shape of the differential cross-section indicate. However, for reasons discussed later in section 6, one could expect a new type of exchange process to dominate at very large $|t|$ with a sizeable relative real part. Whether what now is observed at $|t| = 8$ GeV/c^2 (figure 3-9) corresponds to a transition regime in elastic scattering is still unknown. This is a very interesting question.

While the ISR results have shown that diffraction scattering is far more subtle and complicated than once expected and that the Pomeron, which translates diffractive scattering in terms of an exchange process, is a complicated object, recent Fermilab results have shown that diffraction is also not simple in terms of SU(3) properties[22]. Comparing πp and Kp elastic scattering one can isolate a singlet F_0 and an octet F_8 part in the scattering amplitude which both contribute to the high energy diffractive cross-section. The ratio of πp and Kp differential cross-sections is (to a good first approximation) given by:

$$\frac{(d\sigma/dt)\,\pi p}{(d\sigma/dt)\,Kp} \quad \frac{|F_0|^2 + 4\,Re\,F_0^* F_8}{|F_0|^2 - 2\,Re\,F_0^* F_8} \qquad (3.15)$$

It is larger than 1 at $|t| = 0$ ($F_8 \neq 0$).

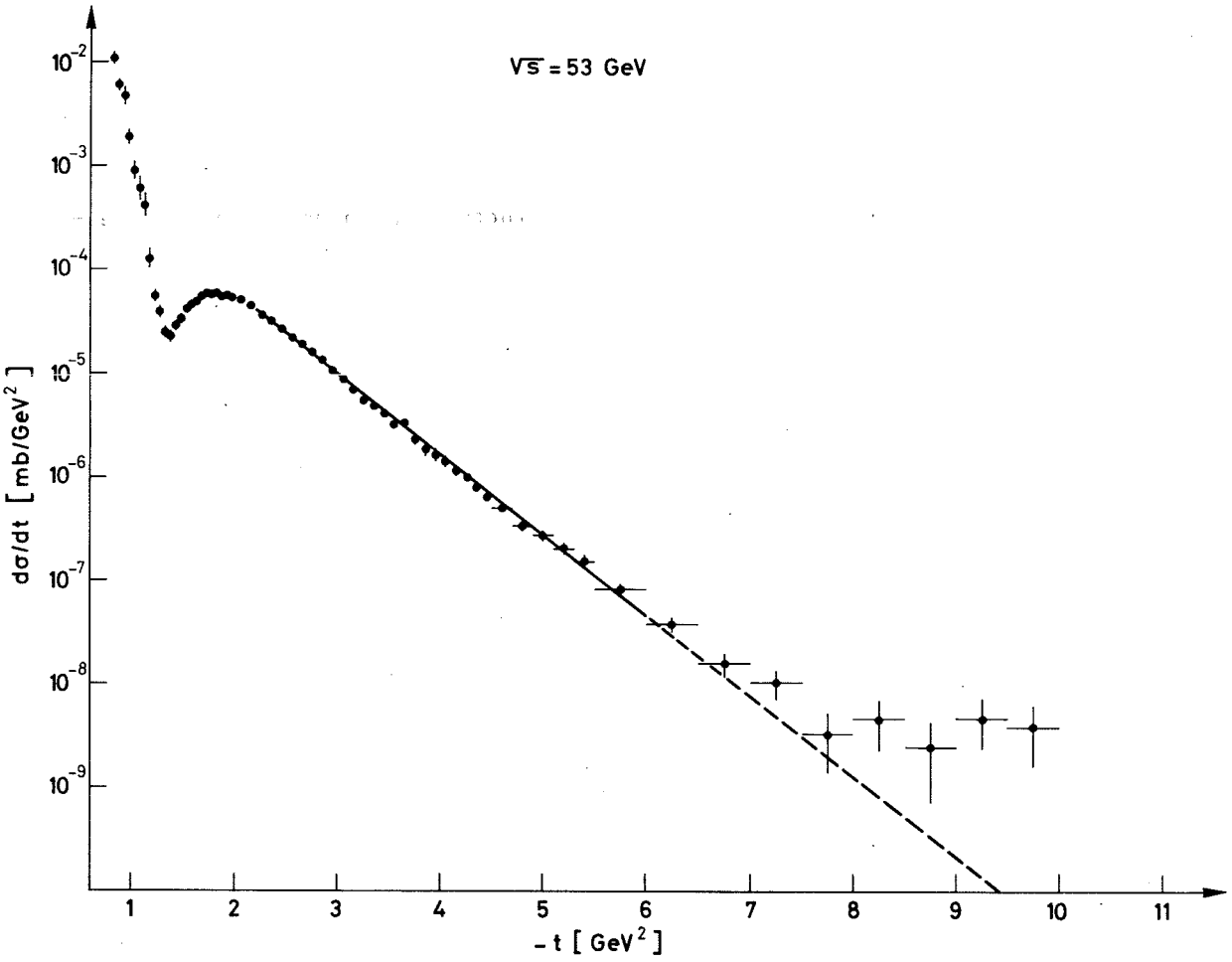

Figure 3-9 : pp differential cross-section at large $|t|$. Data from the CERN-Hamburg-Orsay-Vienna Collaboration (1977)

One finds however that, as $|t|$ increases beyond 0.4 $(GeV/c)^2$, the octet part disappears. The πp total cross-section is larger than the Kp total cross-section. The octet part is important at low $|t|$. At larger $|t|$ the πp and Kp differential cross-sections merge.

To the extent that low $|t|$ values correspond to large impact parameters, where exchange of (light) pions should dominate over (heavier) kaon exchange, such a behaviour is not too surprising. Nevertheless, it further complicates what is referred to as the Pomeron, when all recent theoretical analysis of diffraction scattering lead to involve an exchange process[23].

Table 3-1 lists the ISR experiments, the results of which have been discussed in this section. The picture of diffractive scattering has been deeply modified over the past 5 years. It is still rich in challenging questions.

Table 3-1

ISR experiments with important contributions to the study of total cross-section and elastic scattering.

(i) Discovery of rising cross-sections → See P.R.L. 36B 415, (1971)

601 CERN-Rome

801 Pisa Stony Brook

(ii) Measurement of ρ up to 2000 GeV (elastic scattering down to 0.8 mrad)

805 CERN-Rome

(iii) Differential cross-section at medium $|t|$

602 Aachen-CERN-Genoa-Harvard-Munich

604 CERN-Genoa-Harvard-Munich-Northwestern-Riverside

401 CERN-Hamburg-Orsay-Vienna

4. Particle Production

The mean number of particles produced in a collision increases with energy but relatively slowly (to a first and good approximation, logarithmically). This is the case for all kinds of produced particles. The general trends displayed by pions which are overwhelmingly dominant, is eventually followed by heavy secondaries. This is shown in figure 4-1. At ISR energy there are typically 15 particles produced in each collision, 85% of them being pions. Over the ISR energy range one produces on the average 1.8 extra charged particles per unit increase of $\ell n\ s$. As shown by Fermilab results the increase in multiplicity is due to large multiplicity configurations taking an increasingly important role while that of the low multiplicity ones slowly decreases in relative importance. This is displayed in figure 4-2, which gives the topological cross-sections (number of charged prongs) as a function of energy.

The center-of-mass momentum of a produced particle is usually referred to by its transverse component p_t and its longitudinal component, scaled according to the incident particle momentum

$$x = \frac{p_L}{P} \simeq \frac{2 p_L}{\sqrt{s}} \qquad (4.1)$$

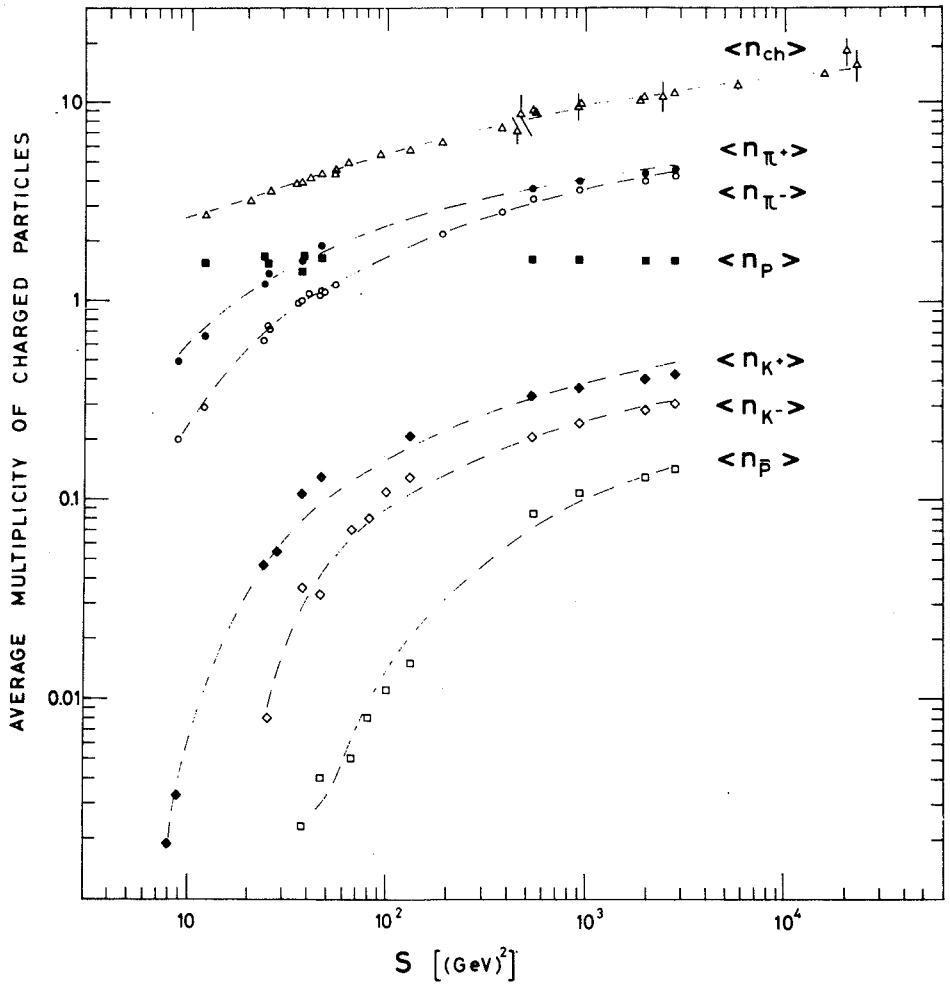

Figure 4-1 : Mean number of particles produced in high energy collisions. The special behaviour of the proton yield is related to the presence of two initial protons. As extra protons are produced in $p\bar{p}$ pairs more frequently, initial protons more frequently appear as neutrons

This choice of variables is motivated by two important properties which are displayed in figure 4-3. Figure 4-3-a) gives the transverse momentum distribution for inclusive distributions at fixed x. An inclusive one particle distribution corresponds here to

$$pp \rightarrow A(x, p_T) + X \qquad (4.2)$$

where A is the observed particle and X any unobserved remainder. The transverse momentum distributions for all types of secondaries hardly vary over the whole ISR energy range. For pions there are even only small changes from PS to ISR energies.

Figure 4-3-b) gives the x distribution at fixed p_t. The data points span the whole ISR energy range. The p_L distribution corresponds to a fixed x distribution. This is referred to as Feynman scaling. Produced particles take on the average fixed fractions of the center-of-mass energy. The phase space configuration does not change appreciably with energy when longitudinal momenta are scaled according to the center-of-mass energy. Scaling, as so defined, can also be described as limiting fragmentation. The momentum distributions of the secondary particles reach limiting values with increasing energy when they are defined in the rest frame of one or other of the incident particles[24]. This is displayed in figure 4-4 in terms of the rapidity variable[25]. Rapidity distributions are simply shifted from one another when going from the center-of-mass system to the rest frame of either of the incident particles. In figure 4-4, the inclusive distributions are given in terms of the rapidity which they have in the rest frame of one of the incident proton (referred to as y_{lab}). As the energy increases the rapidity range increases, but the distribution at already available rapidities remains practically constant. From the point of view of the colliding proton, the momentum distribution of the secondary particle has thus reached a limiting value. One also sees in figure 4-4 that the extending longitudinal phase space (or rapidity range) is filled by particle production with a practically constant density (about two charged particles per unit of rapidity). This results in a central plateau in the rapidity distribution, which one sees developing as y_{lab} exceeds 2 units.

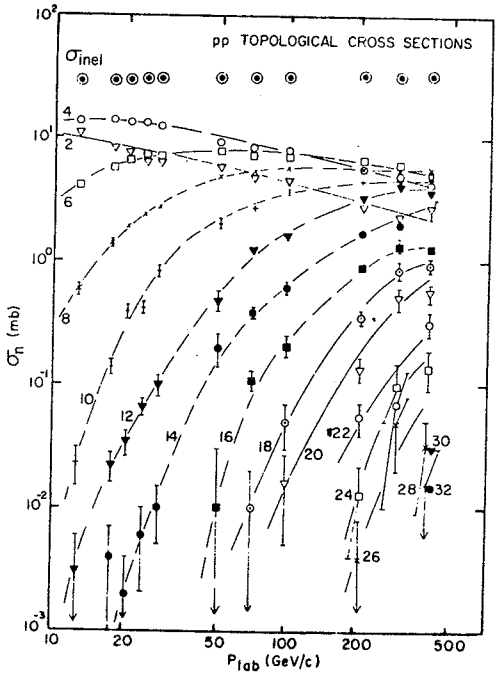

Figure 4-2 : Topological cross sections. Rapid increase of large multiplicity cross-sections and slow decrease of low multiplicity cross-sections. 30" data at Fermilab

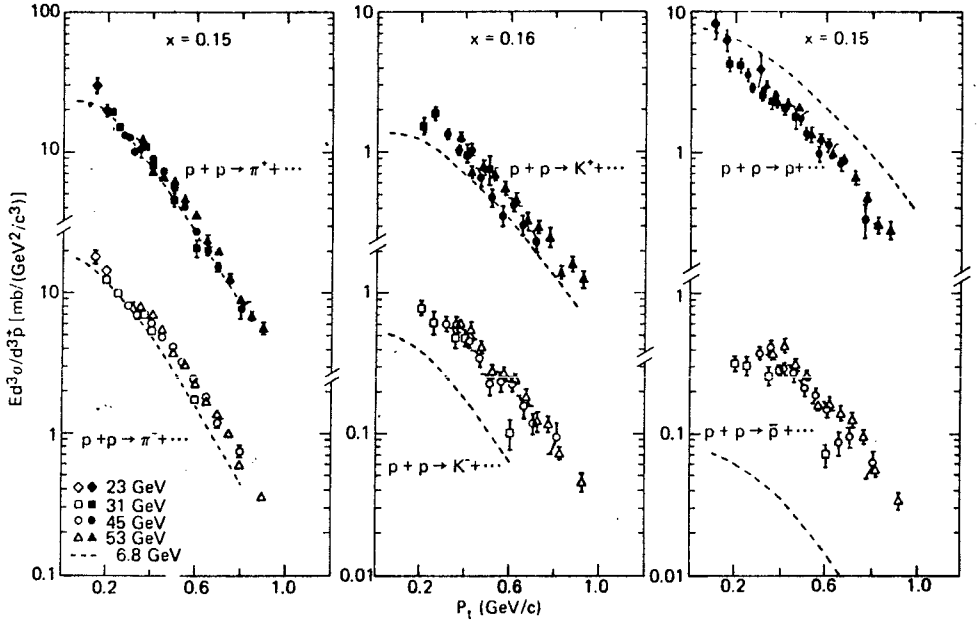

Figure 4-3-a) : Transverse momentum distribution. ISR data and distributions at PS energy (dashed curves). Data from the CERN-Holland-Lancaster-Manchester Collaboration

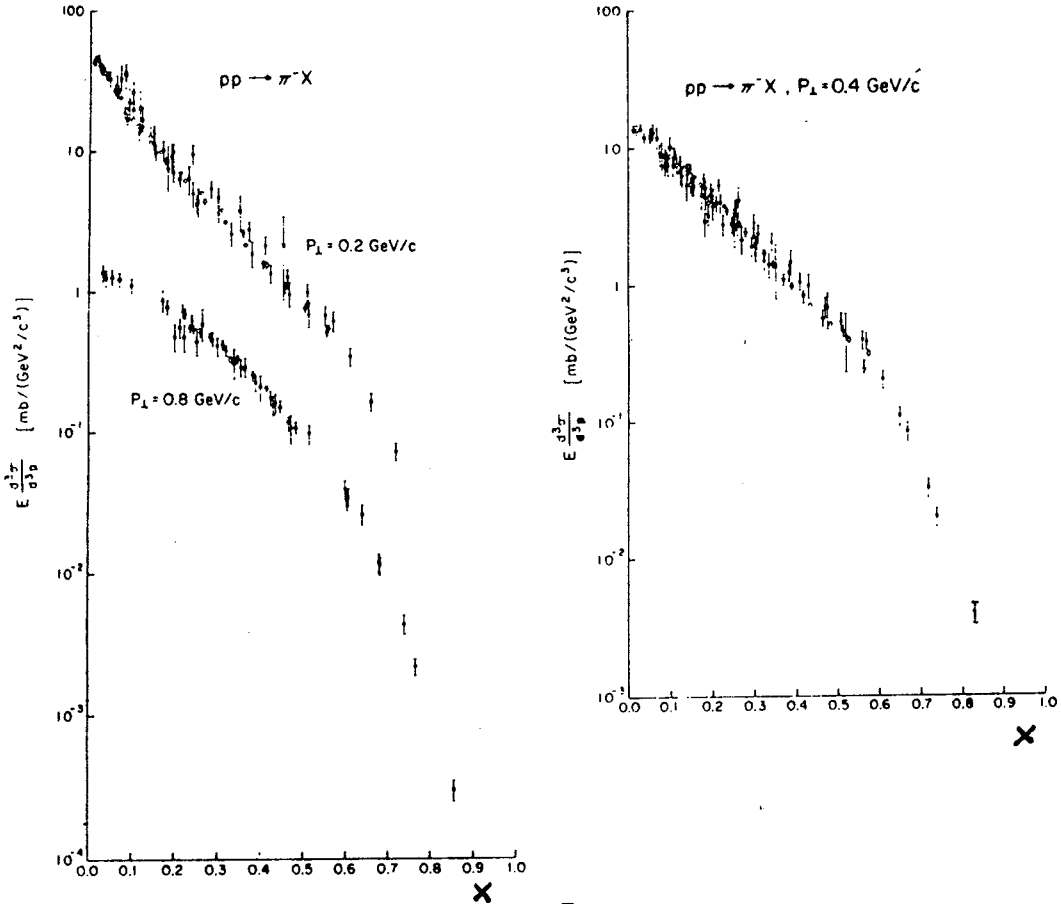

Figure 4-3-b) : Scaling of the inclusive π^- distributions at ISR energies. Data from the CERN-Bologna Collaboration. The inclusive distribution $E\frac{d\sigma}{d^3p}$ is an invariant quantity. $E\frac{d\sigma}{d^3p} = 2\frac{d\sigma}{dydp_t^2d\phi}$ where ϕ is the azimuthal production angle

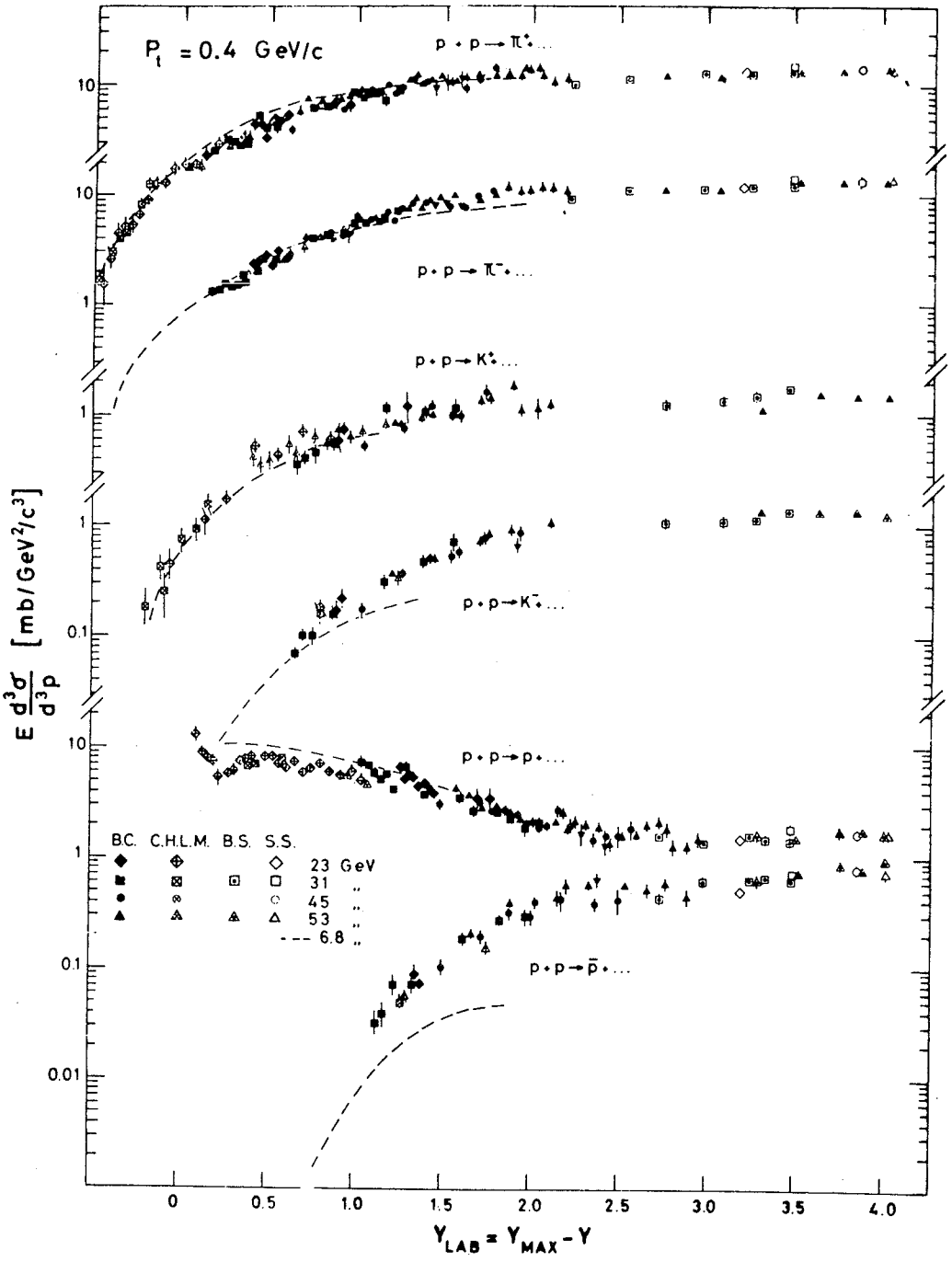

Figure 4-4 : Rapidity distributions referred to that of one of the incident protons. Evidence for the central plateau was first obtained by the British-Scandinavian Collaboration

The mean multiplicity is the integral of the inclusive distribution divided by the total cross-section. The approximate plateau of figure 4-4 corresponds therefore to the approximate logarithmic rise of $\langle n \rangle$ in figure 4-1.

Particle production thus presents a remarkable property. It is limited to low p_t values and the longitudinal phase space density (or rapidity) distribution, which then only matters, is energy independent. At rapidities close to those of the incident particles it remains fixed when taking the rapidity of the relevant incident particle as the origin. This is limiting fragmentation. In the central region, named as such taking now the rapidity of the center-of-mass as the origin, the rapidity density remains constant as the rapidity range increases.

Figure 4-5 gives a beautiful illustration of limiting fragmentation. The inclusive distribution for charged particles is the same whether a proton of 26 GeV has been hit by a proton of 26 GeV or of 15 GeV. At the same time, the distribution obtained from a proton of 15 GeV is the same whether it has been hit by a proton of 26 or 15 GeV. The proton eventually fragments independently of the way it is hit provided it is hit hard enough.

The scaling behaviour and the rapidity plateau were expected properties for a wide range of theoretical models[25]. Nevertheless, ascertaining them was extremely important. As it was also expected, the plateau further shows a lack of correlation with the nature of the incident particles. It reflects the way the vacuum reacts with hadron production to the fact that energy is available through a particle collision. Figure 4-6, which combines Fermilab and Cosmic ray data, shows how the mean multiplicity is independent of the nature of the incident particles. The particle yields simply scale according to the inelastic cross-section.

These general and simple properties of particle production are arrived at in an elegant way through the Mueller formalism which relates the inclusive cross-section in the reaction $A + B \rightarrow C + X$, where particle C is observed, to the total cross-section for $AB\bar{C}$ scattering or to an absorptive part of a three body elastic forward amplitude[26].

$$E \frac{d\sigma}{d^3p} = \frac{1}{s} \sigma_{tot}(AB\bar{C}) = \Delta \{F_{AB\bar{C}}\} \qquad (4.2)$$

A Regge approximation for the $AB\bar{C}$ elastic forward amplitude then leads to limiting fragmentation for the A(B) incident particle when one subenergy only, that for the $(A\bar{C})$ B $((B\bar{C})A)$ system is large (Pomeron exchange Approximation). It leads to a rapidity plateau when both the $A\bar{C}$ and $B\bar{C}$ subenergies are large (Double Pomeron Approximation). The yield for C is then independent of the nature of the A and B particles (factorization of the Regge Amplitude)[26].

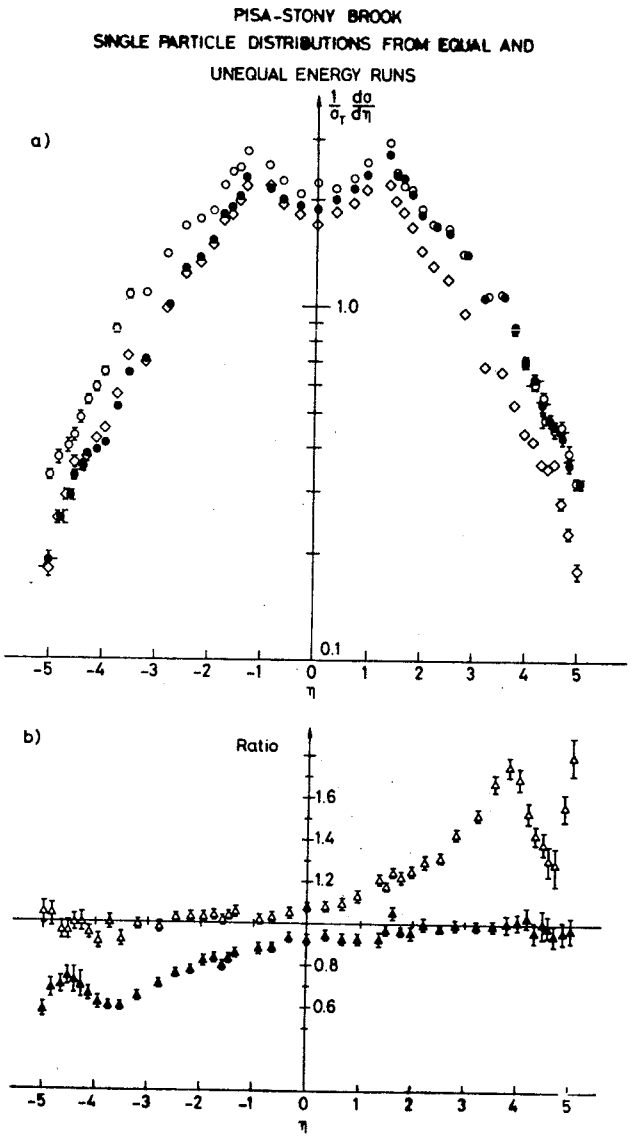

Figure 4-5 : A beautiful illustration of limiting fragmentation. Inclusive rapidity distributions for equal energies (26 - 26 GeV/c open diamonds and 15 - 15 GeV/c full dots) and for unequal energies (26 - 15 GeV/c open dots). The proton fragment, irrespective of the way it has been hit, the ratio of the yield is one. Data from the Pisa-Stony Brook Collaboration

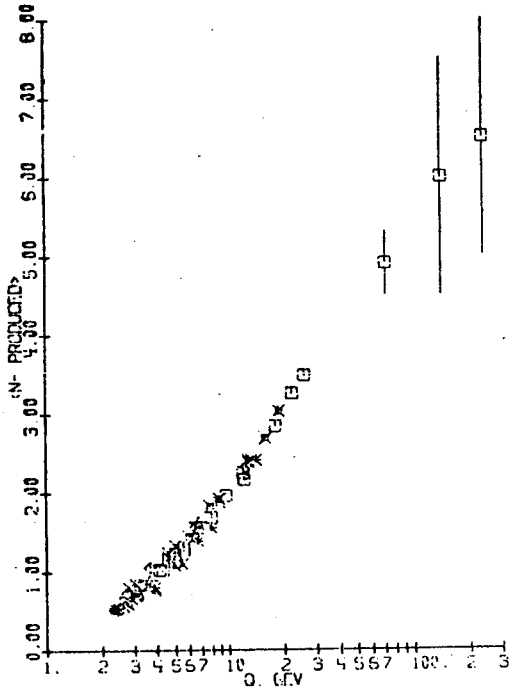

Figure 4-6 : Mean multiplicity as a function of available energy

Mean multiplicity of produced negative particles versus the available energy Q, for π^+p (×), π^-p (□), K^+p (◇), K^-p (☆), pp (□), and $\bar{p}p$ (✳). The data are from the standard set of bubble chamber experiments, except for three cosmic ray measurements at extremely high energies. The latter are from C. B. A. McCusker and L. S. Peak, Nuovo Cimento 31, 524 (1965), at 2800 GeV and from L. S. Peak and R. L. S. Woolcott, Nuovo Cimento 42, 856 (1966), at 11000 and 30000 GeV.

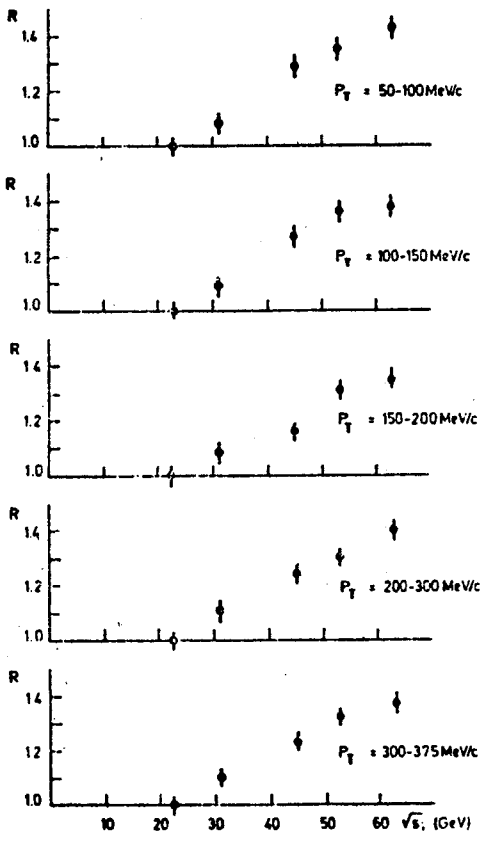

Figure 4-7 : The rise of the central rapidity distribution. It is normalized to the value at $\sqrt{s}$ = 23 GeV. Data from the British-MIT-Scandinavian Collaboration

It is very rewarding to see Regge theory working so successfully and all the particle production data already reviewed thus simply summarized. Nevertheless, Regge theory in this simple form would also lead to constant total cross-sections. If this may be a reasonable first approximation it eventually fails. The same should also apply for the inclusive distributions. This is what is indeed observed. Figure 4-7 shows the rise of the inclusive distribution at center-of-mass rapidity zero. An actual plateau would correspond to a constant value. This is the case to some approximation (figure 4-4). Deviations do occur however when the inclusive distribution is measured with precision. One may argue that this is a relatively small effect (30%) when the equivalent incident energy varies by almost an order of magnitude. It may be only a logarithmic deviation from an otherwise constant value. However, as in the case of the total cross-sections, such relatively small variations from what was the particularly simple expected (and now found) behaviour, are still not understood.

Nevertheless, the constancy of the density in longitudinal phase space, while only an approximate property, remains an impressive one. It required the ISR energy range to assess its value and its limitations.

It may now sound a disappointment that such key features of particle production could be expected from so general assumptions. Learning more about the production mechanisms requires more detailed information. In connection with this, evidence for short range order was a very important point. This leads us to the question of correlations among produced particles.

Observing a secondary particle in a particular region of phase space brings two types of information.

(i) Information about the reaction as a whole. This affects the full rapidity range. They are referred to as long range effects. For instance a fast proton ($x > 0.9$) signals a relatively small associated multiplicity clustered at opposite center-of-mass rapidity, whereas a slow proton ($x < 0.1$) favours a relatively large one clustered in the central region.

(ii) Information about secondaries to be expected in the same region of phase space. They are referred to as short range effects. Typical of such a case is resonance formation and decay since the observation of a daughter particle leads to expect the others nearby in phase space (usually within one unit of rapidity of the first observed particle).

Short and long range effects can never be fully disentangled. Nevertheless, with a global rapidity interval of 6 to 8 units one may clearly point at either of them.

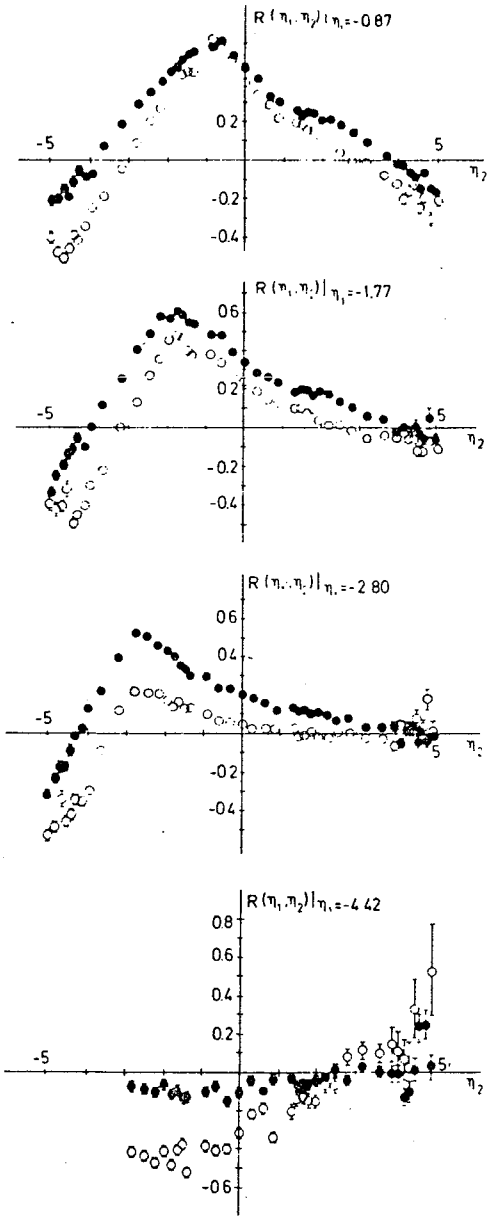

Correlation function $R(\eta_1, \eta_2)$ at values of $\eta_1 \neq 0$. Data are from PSB .; ○: at $\sqrt{s}$ = 23; ●: at $\sqrt{s}$ = 62 GeV.

Figure 4-8 : Rapidity Correlations between two charged particles. The pseudo-rapidity η is used instead of y. Data from the Pisa-Stony Brook Collaboration

Figure 4-8 shows a typical short range effect. The correlation function is defined as

$$R(y_1,y_2) = \frac{\rho_2(y_1,y_2)}{\rho(y_1)\,\rho(y_2)} - 1 \tag{4.3}$$

where

$$\rho(y) = \frac{1}{\sigma_{in}} \int \frac{E}{2} \frac{d\sigma}{d^3p}\, dp_T^2\, d\varphi \tag{4.4}$$

and

$$\rho_2(y_1,y_2) = \frac{1}{\sigma_{in}} \int \frac{E_1 E_2}{4} \frac{d^2\sigma}{d^3p_1\, d^3p_2}\, dp_{T1}^2\, dp_{T2}^2\, d\varphi_{12}\, d\varphi \tag{4.5}$$

are the single and double density distributions. With unpolarized beam the correlation function depends on 5 variables (y_1, y_2, p_{t_1}, p_{t_2} and ϕ_{12}). The latter three variables are integrated over in figure 4-8. The data show that the correlation peaks when the two rapidities are the same. The correlation does not depend appreciably on the rapidity of the particles over a relatively wide central interval $|y| < 2$ (plateau region). In this region it also does not depend appreciably on the center-of-mass energy. Observing a particle makes it more likely to observe a second one in the same region of phase space and this irrespectively of the reaction conditions, provided of course that both particles do not have an important fraction of the center-of-mass energy. This is a typical short range effect. The longitudinal phase space density shows fluctuations but they are of short range order in rapidity. These fluctuations are rather important. The value of R is of the order of 0.6, when the value of $\rho(o)$ is of the order of 2. A typical event corresponds to a rather uniform distribution in rapidity (something which can for instance be expected from a multiperipheral type production mechanism) but with local fluctuations. This is represented by figure 4-9-a). The minimum range which one can consider for fluctuations such as those shown in figure 4-8 (where integration over p_{t_1}, p_{t_2} and ϕ_{12} is performed) is that associated with a set of particle isotropically distributed in their center-of-mass system with the typical p_t distribution. This corresponds to some Gaussian rapidity distribution with a width of the order of two units. This is what defines a cluster of particles. The correlations appearing on figure 4-8 can thus be associated with the formation and fragmentation of clusters. The observation of a particle signals a cluster and one therefore expects other fragments in the same region of phase space. One has however little information about other clusters. A resonance is clearly a cluster. A cluster may however cover a large variety of hadronic effects.

Short range effects, while obvious in figure 4-8, are however not separated from others. While the rapidity configuration of figure 4-9-a) corresponds to the larger fraction of the inelastic collision, there is an important probability (0.25 say) to find very different configurations where a large rapidity gap appears. The configuration of figure 4-9-b) corresponds to a

"show case" diffractive reaction whereby a proton is quasi-elastically scattered, while other secondaries cluster on the other side. The simultaneous occurrence of mutually exclusive configurations of different types (figure 4-9-a) and 4-9-b)) leads to long range effects. The observation of a slow secondary excludes a reaction mode of the show case diffractive type. This therefore enhances the probability of finding a second slow secondary since the inclusive yield combines non-diffractive processes which give some secondary particles and diffractive processes which hardly give any. The actual short range effects in figure 4-8 correspond therefore to a peak over a wide maximum which is associated in part with this long range effect.

If one assumes for the sake of the argument that the reaction is either of the non-diffractive type (figure 4-9-a)) or of the diffractive type with no central contribution (figure 4-9-b)), one easily derives that the correlation function (4-3) should be written as

$$R(y_1,y_2) = \frac{r(y_1,y_2)}{\beta} + \frac{1-\beta}{\beta} \tag{4.6}$$

where $r(y_1, y_2)$ would be the short range correlation effect left over after the elimination of the long range effect, and β the probability not to find a configuration such as that of figure 4-9-b) ($\beta \sim 0.7 - 0.8$ say).

One can then calculate r in terms of a cluster multiplicity K. With a Gaussian parameterization, one finds

$$r(y_1,y_2) = r(\Delta y) = \frac{\langle K(K-1)\rangle}{\langle K\rangle} \frac{1}{2\sqrt{\pi}\delta\rho} e^{-\frac{\Delta y^2}{4\delta^2}} \tag{4.7}$$

One can then reproduce very well present correlation data with $\delta \sim 0.75$, $\rho \sim 2$ and $\langle K\rangle \sim 2$ to 2.5 (for charged particles).

From the obtained value for $\langle K\rangle$, which corresponds to 3 to 4 particles per cluster, one is lead to expect standard resonances to play a very sizeable role in clustering effect. Yet no single resonance (the ρ for instance) appears to have any dominant effect. More data with neutral detection are needed.

The cluster model is devised in such a way as to reproduce the correlation pattern of figures 2-5 and 9-8. In the central region hadronic clusters are produced with but very loose correlation among themselves. Their fragmentation eventually gives the observed short range correlation effects. Increasing the energy increases the rapidity range and the number of clusters. It does not modify however the properties of the clusters. The correlations do not change. The early results from the ISR which provided evidence for this have since been supported by more detailed results from the Fermilab track chamber programme. A rapidity plateau with strong clustering effects is the key and new feature for particle production at high energy.

Figure 4-10-a) shows the improvement allowed by track chamber measurements over the angular distribution measurements of figure 2-5. Figure 4-10-b) shows that short range correlation effects also affect same charge configuration, though they are weaker than in the general charge-charge case. A larger part of the measured value is then due to the long range effects (4.6). Figure 4-10-c) shows that while the key feature corresponds to short range effects, the ridge is distorted. Starting with protons creates a dissymmetry between π^+ and π^- (a long range effect) which has not yet disappeared in the central region at 400 GeV. The dissymmetry is much more pronounced among rapid particles which are readily associated with the fragmentation of the incoming protons. This latter asymmetry should not disappear with increasing energy as opposed to the former one.

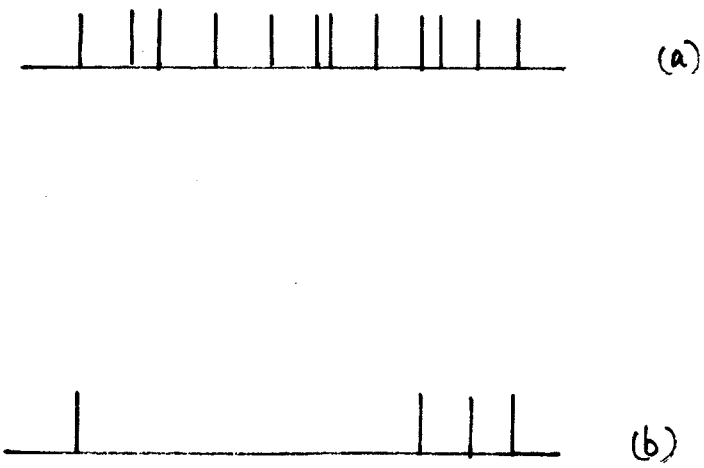

Figure 4-9 :

(a) Typical rapidity distribution. The secondary particle fills almost uniformly the rapidity range.

(b) Diffractive rapidity distribution. A large gap occurs between a quasi-elastically scattered particle and a cluster (hadronic Nova)

(a) (b)

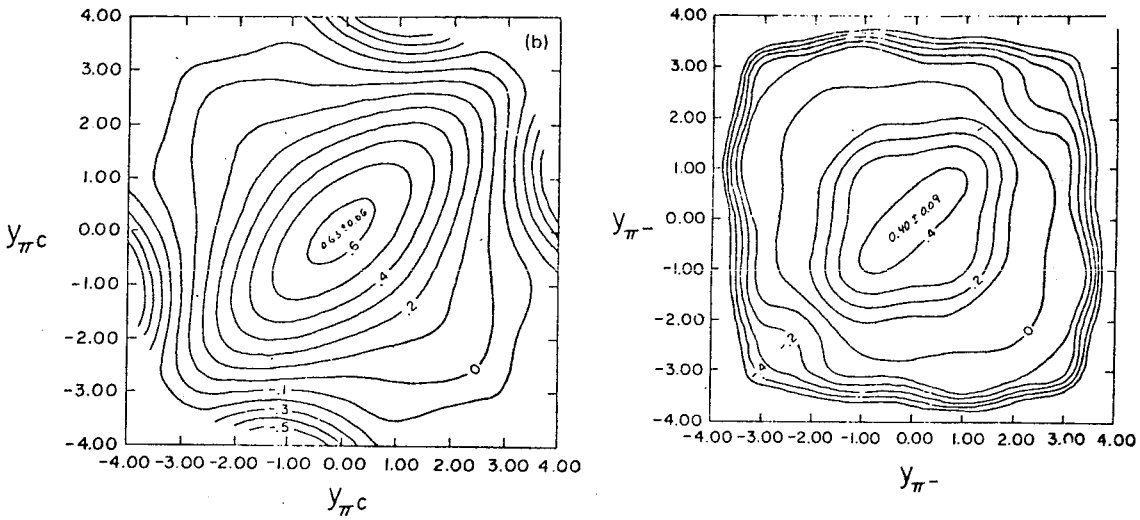

(c)

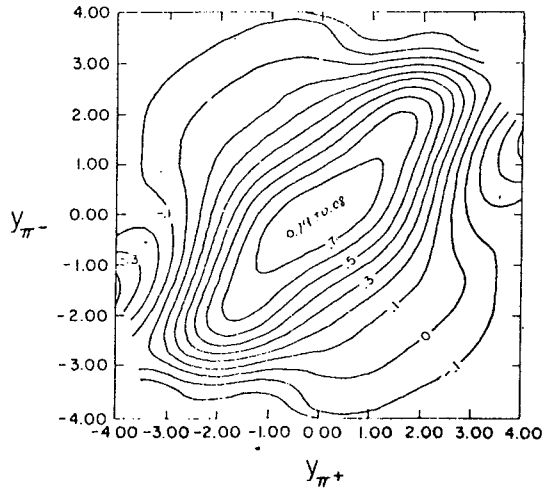

Figure 4-10 :

(a) Rapidity correlations among charged pions at 400 GeV. This is a more refined look (rapidity instead of pseudorapidity and charged pions instead of charged particles) at correlations which improve over figure 2-5. The key features are nevertheless the same.

(b) Correlation among particles with the same sign. Some short range effect remains.

(c) Correlation among π^+ and π^-.

At present the cluster picture of particle production is simple and efficient. Establishing such properties did require large energies. At PS/AGS energies, the available rapidity range is only of 4 units. With two units associated with any cluster it is then impossible to see anything but the fragmentation of the target and of the projectile. At the ISR, with 8 units available, one can clearly see the effect of cluster-type correlations in a central region which can exclude the obvious fragmentation zones of the two protons. This is how short range order could be discovered and the cluster parametrization then derived. The cluster charge multiplicity $\langle K \rangle = 2 - 2.5$ and the cluster size $\Delta y \approx 2$ are however such that no clear clustering effect can be seen on a typical event (figure 4-9-a)). This is somewhat frustrating. One does not see actual clusters in the phase space distribution of the secondary particles. Yet, further tests of the cluster pictures exist. They are of different kinds. On the one hand one may analyze correlations in configurations with different multiplicities. In a model of independent cluster production observing a larger multiplicity implies more clusters of the same kind rather than clusters of larger multiplicities. Figure 4-11 shows how such correlations could be measured. The results matched the predictions. The cluster model went well through a serious test. On the other hand, one may extend the cluster model to production of heavy particles, testing for correlations among baryon (antibaryon) or strange particles. To the extent that the expected cluster mean mass is $M \sim 1.5 - 2$ GeV, this would test in a very important way the tail of the distribution, were the cluster model to apply. More data of the kind now available (charged-charged correlations) would not allow to go much further. Correlation data involving heavy particles are very much needed. Indeed a striking feature of high energy collisions is the sharp rise of the cross-sections for baryon-antibaryon excitation and strange particle production (figure 4-1). One does not yet know however what the corresponding mechanisms are. This is the most important present problem with particle production. At the same time detection of neutrals would help ascertaining the role of standard resonances (ω, η ...) in clustering effects.

In both cases experimentation at the ISR is difficult since it requires particle identification over a wide solid angle. Furthermore, the fact that the reaction occurs in a vacuum chamber with finite thickness walls produces effects which introduce complications. This is still a very interesting domain in particle physics but experimentation with a track chamber (with down stream identifiers) has certainly an edge. Further exploration is therefore more for the Fermilab 30" or the CERN - EHS rather than for the ISR, despite the excess of available energy.

Table 4-1 lists the ISR experiments the results of which have been discussed in this section.

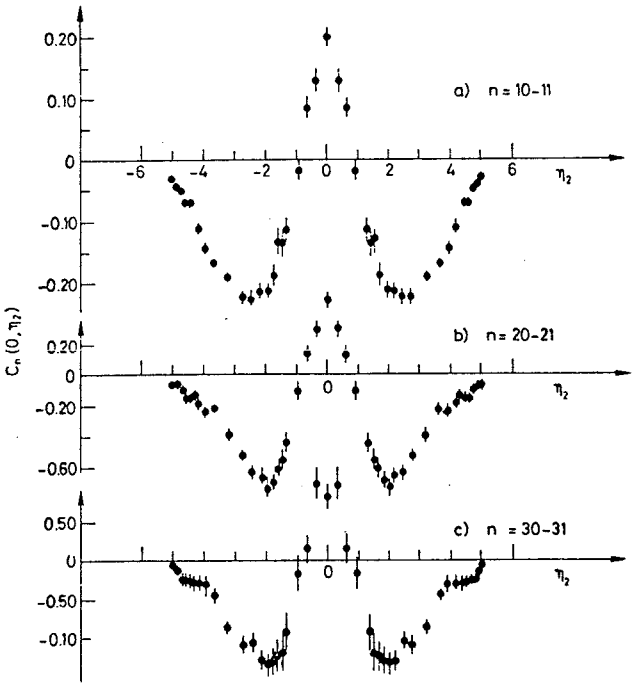

Figure 4-11 : Fixed multiplicity correlations at $\sqrt{s}$ = 63 GeV. Shown is the correlation function $C_n(o,\eta) = \rho_2^{(n)}(o,\eta) - \rho^{(n)}(o)\,\rho^{(n)}(\eta)$ with $\int C_n(y_1, y_2)\, dy_1\, dy_2 = -n$. The observed correlations agree well with what is expected from the cluster model with $\langle K(K-1)\rangle \sim 1.2\,\langle K\rangle$. One can separate two terms in C_n, writing $C_n(y_1, y_2) = \frac{\langle K(K-1)\rangle}{\langle K\rangle_n} n\,\rho_n\, e^{-\frac{\Delta y^2}{4\delta n^2}} - (1 - \frac{\langle K(K-1)\rangle_n}{\langle K\rangle_n})\,\rho_n{}^2$ The first one, which corresponds to short range correlations only varies as $\frac{n}{\ell n\ s}$. The subscripts n correspond to the bias introduced by the choice of n. It depends on the K distribution. It is only a rather small effect in practice provided $\langle n\rangle/2 < n < 1.5\,\langle n\rangle$ say.

Emphasis has been put on rapidity correlations since, for obvious reasons, they have been the object of the first extensive experimental analysis. Correlations involving also the transverse momenta or at least their relative orientations are also very interesting, but more difficult to get with good statistics. Figure 4-12 puts together examples of such data (rapidity and azymuthal) at the ISR and at Fermilab. The pattern is interesting with strong $\phi_{12} = 180^o$ (transverse momentum conservation within clusters?) and $\phi_{12} = 0^o$ (bose statistics?) effects. More detailed data with full p_t correlations are needed.

The key feature seen in figure 4-12 is again the impressive stability of the phase space configuration as the center-of-mass energy increases over a very large domain. The patterns hardly change. This is a very important feature in particle physics. This is a beautiful success of research at the ISR in 1973-1974.

(a)

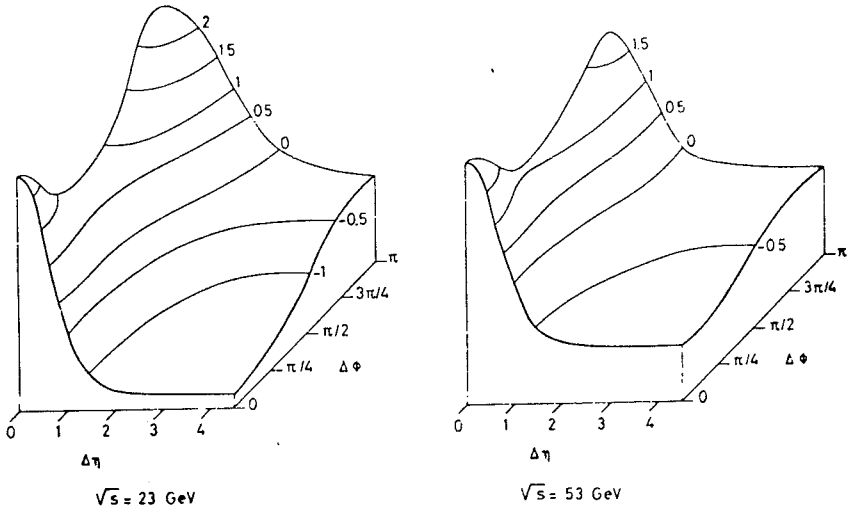

(b)

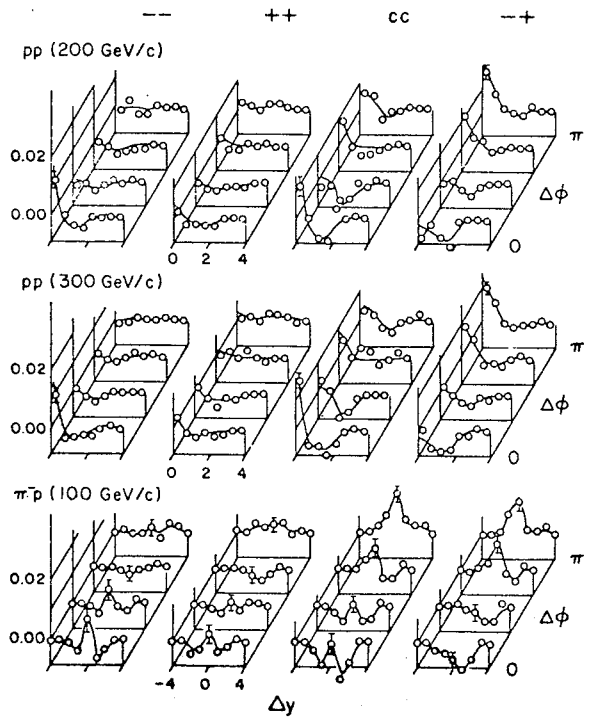

Figure 4-12-a) : Correlations in η and ϕ among charged particles (ISR). Data from the Aachen-CERN-Munich Collaboration

4-12-b) : Correlation in y and ϕ at Fermilab (30" data)

This completes the review of the particle production properties itemized in section 2.

Table 4-1

ISR experiments with important results on particle production.

(i) Inclusive distributions and tests of scaling in the fragmentation region

201 CERN-Holland-Lancaster-Manchester (small angle)

202 Argonne-Bologna-Michigan (medium angle)

603 Aachen-CERN-UCLA-Harvard (inclusive production of Δ)

802 CERN-Rome

405 CERN-Karlsruhe

(ii) The central rapidity plateau

101 CERN-Cracow-Bucharest-Tata (Emulsion)

203 British-Scandinavian (first evidence for the rapidity plateau)

803 British-Scandinavian-MIT

(iii) Correlations and short range order

801 Pisa-Stony Brook

404 CERN-Hamburg-Vienna

701 Aachen-CERN-Munich (Streamer Chamber)

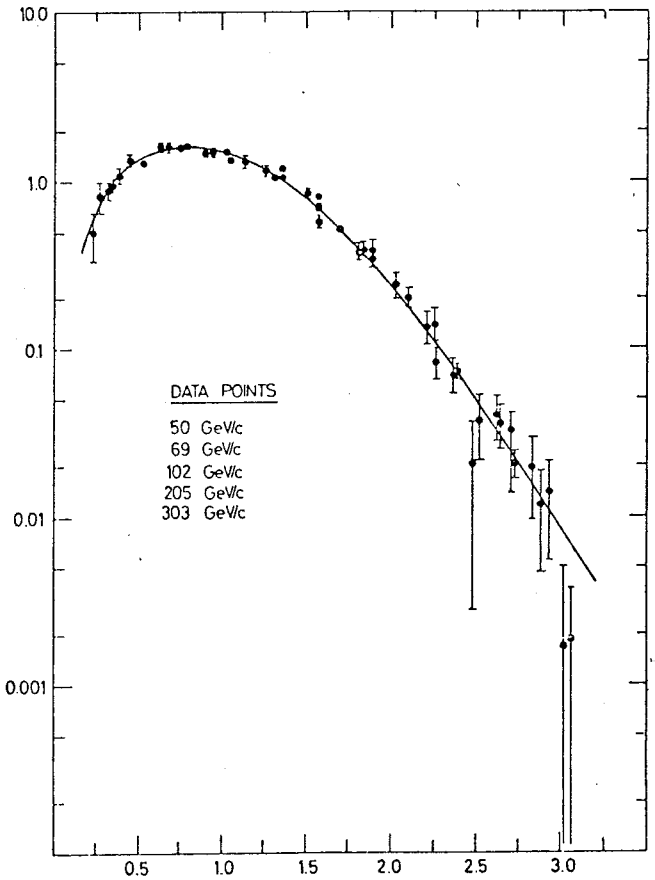

Figure 4-13-a) : $\langle n \rangle \sigma n/\sigma$ as a function of $n/\langle n \rangle$. Koba-Nielsen-Olesen relation. Fermilab track chamber data

For the sake of completeness one should mention some striking properties of multiplicity distribution at high energy. They came as very interesting early results before detailed rapidity correlation data were available[27]. As integrals only over such correlation they are now of a lesser interest. They remain nevertheless quite remarkable. Figure 4-13-a) shows how topological cross-sections obey a simple scaling behaviour (Koba-Nielsen-Olesen relation) and figure 4-13-b) shows the relation between the dispersion parameter $D = \sqrt{\langle n^2 \rangle - \langle n \rangle^2}$ and $\langle n \rangle$, proposed long ago by Wroblewski. The latter one is now well verified by recent ISR data.

Such relations correspond to a simple (but still partially empirical) relation among moments

$$\langle n^q \rangle = C_q \langle n \rangle^q \tag{4.7}$$

where C_q is energy independent. The observed behaviours correspond to the existence of mutually exclusive mechanisms (figure 4-9) and to the fact that any rate of change is eventually related to the available rapidity range and appears therefore as a logarithmic effect only.

There is finally a topic about which very little is known and which deserves further studies. It is related to the question of correlations among heavy particles which was previously mentioned. We conclude this section with a few words about it. Observing a proton at wide angle makes it more likely to observe another one than when the reaction is selected by a pion at wide angle (typical non-diffractive process). A double arm spectrometer study at 90° (CERN-Columbia-Rockefeller-Saclay) indicates a gain by a factor of the order of 2. Yet, the slow proton does not only signal a particularly large multiplicity reaction which should obviously result in more frequently produced $p\bar{p}$ pairs. Indeed there are twice as many protons than anti-protons seen in association with a slow proton. One has therefore to conclude that there are configurations in which the two incident protons stop. There is also direct evidence from a correlation experiment (CERN-Holland-Lancaster-Manchester) that as the energy of a final proton decreases ($x < 0.1$), the associated multiplicity at wide angle sharply increases. There could therefore be a new class of reactions with slow protons in the final state and a relatively large multiplicity. Track chamber data at PS energy have reported such correlations (Scandinavian Collaboration). They also appear to be present at ISR energy where bringing the two protons to rest requires a far more violent interaction. There is however little evidence still[28].

Studying such processes is obviously very interesting. It may however be easier to achieve something with a track chamber and a downstream analyzer (EHS) at the SPS, than at the ISR, where particle identification with large multiplicity is difficult. Yet the upgraded SFM, with its time of flight device, could justify an attempt in that direction.

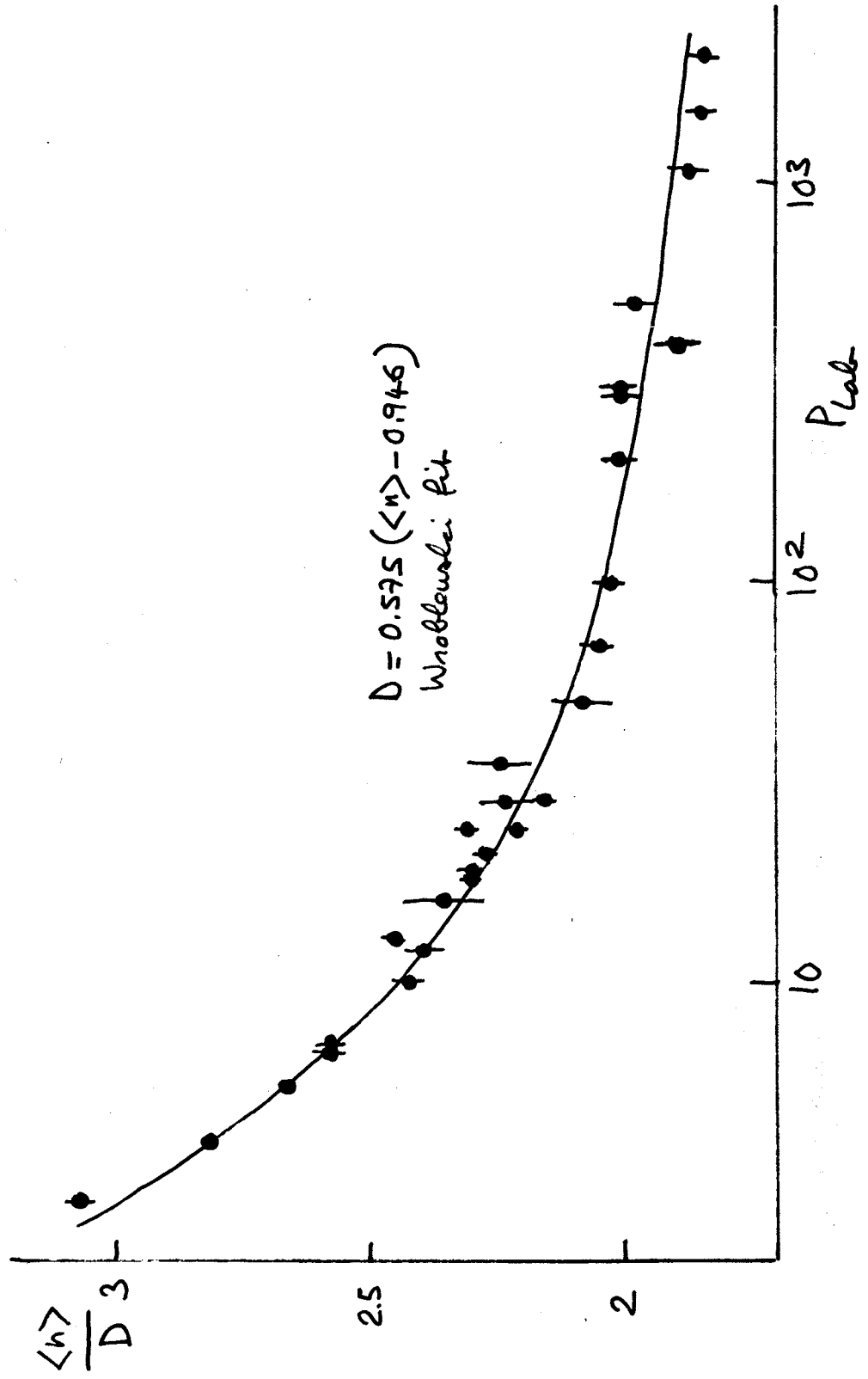

Figure 4-13-b) : The Wroblewski relation between D and ⟨n⟩. ISR data from the Aachen-CERN-Munich Collaboration Streamer Chamber

5. Diffractive Excitation

The fact that high energy elastic diffractive scattering is associated with diffractive excitation is a general consequence of hadron structure[29]. While a proton may suffer but a relatively very small energy loss ($X > 0.98$ say) its internal degree of freedom may be excited. The final state then consists of a hadronic system with the same internal quantum numbers. The differential cross-section is sharply peaked in the forward direction and hardly changes with energy, as for elastic scattering. In most cases one particle only is excited while the other one is only quasielastically scattered. This is referred to as single diffractive excitation with a cross-section (excitation of either of the particles) σ_D. Such a process is important. One finds that $\sigma_D \approx \sigma_{el}$. The corresponding rapidity configuration is rather special. It is shown in figure 4-9-b).

Elastic scattering and diffractive excitation have a common description in terms of Pomeron exchange. Each vertex can be either excited or not excited. The Pomeron can be exchanged once or several times. Figure 5-1 shows the different amplitudes together with the relevant rapidity distribution. Pomeron dominance implies a rapidity gap of about 3 units. The ISR energy range is therefore still marginal for the observation of Double Pomeron exchange! There is now rather good evidence for it[29]. With the use of factorization one may expect cross-sections in the ratio of 1 to 0.25 to 0.0025 for the three types of processes of figure 5-1 at ISR energy[30]. This meets present experimental values which are however known with rather large uncertainties only.

Diffractive excitation was already well known at PS/AGS energies. It was however then limited to the excitation of relatively low mass hadronic states ($M < 2$ GeV). Such low mass diffractive reactions, the cross-sections for which hardly change with energy, could be studied at the ISR. The rapidity gap is then large enough that other exchange mechanisms completely disappear and that evidence for double diffractive excitation (with expected factorization property) can be obtained. Figure 5-2 gives the differential cross-section obtained for the reaction $pp \rightarrow pn\pi^+$. The dip at low $|t|$ ($|t| \sim 0.2$ (GeV/c)^2) observed for low mass excitation is responsible for the anomalously large slope. It corresponds to a peripheral production process. The production reaction is almost limited to a ring in impact parameter. This is an expected feature in an optical model approach. On the other hand, figure 5-3 shows the mass distribution observed at one vertex whether one requires at the other a quasielastically scattered proton (figure 5-1-a)) or an N*(1688) (figure 5-1-b)). The two distributions are compatible. This is an expected effect in a Pomeron exchange approach.

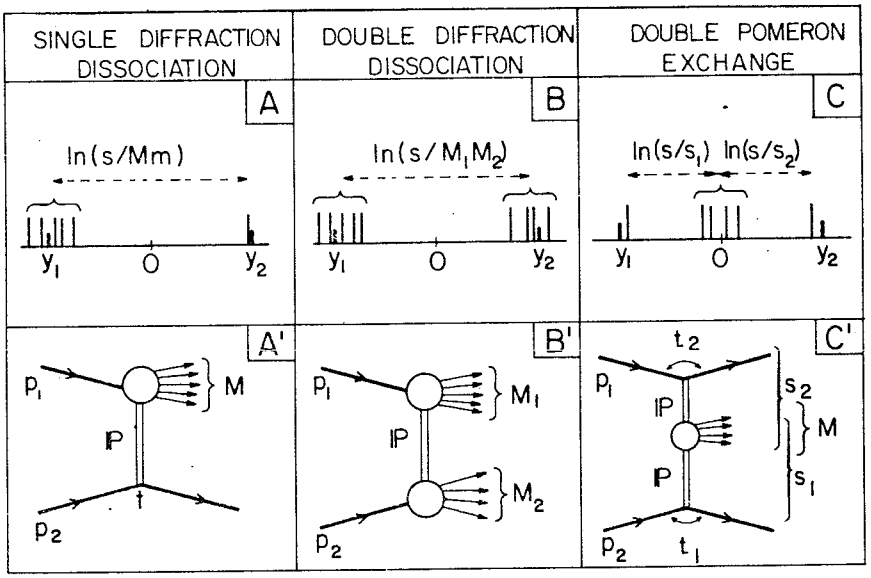

Figure 5-1-A), B) and C) show typical configurations in rapidity of single diffraction dissociation, double diffraction dissociation and double Pomeron exchange. The corresponding Pomeron exchange graphs are shown in A'), B') and C') respectively.

The key qualitative advance in diffractive excitation studies are however summarized in figure 5-4. It corresponds to diffractive excitation of high mass object (M $\sim$ 10 GeV) for which the ISR had the pioneering role.

Considering inclusive proton scattering which, as X approaches 1, should eventually correspond to single diffractive excitation, one writes

$$E\frac{d\sigma}{d^3p} = \frac{x}{\pi}\frac{d\sigma}{dx\,dp_T^2} = \frac{s}{\pi}\frac{d\sigma}{dM^2\,dt} \qquad (5.1)$$

with

$$M^2 = s(1-x) \qquad t = -\frac{p_T^2}{x} \qquad (5.2)$$

All relations are written in the high energy limit ($s \gg m^2$). One denotes by M^2 and t the excited mass and the momentum transfer squared (figure 5-5). Analyzing the amplitude of figure 5-5 in terms of Pomeron exchange, one readily obtains

$$E\frac{d\sigma}{d^3p} = \sum_i G_i(t)\left(\frac{s}{M^2}\right)^{2\alpha(t)-\bar{\alpha}_i(0)} s^{\bar{\alpha}_i(0)-1} \qquad (5.3)$$

where $\alpha(t)$ is the Pomeron trajectory ($\alpha(0) = 1$) and $\bar{\alpha}_i$ are the trajectories used at describing the M^2 dependence of the Pomeron-proton amplitude appearing at the lower vertex. The elastic forward amplitude is written as a sum of terms behaving as $(M^2)^{\bar{\alpha}_i(0)}$. The corresponding contributions in the Pomeron-proton cross-section behave as $(M^2)^{\bar{\alpha}_i(0)-1}$.

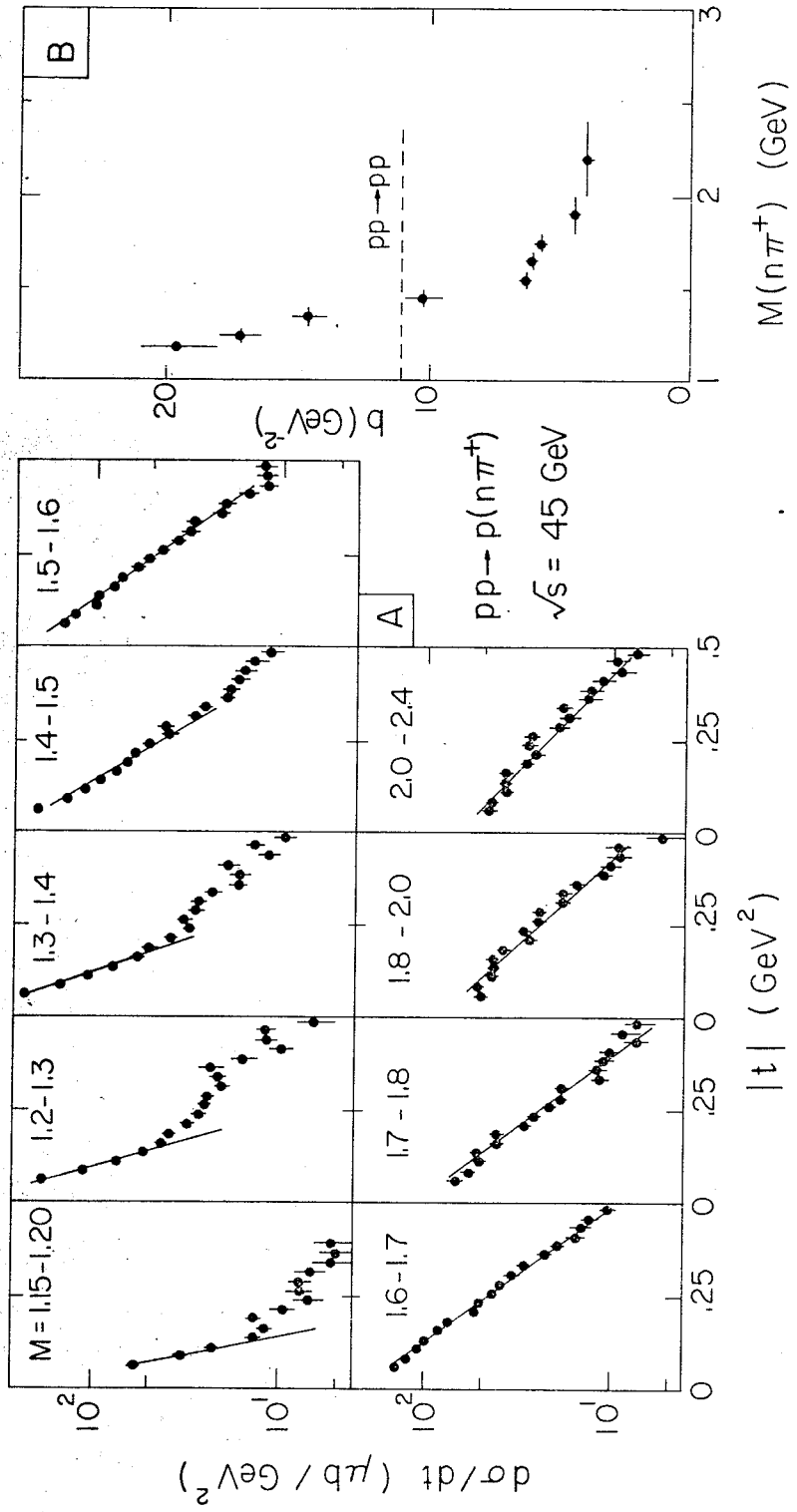

Figure 5-2 : (A) Momentum transfer distributions for the reaction $pp \rightarrow p(n\pi^+)$ at $\sqrt{s}$ = 45 GeV in different intervals of the $n\pi^+$ effective mass M.
(b) Dependence of the forward slope be on the $n\pi^+$ mass.
Data from the CERN-Hamburg-Orsay-Vienna Collaboration

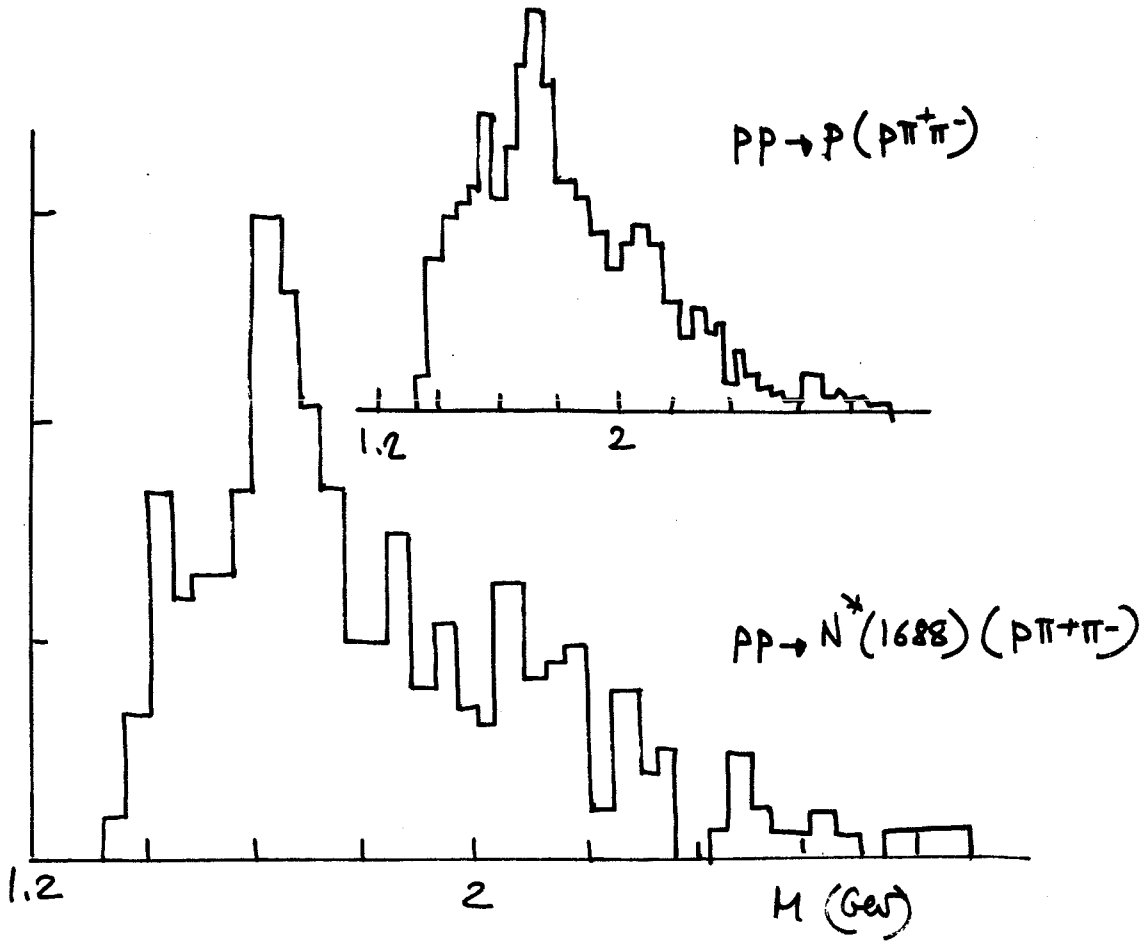

Figure 5-3 : Mass distribution for a diffractively excited pπ+π- system in single and double diffractive excitation $\sqrt{s}$ = 23 GeV. Data from the Princeton-Pavia Collaboration

Relation (5.3) corresponds to a triple Reggeon approximation[31]. The quantity (s/M^2) depends only on X(5.2). If $\bar{\alpha}(o) = 1$, or if the Pomeron-proton total cross-section has a constant value when the Pomeron-proton center-of-mass energy M varies, the inclusive distribution (5.3) is energy independent. The relevance of diffraction excitation $\alpha(t) \approx 1$ then implies a $(1-x)^{-1}$ fall off after a sharp rise associated with threshold behaviour. The higher the energy the sharper the rise. An energy independent inclusive distribution implies in turn an excitation mass distribution at fixed t behaving as $d\sigma/dM^2 \sim (M^2)^{-1}$, according to (5.1). All these features are in remarkable agreement with the data of figures 5-4-a) and 5-4-c).

Diffractive excitation extends to large mass. The excitation cross-section at large mass decreases as $(M^2)^{-1}$, thus contributing an integrated cross-section in the peak of figure 5-4 which increases as ℓn s first ignoring shrinking. It was an important discovery at the ISR to find that such an effect actually exists and that the relevant cross-section is rather large ($\sigma_D \simeq \sigma_{el}$). It is all

the more interesting that it can be easily summarized in the exchange picture of diffraction. It simply implies that the Pomeron-proton total cross-section approaches a constant as M^2 increases. The numerical value of the cross-section is actually not unambiguously defined in the framework of a Regge parameterization, but its M^2 behaviour is. In any case it is of the order of 1 mb, hence hadronic. Conversely one may say that the properties of high mass diffraction provide the best present rationale for an exchange approach (Pomeron exchange) to diffractive processes, while elastic scattering and low mass diffraction (figures 3-8 and 5-2) are certainly more easily described in terms of an optical picture.

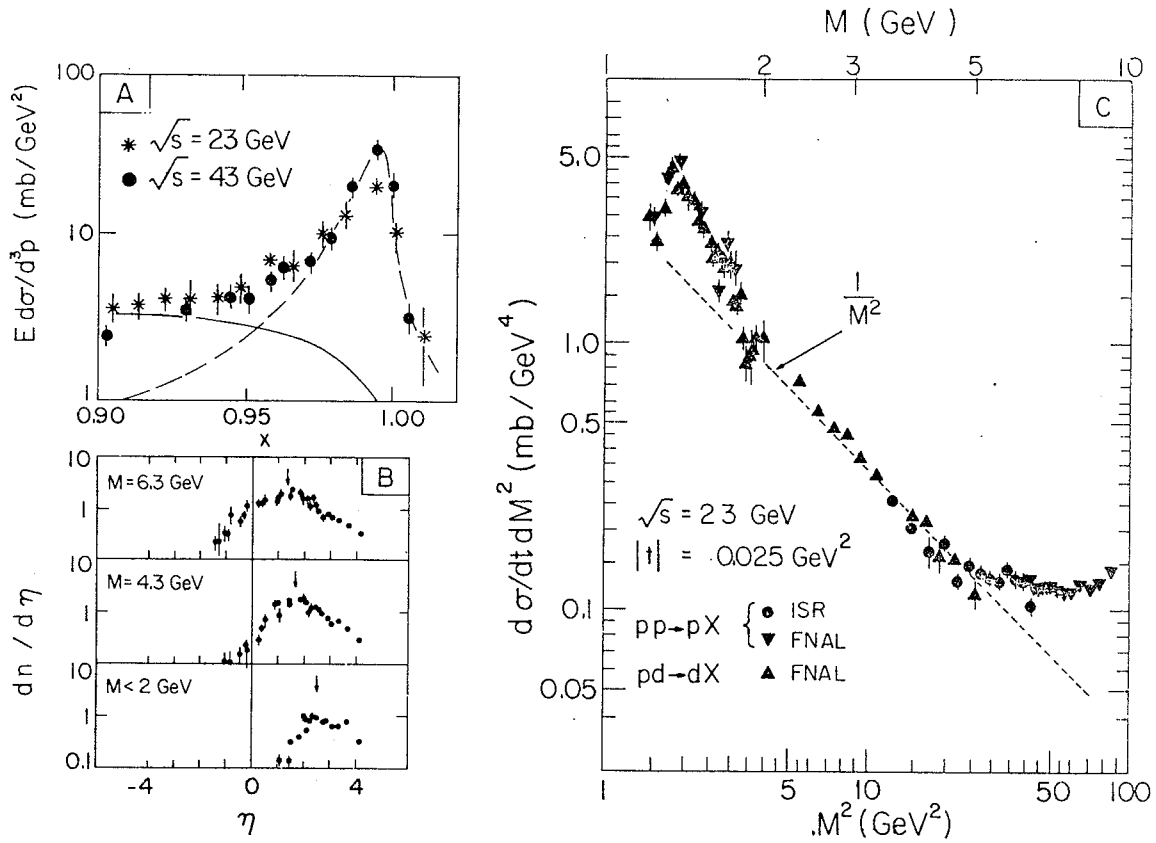

Figure 5-4 : (A) ISR data showing the x distribution of quasi-elastically scattered protons at p_t = 0.525 GeV/c
(B) "Pseudo-rapidity" distribution resulting from the fragmentation of large mass M systems diffractively produced. The arrows indicate the centre of the distribution as expected from kinematics
(C) Compilation of data on M^2 dependence at fixed s and t
Data from the CERN-Holland-Lancaster-Manchester Collaboration

Following the exchange approach, one may further analyze Pomeron-proton interaction. Correlation studies involving a quasi-elastically scattered proton and charged particles associated with the fragmentation of the excited proton show that the inclusive distribution is very similar to that found for hadron-hadron interactions. The rapidity distributions of figure 5-4-b) extend logarithmically with M. The maximum value does not change much as a plateau eventually develops. The distribution is symmetrical with respect to the center-of-mass rapidity of the hadronic cluster $Y = \ell n \frac{\sqrt{s}}{M}$. Present information is limited. Yet, at the inclusive level Pomeron-proton interactions are similar to standard hadronic ones. Nothing yet is known about leading particle effect (the fraction of the energy typically kept by a proton in Pomeron-proton scattering). Nothing yet is known about correlation effects associated with Pomeron fragmentation. This requires however particle identification and momentum analysis over a wide solid angle. Further studies are therefore more for the SPS EHS than for the ISR.

The ISR retains however an edge for a very particular type of process which has to be present in the exchange approach. It corresponds to large enough values of the diffractive excitation mass that a diffractive sub-process can be isolated. One thus obtains Double Pomeron exchange as shown in figure 5-6. The excitation mass is given by

$$M^2 = s(1-x_1)(1-x_2) \tag{5.4}$$

With the same notation one can respectively write the single diffractive cross-section (figure 5-5) and the Double Pomeron exchange cross-section (figure 5-6) as

$$x \frac{d\sigma}{dx dp_T^2} = \frac{1}{(4\pi)^2} \gamma^2(t) |\eta(t)|^2 \frac{\sigma_P(M^2,t)}{(1-x)^{2\alpha(t)-1}} \tag{5.5}$$

$$x_1 x_2 \frac{d^2\sigma}{dx_1 dp_{T_1}^2 dx_2 dp_{T_2}^2} = \frac{1}{(4\pi)^2} \gamma^2(t_1)\gamma^2(t_2)|\eta(t_1)|^2|\eta(t_2)|^2 \frac{\sigma_{PP}(M^2,t_1,t_2)}{(1-x_1)^{2\alpha(t_1)-1}(1-x_2)^{2\alpha(t_2)-1}} \tag{5.6}$$

where $\gamma(t)$ is the Pomeron-proton vertex function, $\eta(t)$ the Pomeron signature factor and σ_P and σ_{PP} the Pomeron-hadron and the Pomeron-Pomeron total cross-sections as (somewhat arbitrarily) defined by our writing of scattering amplitude factorizing out signature factors.

Relation (5.6) corresponds to phase space distributions which are quite special. Nevertheless the two rapidity gaps, the extent of which could justify Pomeron dominance, are hardly large enough to bring the background (Pomeron-Reggeon exchange or, experimentally, the large mass low multiplicity tail of single diffractive excitation) to a level low enough for an obvious kinematical separation.

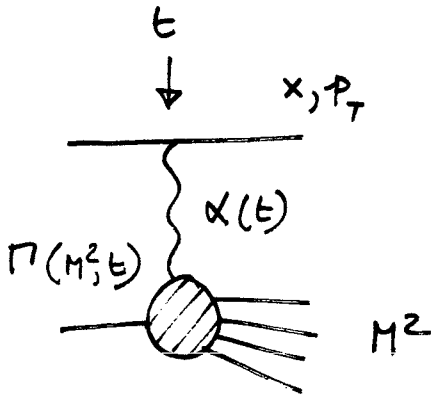

Figure 5-5 : Single Diffractive Amplitude $F = \alpha(t)\ \eta(t)\ (\frac{s}{M^2})^{\alpha(t)}\ \Gamma(t,M^2)$

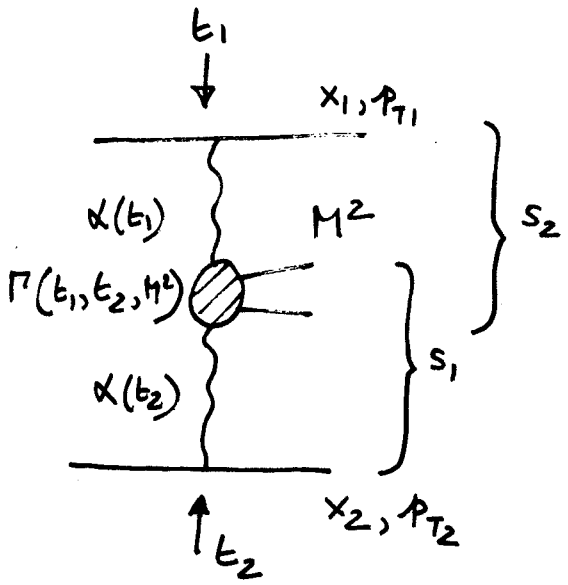

Figure 5-6 : Double Pomeron Exchange Amplitude

$$F = \alpha(t_1)\ \alpha(t_2)\ \eta(t_1)\ \eta(t_2) \left(\frac{s}{s_1}\right)^{\alpha(t_2)} \left(\frac{s}{s_2}\right)^{\alpha(t_2)}\ \Gamma(t_1,\ t_2,\ M^2)$$

Applying drastic cuts and studying dependence in the different variables it is however possible to collect evidence for a contribution with all expected properties of double Pomeron exchange[32]. Figure 5-7 shows the cross-section associated with specific cuts on the reaction $pp \rightarrow pp\ \pi^+\pi^-$. In the two cases ($|y_\pi| < 1$, X_1 and $X_2 > 0.9$) and ($|y_\pi - y_p| \geq 3$, X_1 and $X_2 > 0.9$) one expects cross-sections which are constant and rising as $\ell n\ s$ respectively. The data are compatible with such a behaviour. The cross-section values, calculated on the basis of figure 5-6 using factorization properties are also compatible with those measured[32].

This is very encouraging. Nevertheless further studies are needed. At the ISR, the Split Field Magnet provides a large solid angle detector for the slow particles. However it does not provide yet a momentum determination good enough for the two fast protons. A Double Arm Spectrometer could do that but at the expense of covering relatively small solid angles. It is also necessary then to add an efficient wide angle detector. Nevertheless, despite difficulties, this is a process which may be worth more effort at the ISR since the extra energy appears in that particular case as an important asset. One can really make use of as large a rapidity interval as possible.

It is of course important to obtain a better determination of the Double Pomeron exchange contribution to the cross-section. Next comes the study of the SU(3) properties of the Pomeron, which should have important bearing on the hadronic states obtained through Pomeron-Pomeron scattering (figure 5-6). The low mass distribution in the ε region, the f/f' ratio are important features to analyze. From duality arguments one may expect similarities with what is observed in the hadronic decay of the new particles ($\psi' \rightarrow \psi + X$ for instance). In both cases one has disconnected graphs with low transfers. Similarities and differences are still to be explored.

Table 5-1 lists experiments the results of which have been reviewed in this section.

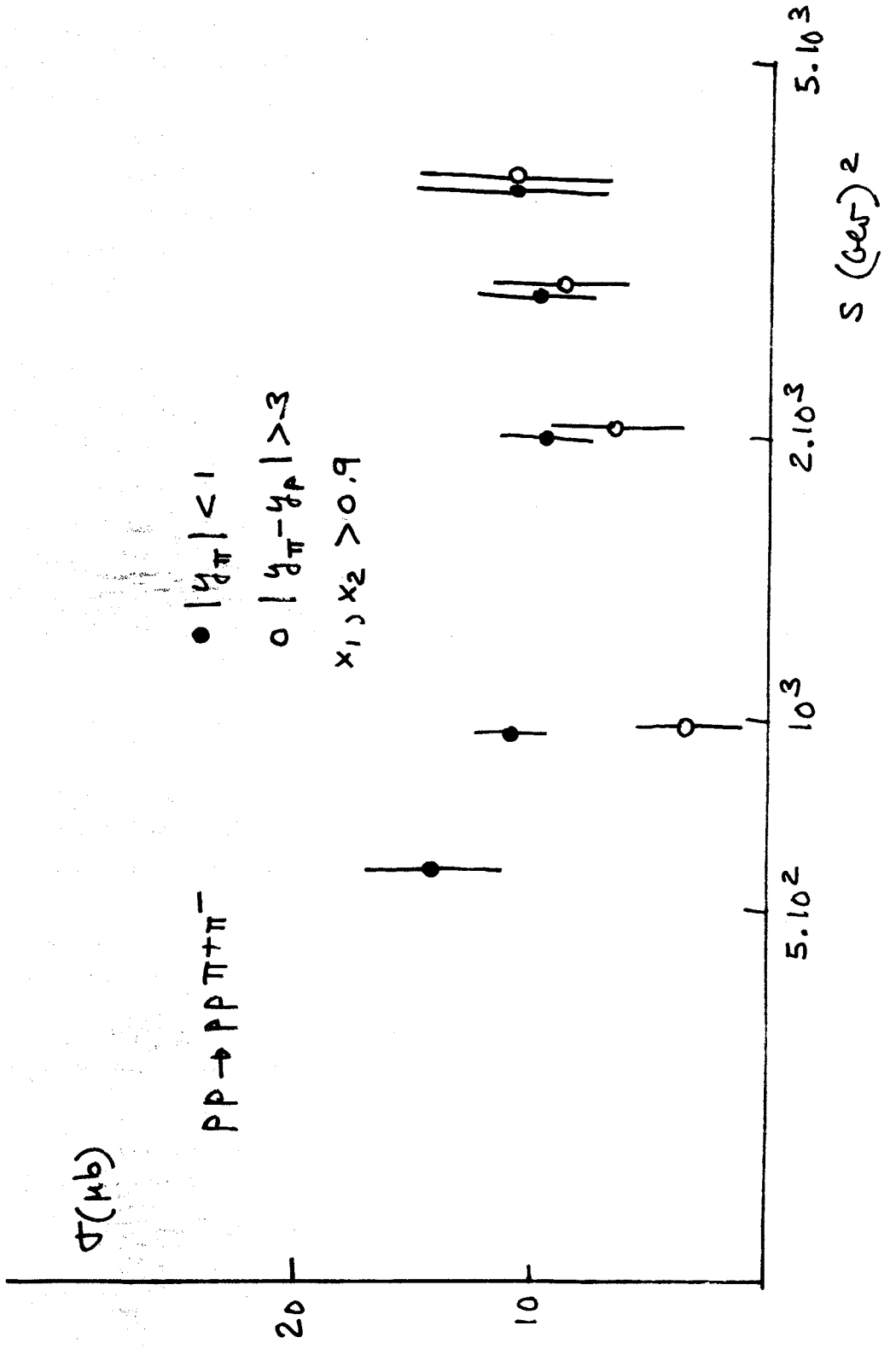

Figure 5-7 : Double Pomeron exchange contribution to the reaction pp → pp π+π−. The two pions are either both required to be in the central region or to leave a rapidity gap next to the leading protons. Data from the CERN-Collège de France-Heidelberg-Karlsruhe Collaboration

Table 5-1

ISR experiments with important contributions to the study of diffractive processes.

(i) Study of single diffractive excitation

201 CERN-Holland-Lancaster-Manchester (First evidence for large mass diffractive excitation)

206 CERN-Holland-Lancaster-Manchester

801 Pisa-Stony Brook

(ii) Diffractive excitation of exclusive system

603 Aachen-CERN-UCLA-Harvard

401 CERN-Hamburg-Orsay-Vienna

411 Pavia-Princeton (including studies with deuteron beams)

(iii) Special study of Double Pomeron exchange

604 CERN-Genoa-Harvard-Munich-Northwestern Riverside

407/408 CERN-Collège de France-Heidelberg-Karlsruhe

401 CERN-Hamburg-Orsay-Vienna

207 CERN-Holland-Manchester

6. Large Transverse Momentum Reactions

The discovery of large transverse momentum phenomena is one of the major contributions of research at the ISR[33]. Any surprise notwithstanding, it has opened up the most promising field of research there. The key feature is the production of hadronic jets at wide angle. Their studies are of great topical interest.

The overwhelming majority of secondary particles is produced with low p_t ($\langle p_t \rangle$ = 0.35 GeV/c). The initial exponential fall off, which extends up to 1 GeV/c, is however followed by a much less rapid decrease, which is amenable to an inverse power parameterization at least from 2 to 8 GeV/c. The inclusive distribution of π^o, as observed at 90°, is shown in figure 6-1. The inclusive distribution does not actually change appreciably with production angle over a rather wide range $40^o < \theta < 140^o$. It eventually falls more sharply as one approaches the forward directions in the center-of-mass system. In contradistinction with what occurs at low p_t ($p_t < 1$ GeV/c), the large p_t distributions rise

with energy. This was already emphasized in section 2 and figure 2-6 shows that the energy dependence is the more pronounced the larger p_t is. It is then convenient to choose as variables p_t, $x_t = 2p_t/\sqrt{s}$ and θ, the center-of-mass production angle. The inclusive distribution

$$E\frac{d\sigma}{d^3p} = f(p_T, x_T, \theta) \tag{6.1}$$

is practically independent of θ and compatible with a limiting behaviour as x_t approaches zero. It can be parametized as

$$E\frac{d\sigma}{d^3p} \approx \frac{1}{p_T^n} G(x_T) \tag{6.2}$$

with

$$G(0) \neq 0 \qquad n \approx 8$$

Figure 6-2 shows how such a parametization works. This is very satisfactory. The power is close to 8.

As emphasized in sections 3 and 4, the low p_t behaviour is most generally associated with a process which is coherent over the transverse dimensions of the interacting hadrons. It fits very well a thermodynamical equilibrium distribution over the interaction volume. Conversely, a structure in the p_t distribution most generally stands for a structure in the source of secondary particles. If an exponential behaviour corresponds to an extended object, an inverse power stands for a point-like origin. These simplistic Fourier transform arguments are far from compelling. Nevertheless, an anomalous large p_t behaviour in hadron interactions could be expected as a tentative generalization of what is observed in deep inelastic lepton scattering[34]. The parton model of Feynman indeed implies relations among 4 different types of processes[35]. They can be associated with impulse approximations applied to hadron constituents (partons), as shown in figure 6-3.

Figure 6-3-a) corresponds to deep inelastic lepton-hadron scattering. At large momentum transfer one can sum incoherently over the parton contributions when calculating reaction yields. This results in the Björken scaling behaviour. There is now very good evidence to identify partons and quarks[35]. Figure 6-3-b) corresponds to high energy e^+e^- annihilation into hadrons, a process already well studied at SPEAR and DORIS. One can again sum incoherently over parton (quark) pair production when calculating the hadron yield, the parameter R. Figure 6-3-c) corresponds to large mass lepton pair formation in hadronic interactions. A quark and an anti-quark annihilate into a lepton pair. We shall come back to this in section 7. Finally, figure 6-3-d) corresponds to the impulse approximation presently used at calculating yields in large p_t hadron interactions. Two constituents scatter at wide angle and one can sum incoherently over

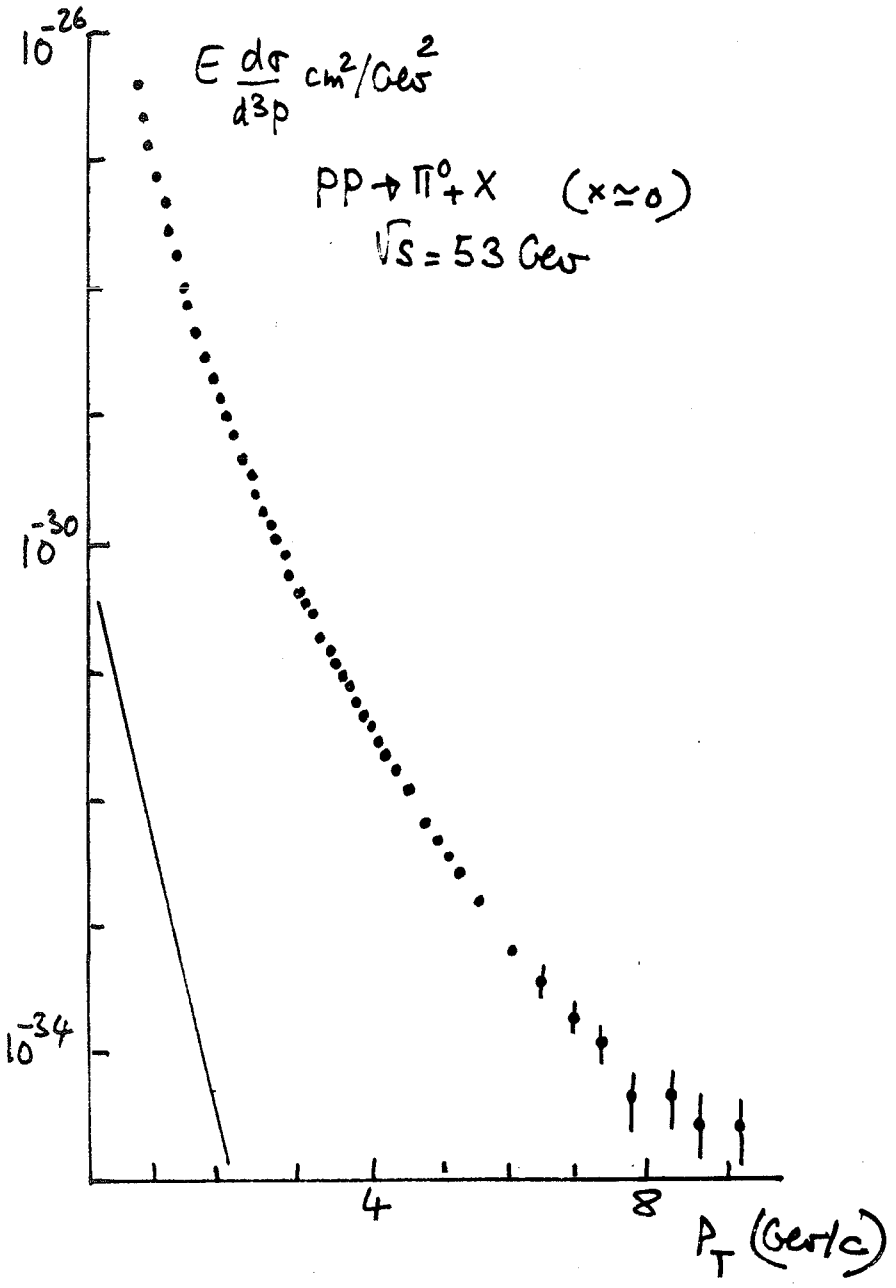

Figure 6-1 : Inclusive π^0 distribution at 90°. The solid line corresponds to the low p_t (unormalized) behaviour.
Data from the Aachen-CERN-Heidelberg-Munich Collaboration

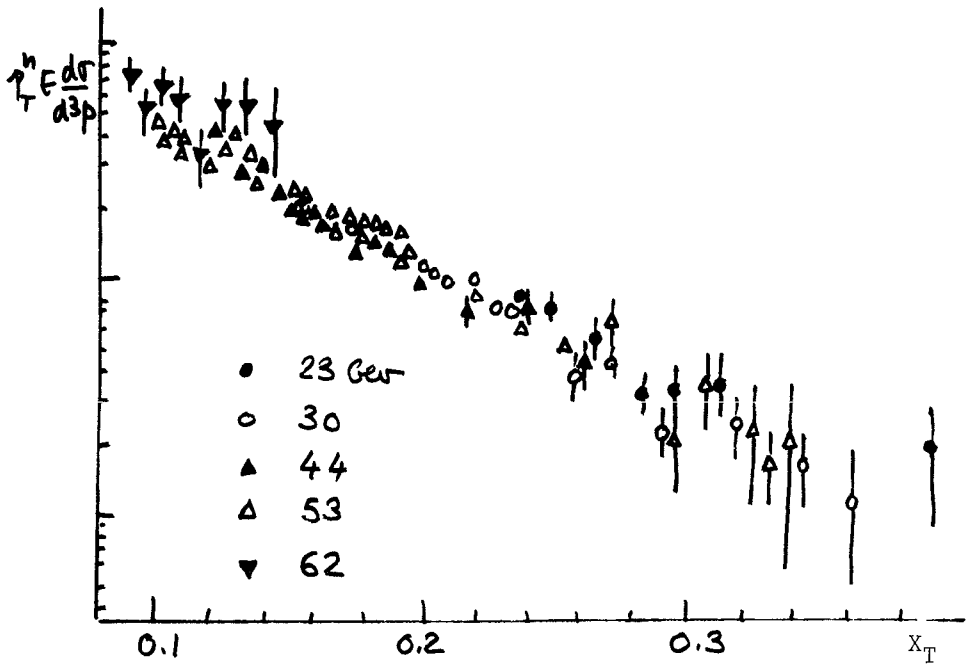

Figure 6-2 : Scaling behaviour of the large p_t yields. Data from the CERN-Columbia-Rockefeller Collaboration. Shown is $p_t^{8.26} E\frac{d\sigma}{d3p}$ as a function of x_t. The chosen value, 8.26 corresponds to a best fit

such pair contributions. While in all such calculations, one deals with constituents (identified in some cases with quarks) only hadrons are observed in the final state or present in the initial state. Quark distributions inside hadrons are now relatively well parametized from the analysis of deep inelastic lepton scattering and, in particular, of neutrino reactions. One is also led to expect that, when scattered at wide angle (in a region of phase space which is well separated from that occupied by the hadron remainder(s) to be found predominantly in the forward and backward direction), a constituent will result in a jet of hadrons.

A hadronic jet is tentatively defined according to the rule of hadron production provided by the analysis of particle production as discussed in section 4. The final state hadrons have only a small transverse momentum with respect to the constituent (mean jet) direction ($\langle q_t \rangle \simeq 0.35$ GeV/c). They take on the average a fixed fraction x of the global jet (constituent) momentum. An x^{-1} distribution at low x eventually gives a plateau behaviour in rapidity and a logarithmic jet multiplicity. At the same time, the behaviour of the distribution as x approaches 1 corresponds to a widening rapidity gap. With a Poisson distribution for the multiplicity this implies a $(1-x)^{\gamma}$ behaviour. Figure 6-4

shows that this is indeed well satisfied by the hadron jets observed at SPEAR (figure 6-3-b)) which one is tentatively led to identify with the fragmentation of a quark. The formation of hadronic jet is associated with the paramount problem of quark confinement. The phenomenological and oversimplified definition thus presented (this is a parametization for the hatched blobs in figure 6-3) is however satisfactory for the analysis of present data.

The dynamics associated with figure 6-3 is not yet on firm ground. Nevertheless several predicted types of behaviour could already be confirmed. We shall therefore organize this presentation of large p_t data with such an approach in mind.

Associating large p_t reactions to scattering among hadron constituents, one is however led to consider the most simple scaling behaviour $d\sigma/dp_t^2 \sim p_t^{-4}$, as what should a priori prevail. Such a scale independent result is for instance what one would obtain in perturbation theory (simple gluon exchange) in the subprocess of figure 6-3-d). Asymptotic freedom as expected to apply to quark interactions would predict only a logarithmic departure from such a behaviour[35]. As previously said one does find an inverse power but with $d\sigma/dp_t^2 \sim p_t^{-8}$ instead of $d\sigma/dp_t^2 \sim p_t^{-4}$. We shall come back to this question later.

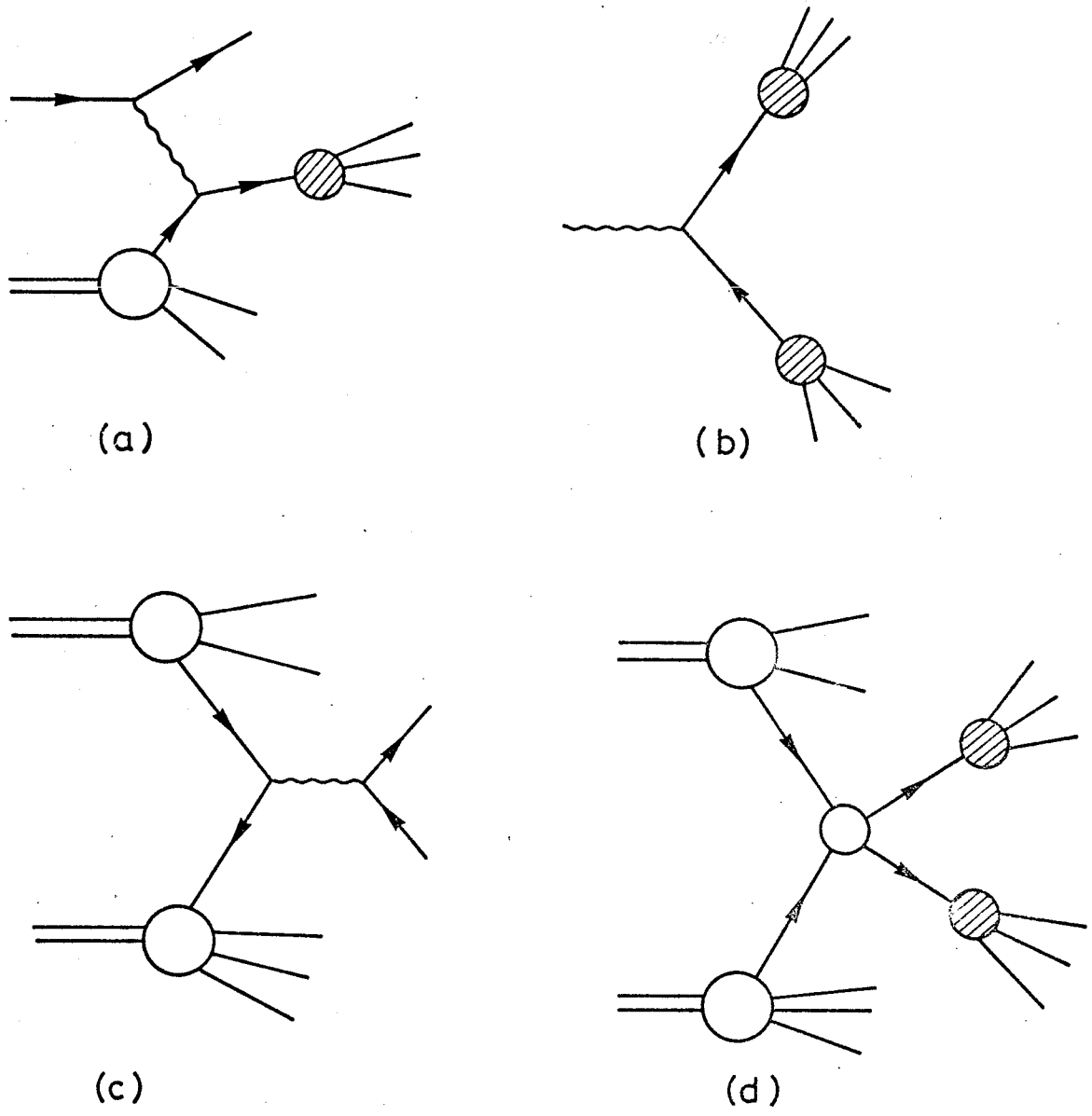

Figure 6-3 : 4 processes which are related in the parton model
(a) deep inelastic lepton scattering, (b) hadron production in e^+e^- annihilation, (c) large mass lepton pair production, (d) large p_t production

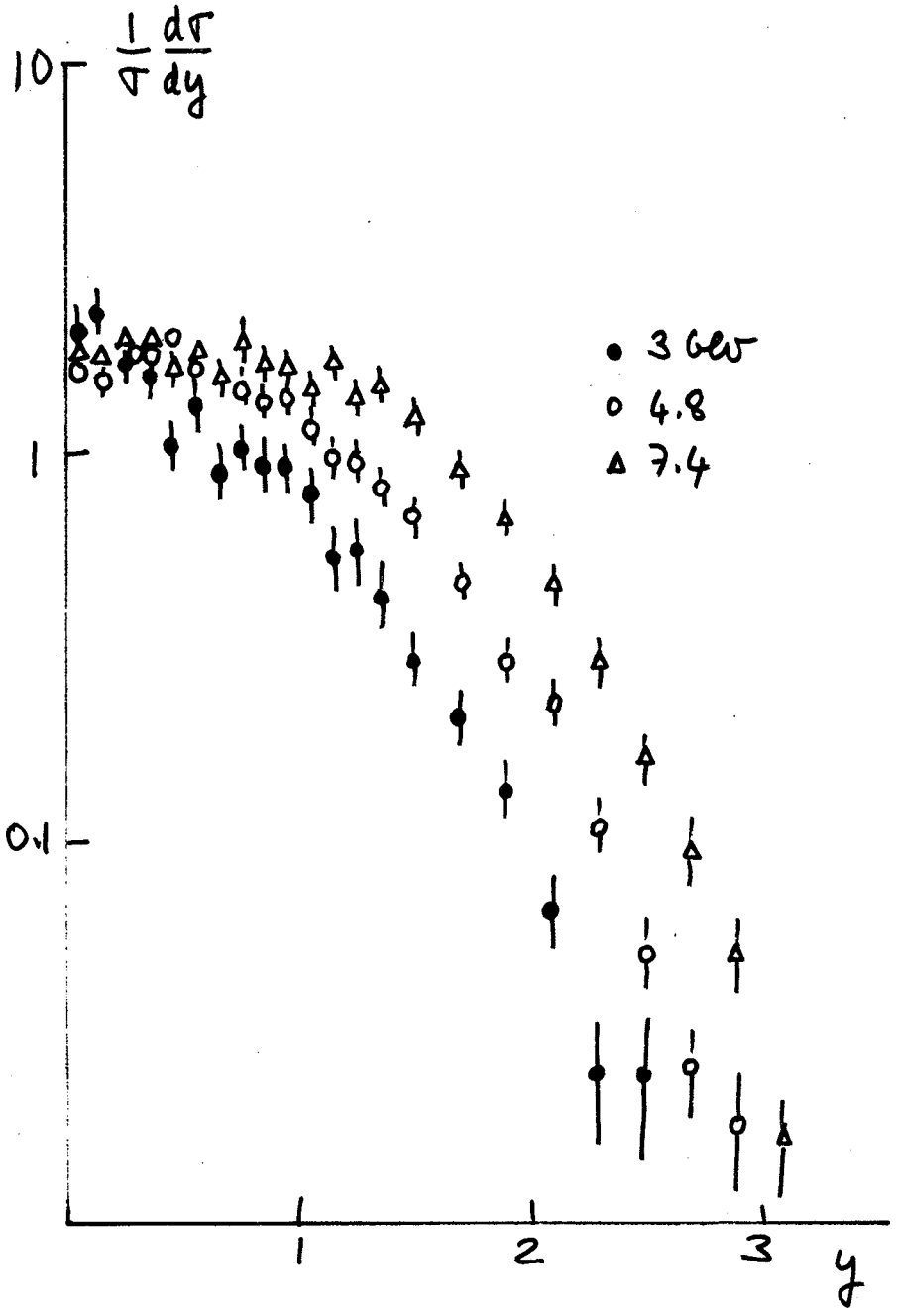

Figure 6-4 : Rapidity distributions in jet fragmentation. Results from SPEAR. Scaling in the fragmentation region (the large y curves are translated from one another) and rapidity plateau.
Key features from section 4 do appear

Large p_t production distinguishes itself by further important qualitative effects. They are summarized in table 6-1, and briefly considered in turn. The overwhelming role of the pions, a key feature at low p_t, disappear at large p_t. Figure 6-5-a) shows charged particle ratios as functions of p_t. The ratios do not vary much with energy. The K^+/π^+ and p/π^+ ratios, which are less sensitive than others to threshold effects, do not vary much with p_t beyond $p_t \simeq 1.5$ GeV/c. This is shown by figure 6-5-b). The relative importance of K^+ is not surprising to the extent that the important parameter in many particle production model calculations is $m_t = \sqrt{p_t^2 + m^2}$. At large p_t, and with SU(3) symmetric couplings, K^+ production should not be much disfavored as compared to that of π^+'s. The relative importance of the proton yield ($p/\pi^+ \sim 0.3$) is however a striking feature of large p_t production which is not well understood yet.

Altogether there is a positive excess at large p_t which is already seen among pions. The value seen on figure 6-5-a) (~ 1.2) differs from that found among low p_t particles, which is practically 1 at ISR energies. As p_t increases the positive over negative ratio increases. Figure 6-5-c) contrasts the behaviour observed in pp collisions to that observed in pn collisions where (from charge symmetry) the ratio between the positive and negative pion yields at 90^o has to be 1. This positive excess cannot be associated with the positive charges of the incident protons since the associated multiplicity in large p_t reactions is larger than that of typical reactions. It is rather associated with the fact that positive constituents are more abundant than negative ones.

Another specific effect is concerned with production off nuclei. High energy reactions in nuclei offer many interesting effects which are associated with the fact that hadron formation time becomes much longer than transit time through nuclei. There are much data already available[36] but with an emphasis on ISR data this will not be discussed here. Figure 6-6 shows the A dependence of large p_t yields. At low p_t production rates are proportional to the nuclear surface ($\alpha \sim 2/3$). At large p_t they increase faster than A. An A dependence is easily connected to a reaction among hadron constituents which are not screened as such by interactions with the outer nucleons. A faster than A dependence corresponds however to further coherent effects which are not yet understood.

Figure 6-7 shows another important effect at the inclusive level. Pions are more efficient than protons at producing large p_t particles, when the converse occurs for the production of the low p_t dominant secondaries (section 4). As $x_t(p_t)$ increases the ratio of the proton to pion induced pion yields changes dramatically. This is expected for a reaction at the constituent level to the extent that the fewer pion constituents have on the average a larger fraction of the hadron momentum than those of the proton. The data agree with expectations (solid curve).

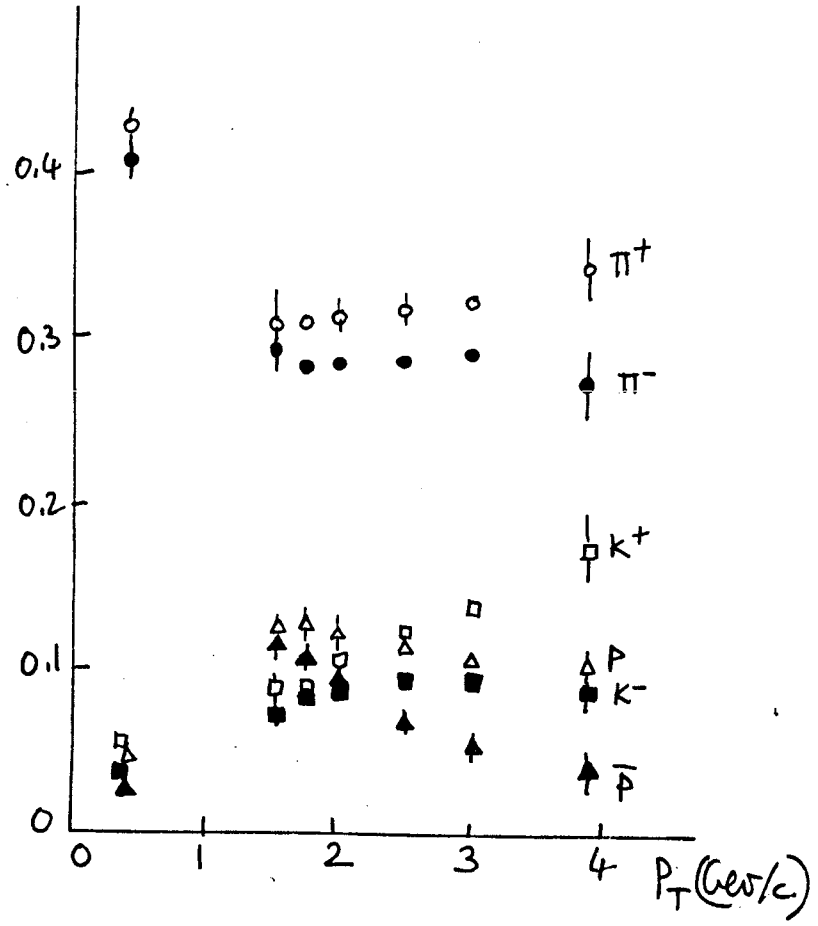

Figure 6-5-a) : Fractions of the charged particle production carried by each type of secondaries. Data from the British-Scandinavian Collaboration. $\sqrt{s}$ = 53 GeV

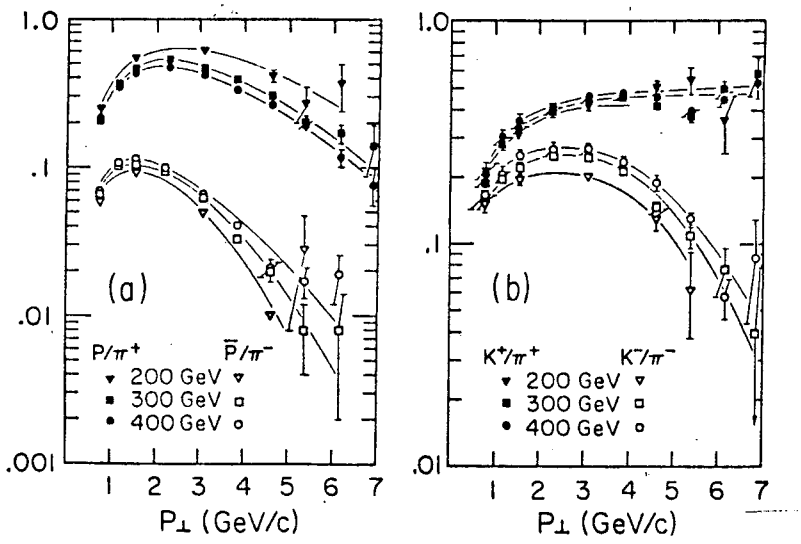

Figure 6-5-b) : Particle ratios at Fermilab (larger p_t values). Data from the Chicago-Princeton Collaboration

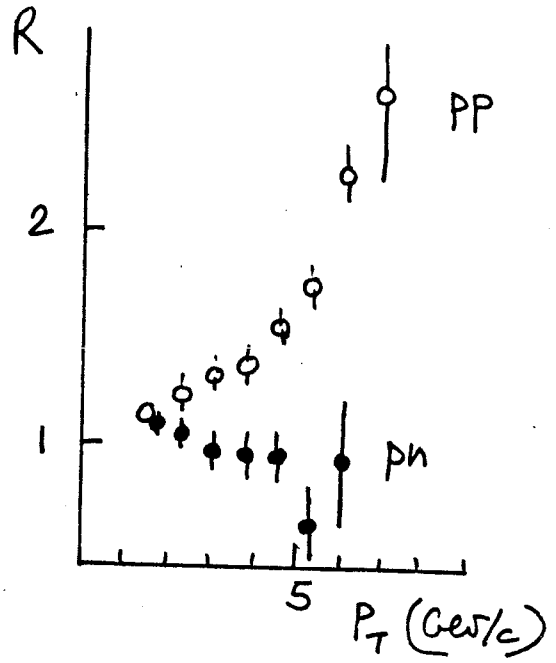

Figure 6-5-c) : Positive over Negative ratio as a function of p_t in pp (open circles) and pn (full circles) reactions at 90^{o}.
Data from the Chicago-Princeton Collaboration

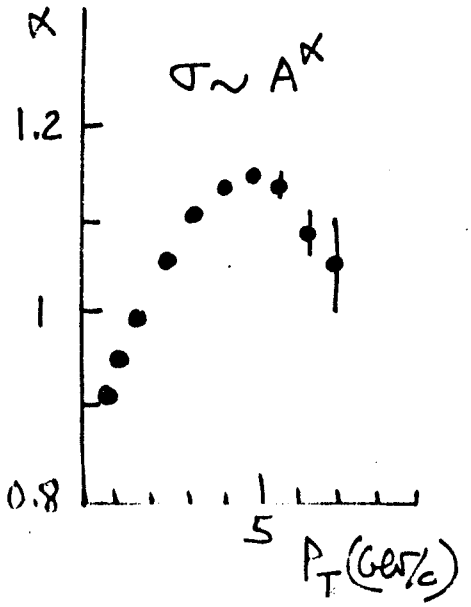

Figure 6-6 : A dependence of the pion yields in large p_t production of Nuclei → off nuclei.
Data from the Chicago-Princeton Collaboration at Fermilab

Table 6-1

Qualitative differences between large p_t and typical particle production. Large p_t here means $1.5 < p_t < 5$ GeV/c (available data).

	low p_t	large p_t
$\frac{d\sigma}{dp_t^2}$ at x = 0	e^{-6p_t}	p_t^{-8}
Energy dependence	no	rising
Positive/negative	1	>1
Pion/Heavy particles	~ 6	1.5 - 2
p/π induced reaction yields	>1	<1
A^{α} dependence in nuclear reaction	$\alpha \sim 2/3$	$\alpha > 1$
Associated multiplicity	positive correlations	larger positive correlations

There is also a very important effect when considering the associated particles to a large p_t trigger. The associated multiplicity is larger than in a typical event at the same energy. It increases with p_t (to a first approximation linearly with about 2/3 extra charged particle per extra GeV/c required for the particle signaling a special large p_t reaction (trigger particle). Figure 6-8-a) shows the rapidity distribution of the charged particles seen together with a large p_t π^o trigger at 90°. The distribution peaks at 90° while being very broad. The rapidity distribution is practically independent of the direction of the triggering particle ($40^o < \theta < 140^o$). The integrated value can be compared to the mean multiplicity for a reaction at center-of-mass energy $\sqrt{s} - 2p_t$, thus excluding the minimum energy required by the trigger and its p_t balance. This defines an excess of multiplicity which is found to be energy independent. It increases with p_t. This is shown in figure 6-8-b). Finally figure 6-8-c) gives the azimuthal distribution for the charged particles associated with a large p_t π^o at $\phi = 0^o$. There is a maximum in the opposite direction. However it is rather broad. One has therefore to conclude that a large fraction of the associated multiplicity consists of low p_t particles which have hardly any angular correlation with the trigger particle.

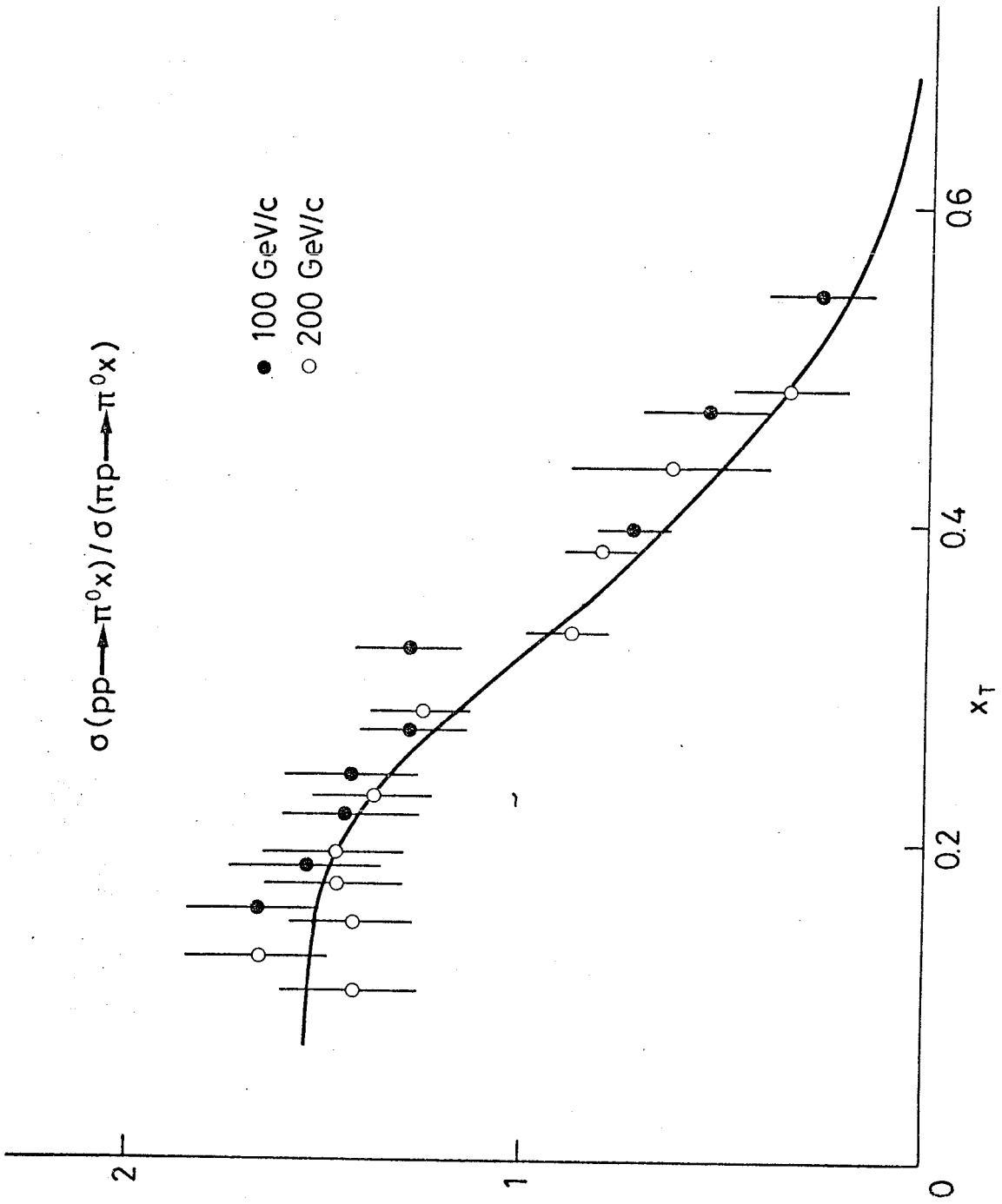

Figure 6-7 : Ratio of π yield in proton and pion induced reactions. Results from the Caltech-Berkeley Collaboration at Fermilab

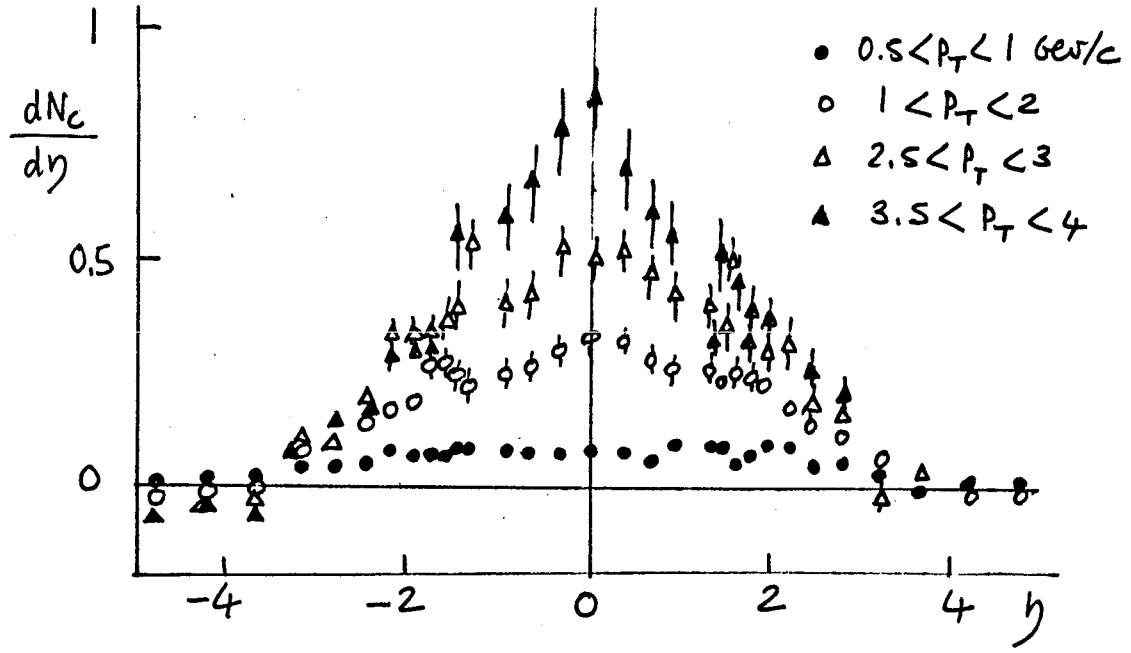

Figure 6-8-a) : Rapidity distribution of the associated charged secondary particles to a large p_t π^o trigger at 90^o
Data from the Pisa-Stony Brook Collaboration

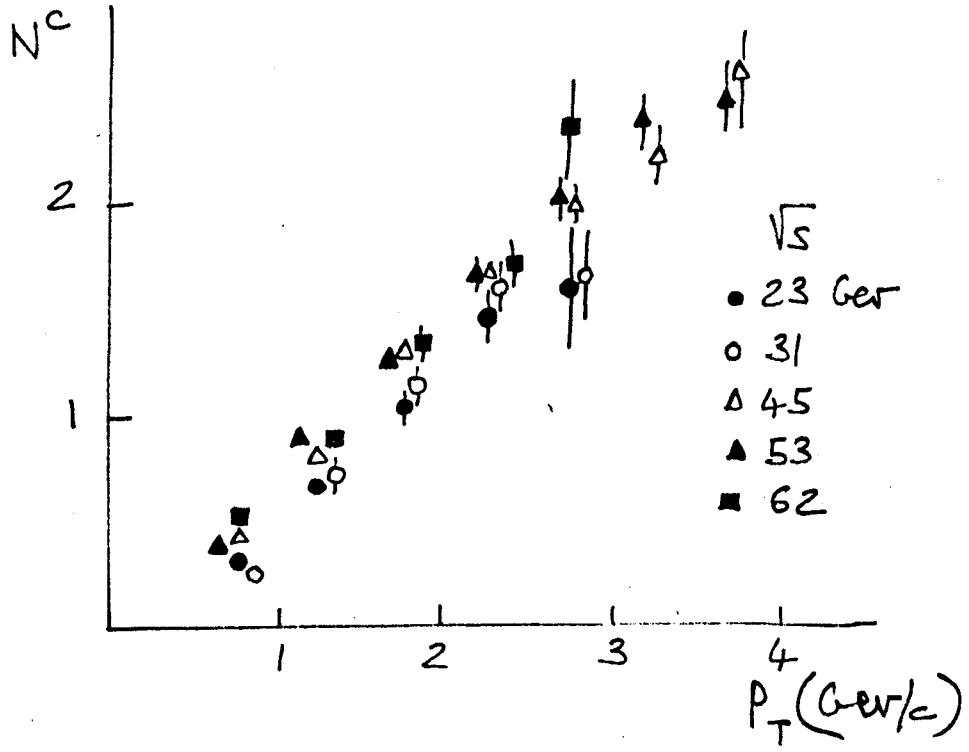

Figure 6-8-b) : Charged particle excess in the integrated distribution

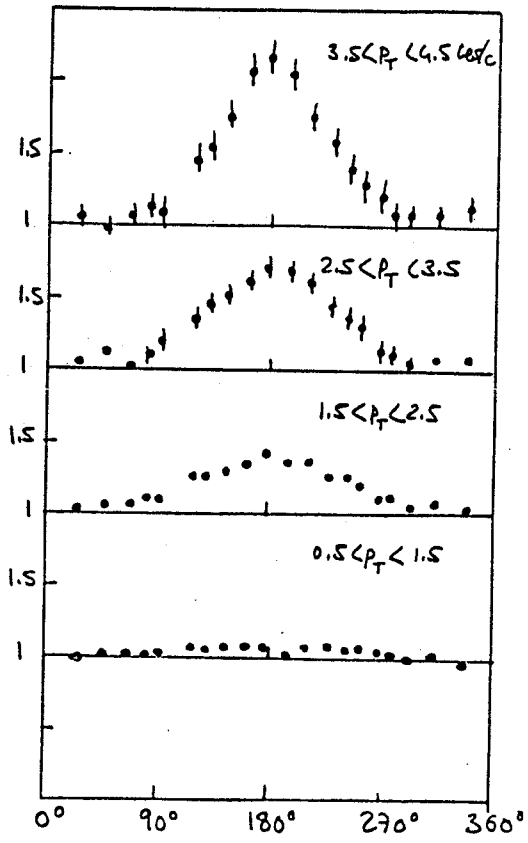

Figure 6-8-c) : Azimuthal distribution of the associated charged particles to a large p_t π^o trigger at $\phi = 0$, $\theta = 90^o$. Data from the Pisa-Stony Brook Collaboration. The data of figures 6-8-a) and 6-8-c) correspond to $\sqrt{s} = 53$ GeV. There is no important energy dependence.

Figure 6-9 : Leading particle effects in reactions with and without a large p_t particle. Data from the CERN-Collège de France-Heidelberg-Karlsruhe Collaboration

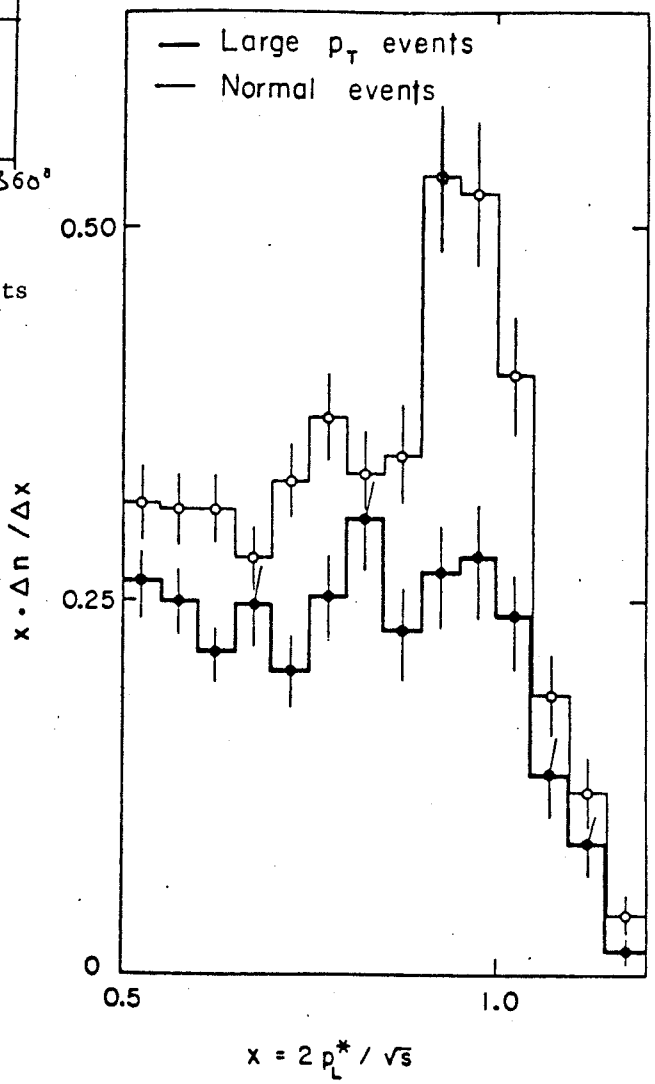

The observation of large p_t particles does not exclude rapid forward and backward particles and in particular leading protons, as present in typical events. This is expected from a process associated with that of figure 6-3-d) with the remainders resulting in forward and backward jets. Figure 6-9 shows the distribution for positive particles (leading protons) in reaction with a large p_t particle and in typical events. The quasi-elastic peak associated with diffractive excitation disappears (section 5). Leading protons are otherwise present. More recent data from the British-Scandinavian Collaboration have checked the expected factorization properties among forward and backward leading particles.

A process such as that of figure 6-3-d) should imply important angular correlations among produced particles. Nevertheless, in view of the large associated multiplicity they can appear clearly only when the analysis is restricted to large p_t particles. This requires momentum analysis over a large solid angle. This took much time and effort at the ISR. A series of experiments (1973 to 1976) could eventually provide evidence for a jet configuration. This corresponds to a major advance in the understanding of these processes. The general expected pattern is presented in a schematic way in figure 6-10. Two constituents A and B, with (small) transverse momentum k_t collide and two constituents C and D are produced at wide angle, resulting in two hadronic jets. To a good approximation the two jets should balance out their transverse momentum p_t since k_t is small. They will however not in general balance out their longitudinal momentum since A and B have a priori different fractions x_1 and x_2 of the incident hadron momentum. The trigger particle signals a jet. Any large p_t particle on the same (toward) side, if present, should be in the same direction, since they should belong to the same jet. There should be a jet on the other side. Nevertheless, it is expected not to have strong angular correlation with the trigger particle. A large p_t particle on the other (away) side is widely distributed in angle (fan-like distribution). However, when two are seen, they should be in the same direction as belonging to the same jet. All large p_t particles belonging to two jets which balance (to a first approximation) their transverse momenta, should all lay in a plane. The momentum distribution perpendicular to the plane defined by the trigger particle and the incident particles should be exponentially cut off. One has thus three properties which are specific of the jet structure. Figures 6-11, 6-12 and 6-13 summarize present evidence. Figure 6-11 gives the coplanarity test. Figure 6-12 gives rapidity distributions of same side charged secondaries asssociated with a large p_t trigger. The distribution peaks at the rapidity of the trigger particle and the more so the larger the transverse momentum. One further checks that the rapidity distribution corresponds to a limited transverse momentum distribution with respect to the global momentum of the jet (q_t distribution on figure 6-12-b)).

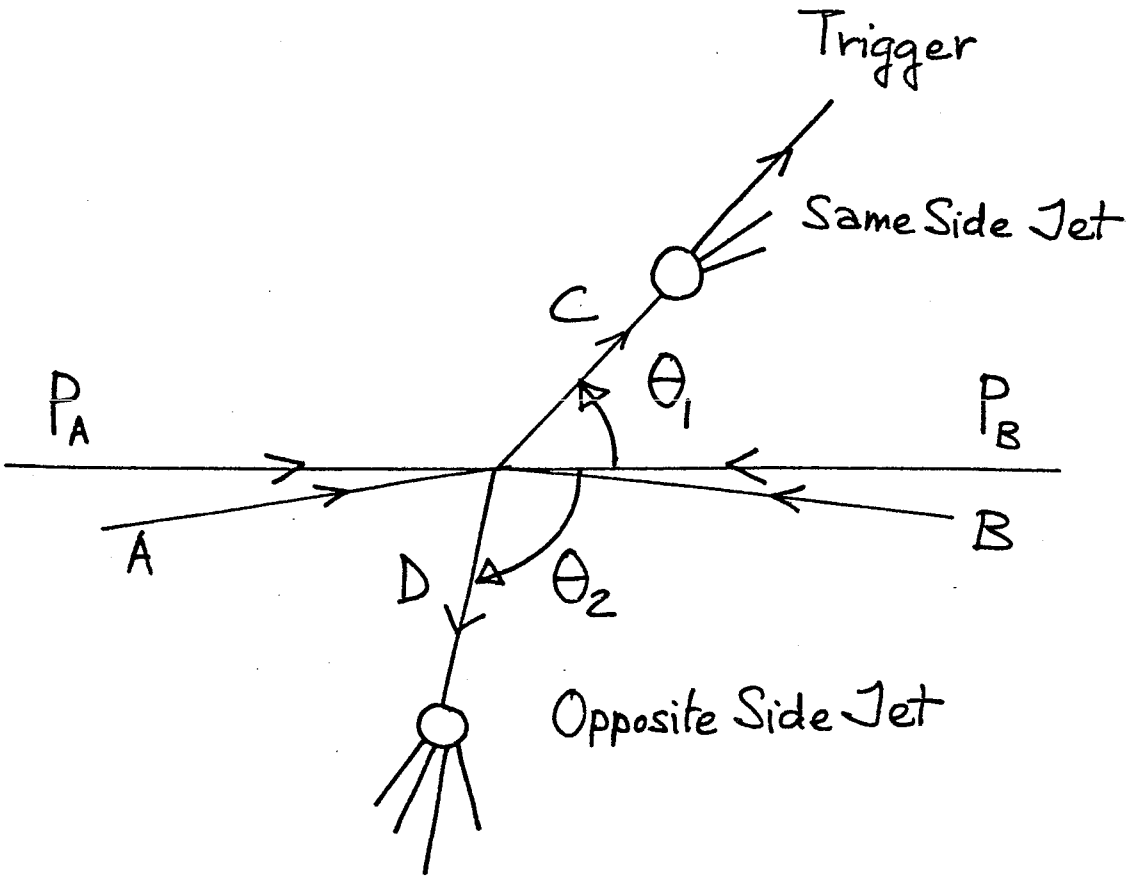

Figure 6-10 : Two jets at wide angle as the result of the hard scattering between hadron constituents. In practice the angular correlations are smeared out by the presence of many low energy particle (figure 6-8-a))

Figure 6-13 gives the rapidity difference distribution for two large p_t particles observed on the away side. The trigger is a π^o with $p_t > 2.5$ GeV/c. Configuration with two charged particles with $p_t > 1.2$ GeV/c on the away side are analyzed. Even though large p_t particles on the away side show a fan-like distribution (figure 6-12-c)), whenever two are seen, they are in the same direction as the fragments of a jet should.

Figures 6-11, 6-12 and 6-13 illustrate the type of data now available in support of the jet picture. The three phenomenological conditions are met. As far as the analysis can go, large p_t reactions show a two-jet structure. It is now extremely important to push such an analysis to higher p_t values ($p_t \gtrsim 5$ GeV/c as opposed to 2 GeV/c as now available). Jet effects are expected to be far more pronounced. Surprises may appear.

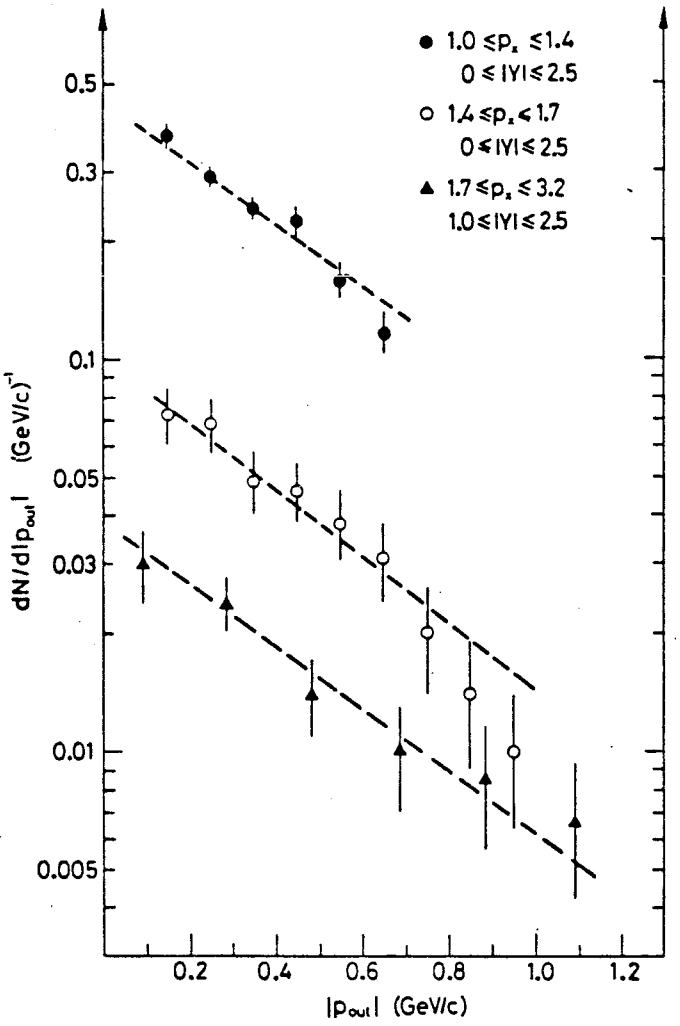

Figure 6-11 : Coplanarity test. One denotes as p_{out} the component normal to the plane defined by the trigger particle and the incident particle. The observed mean value agrees with what is expected from the smearing associated with the constituent transverse momentum inside the hadron and the fact that the trigger particle does not give precisely the direction of the jet. With jet triggering, Fermilab experiment 260 gets a still neater coplanarity effect.

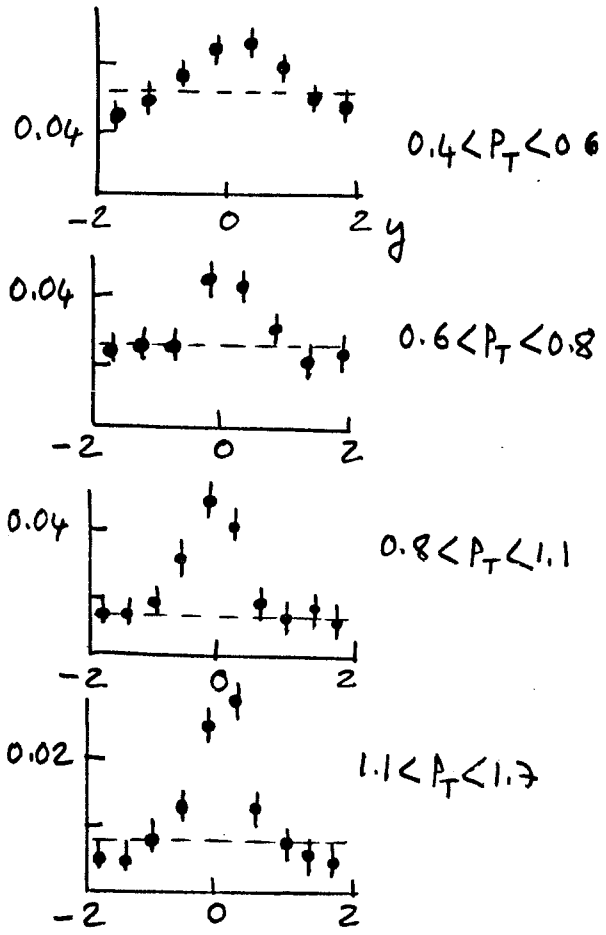

Figure 6-12-a) : Rapidity distribution on the same side (trigger π^o of $p_t \simeq 2.5$ GeV/c at 90^o). The number of associated secondaries drops as the required value of p_t increases. When present they are however the more so correlated with the trigger. Data from the CERN-SFM Collaboration

Figure 6-12-b) : Transverse momentum distribution with respect to the global jet momentum. Data from the British-Scandinavian Collaboration

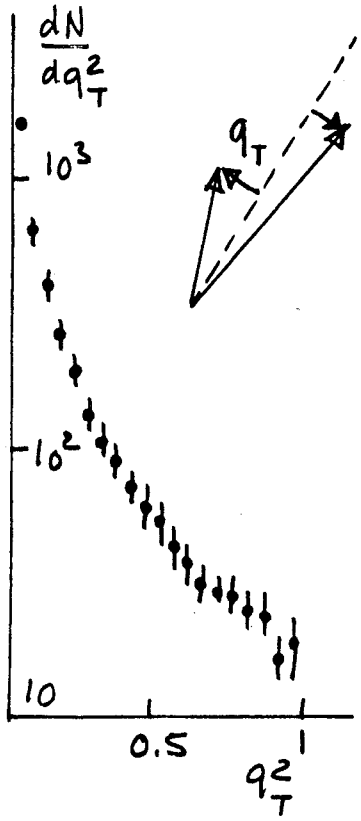

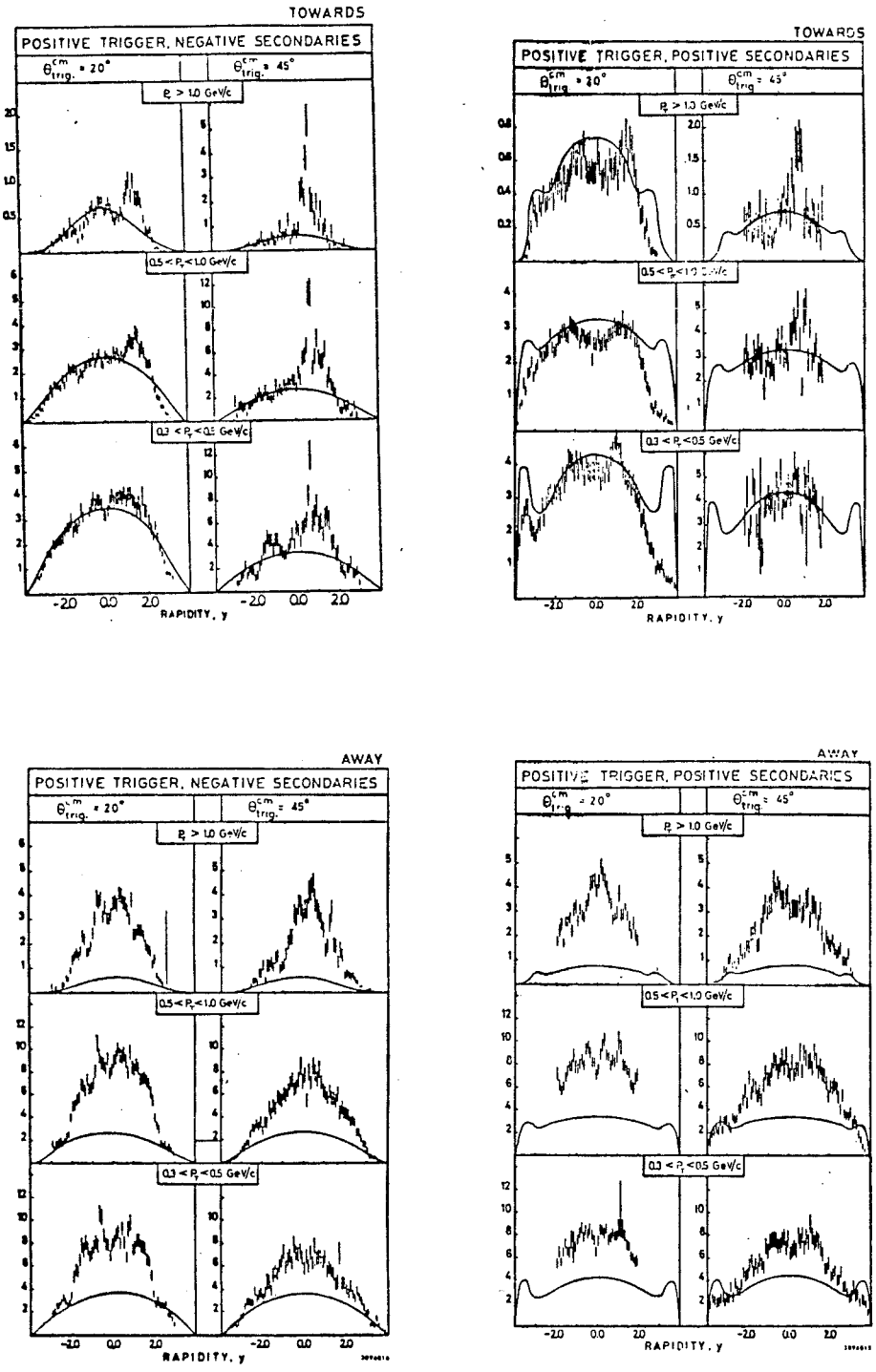

Figure 6-12-c) : Rapidity distributions of the charged particles associated with a charged particle trigger at θ with $p_t \gtrsim 2$ GeV/c. Opposite signs (left) and same side (right). Towards (up) and away (down). Data from the CERN-Collège de France-Heidelberg-Karlsruhe Collaboration

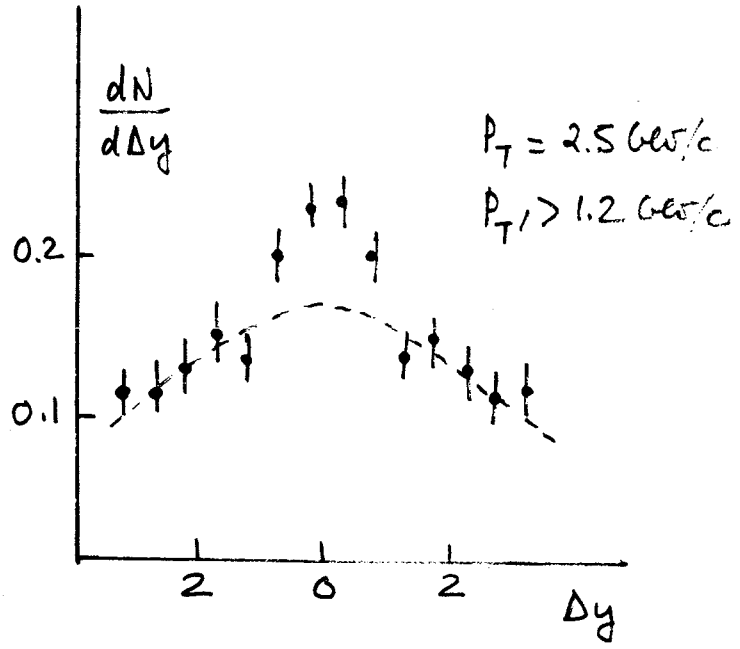

Figure 6-13 : Jet correlations on the away side. The dashed line corresponds to what was expected from uncorrelated particles. Results from the CERN-SFM Collaboration

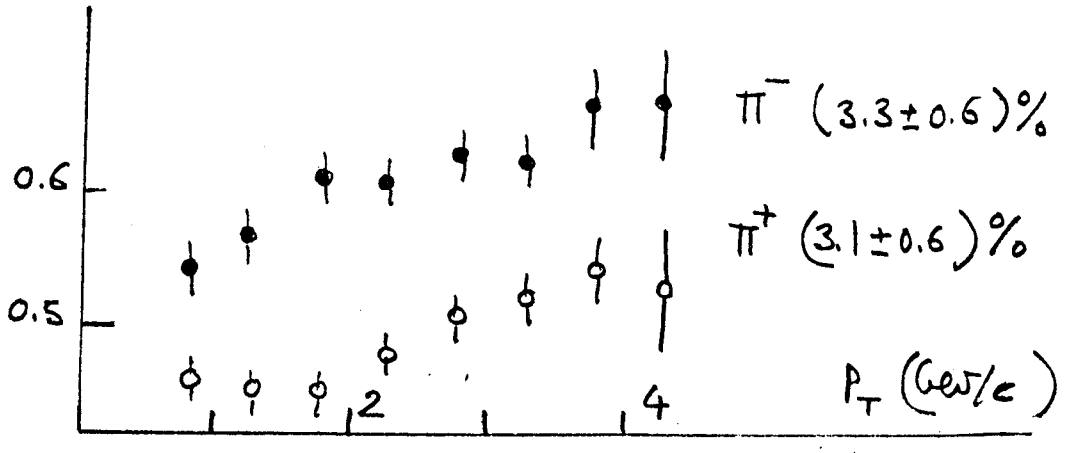

Figure 6-14 : Momentum flow on the trigger side. Momentum of the charged particles found together with a π^+ and a π^- trigger. Results from the British-French-Scandinavian Collaboration

Having ascertained the jet structure, the next point is to describe jet fragmentation[37]. As previously said, the general properties of hadron production are expected to apply. A fragment of type i is expected to take a fraction x of the jet momentum P_T, with a distribution $F^i(x)$. The inclusive distribution reads

$$\frac{d\sigma^i}{dp_T} = \int \phi(P_T)\,\delta(p_T - xP_T)\,F^i(x)\,dx\,dP_T \tag{6.3}$$

where $\phi(P_T)$ is the cross-section for jet production.

This gives

$$\frac{d\sigma^i}{dp_T} = \int \phi\left(\frac{p_T}{x}\right)\frac{F^i(x)}{x}\,dx \tag{6.4}$$

and with

$$\phi(P_T) = A\,P_T^{-n} \tag{6.5}$$

$$\frac{d\sigma^i}{dp_T} = \frac{1}{p_T^n}\int_0^1 F^i(x)\,x^{n-1}\,dx \tag{6.6}$$

This is the well known parent-child relationship. The inclusive distribution of the daughter particle has (in general only asymptotically) the same behaviour as that of the parent particle. Relation (6.6) shows that values close to x = 1 are over emphasized since n is large ($n \simeq 8$) but this is where F is small. It is instructive to consider at this stage a 3 fragmentation mode model. One mode corresponds to a single hadron taking practically all the jet momentum $F_I^i(x) = K^i\delta(x - 1)$. Another mode corresponds to a resonance (with two body decay) taking practically all the jet momentum $F_{II}^i(x) = R^i$. A third mode corresponds to a typical fragmentation $F_{III}^i(x) = B^i\frac{(1-x)^2}{x}$. This would reproduce rather well the distribution of figure 6-4. With the fragmentation function

$$F^i(x) = B^i\frac{(1-x)^2}{x} + R^i + K^i\delta(x-1) \tag{6.7}$$

Combined with (6.6), one gets

$$\frac{d\sigma^i}{dp_T} = \frac{1}{p_T^n}\left(\frac{2B^i}{(n+1)n(n-1)} + \frac{R^i}{n} + K^i\right) \tag{6.8}$$

This illustrates the key point to make. In view of the steep fall off ($n \simeq 8$), even if a mode whereby most of the jet momentum is found on one particle is a minority one (at the percent level say) and would not practically affect the inclusive distribution (figure 6-4), it may take a major role when triggering on a large p_t particle. Conversely, if one would trigger on a whole jet (collecting momentum over some solid angle as estimated from figures 6-12 and 6-13) one should get a much larger yield at fixed p_t (typically two orders of magnitude larger) than triggering on a single particle. This very important properties which follow

from scaling in jet fragmentation, and which are referred to as trigger bias, have recently been verified at Fermilab using a wide angle spectrometer with a calorimeter trigger. Triggering on a jet of global transverse momentum P_T, one observes a yield which is two orders of magnitude greater than that found with a single particle trigger at the same P_T. The ratio is (within errors) independent of P_T[38].

For the same reasons, the momentum flow in the direction of a trigger particle is expected to increase with P_T while remaining small, since one very frequently triggers on a jet with only one large p_t fragment. This is shown in figure 6-14 which gives the transverse momentum excess (almost a fixed fraction) seen in association with π trigger at large p_t. The trigger particle may take about 90% of the mean jet momentum which it signals. In any case, getting the jet momentum directly from a trigger particle (in the latter case a mean momentum), one can check for a scaling behaviour in the transverse momentum distribution of the particles associated with the jet on the other side. Distribution should depend on $x = p_t/P_T$ and not on the trigger momentum. Figure 6-15 puts together some recent results. The Fermilab results (at large p_t) are in good agreement with scaling (figure 6-15-a)). The ISR results are in agreement with a scaling behaviour which would apply for $P_T \gtrsim 3$ GeV/c. This belated scaling could be associated with the transverse momentum of constituents within hadrons ($k_t \sim 0.5$ GeV/c). Scaling would apply when $P_T >> k_T$ only. This point is still not well understood.

Figure 6-16 gives a further test of scaling in jet fragmentation. When defined in terms of a scaling fragmentation function the two particle distribution is given by:

$$\frac{d^2\sigma}{dP_{T_1}\,dP_{T_2}} = \int \frac{B_2^{ij}(x_1,x_2)}{x_1 x_2}\,\delta(P_{T_1}-x_1 P_T)\,\delta(P_{T_2}-x_2 P_T)\,\phi(P_T)\,dx_1\,dx_2\,dP_T \qquad (6.9)$$

Integrating over P_T ($p_{t_1} - p_{t_2}$) one readily gets an inclusive distribution $\frac{d\sigma}{dp_t}$ ($p_t = p_{t_1} + p_{t_2}$) which is proportional to the single particle distribution (6.6). The data displayed in figure 6-16 are compatible with this. Nevertheless scaling is so important a property that more data than those already available are certainly needed.

At present, there is evidence for an approximate factorization between the two jets, the only correlation being the common value of $|P_T|$. There are however certainly some quantum number correlation effects. This requires further study.

The nature of the constituents, which can be identified with quarks in the processes of figures 6-3-a) and 6-3-b), is still open for large p_t phenomena.

The inclusive distribution, calculated according to the impulse approximation of figure 6-3-d) reads

$$E\frac{d\sigma}{d^3p} = \int F^A(x_1)\, F^B(x_2)\, \frac{F(x)}{x}\, \frac{1}{\pi}\, \frac{d\tilde{\sigma}}{d\bar{t}} \qquad (6.10)$$

where $F^A(x_1)$ and $F^B(x_2)$ are the constituent distributions inside the incident hadron and F(x) describes the fragmentation of the scattered constituent. The differential cross-section at the constituent level (with Mandelstam variables $\bar{s} = sx_1x_2$, $\bar{t}$ and $\bar{u}$) is denoted by $\frac{d\tilde{\sigma}}{d\bar{t}}$. In order to get eventually a p_t^{-8} behaviour, one has to impose a differential cross-section of the type (large $\bar{s}$ and $\bar{t}$) $\frac{d\tilde{\sigma}}{dt} \sim \frac{1}{\bar{t}^4}\left(\frac{\bar{t}}{\bar{s}}\right)^{\alpha}$. If the constituents are quarks, F^A, F^B and F can be taken from the analysis of different processes, 6-3-a) and 6-3-b). As discussed by Feynman and Field, one can then get a good description of existing data with $\alpha = 1$[39]. If the relevant constituents are not all quarks one may get a rationale for the observed power 8. A meson-quark interaction involves for instance an extra form factor, with a resulting extra p_t^{-4} factor in the inclusive yield. This is expected in the constituent interchange model of Brodsky, Blankenbecler and Gunion[40]. This model had much success with inclusive yields. It fails however with recent correlation data where the Feynman and Field approach is quite successful. An improved CIM may still correspond to the p_t range explored so far.

If large p_t phenomena involve quark-quark scattering, one should expect that, provided p_t is large enough, the perturbation theory result should apply with eventually a p_t^{-4} behaviour.

The differential cross-section for quark-quark scattering with gluon exchange reads

$$\frac{d\tilde{\sigma}}{d\bar{t}} = \frac{1}{8\pi\bar{s}^2}(4\pi\alpha_s)^2\left(\frac{\bar{s}^2+\bar{t}^2}{\bar{u}^2} + \frac{\bar{s}^2+\bar{u}^2}{\bar{t}^2}\right) \qquad (6.11)$$

with $\bar{s} + \bar{t} + \bar{u} \simeq 0$.

The running coupling constant squared is denoted by α_s. It can be inferred from the study of Charmonium ($\alpha_s \simeq 0.2$ at present p_t). Relation 6.11 then gives a computable yield for jet production which is however much smaller than what is observed. Nevertheless, since this predicted yield behaves at p_t^{-4} when the measured yield falls as p_t^{-8}, it should eventually take over. This may occur for $p_t \gtrsim 10$ GeV/c, where the calculated yield would compare with the measured one. Whether the p_t behaviour will change at very large p_t, thus revealing a still more basic interaction than that relevant for large p_t phenomena below 10 GeV is certainly the most challenging question at present.

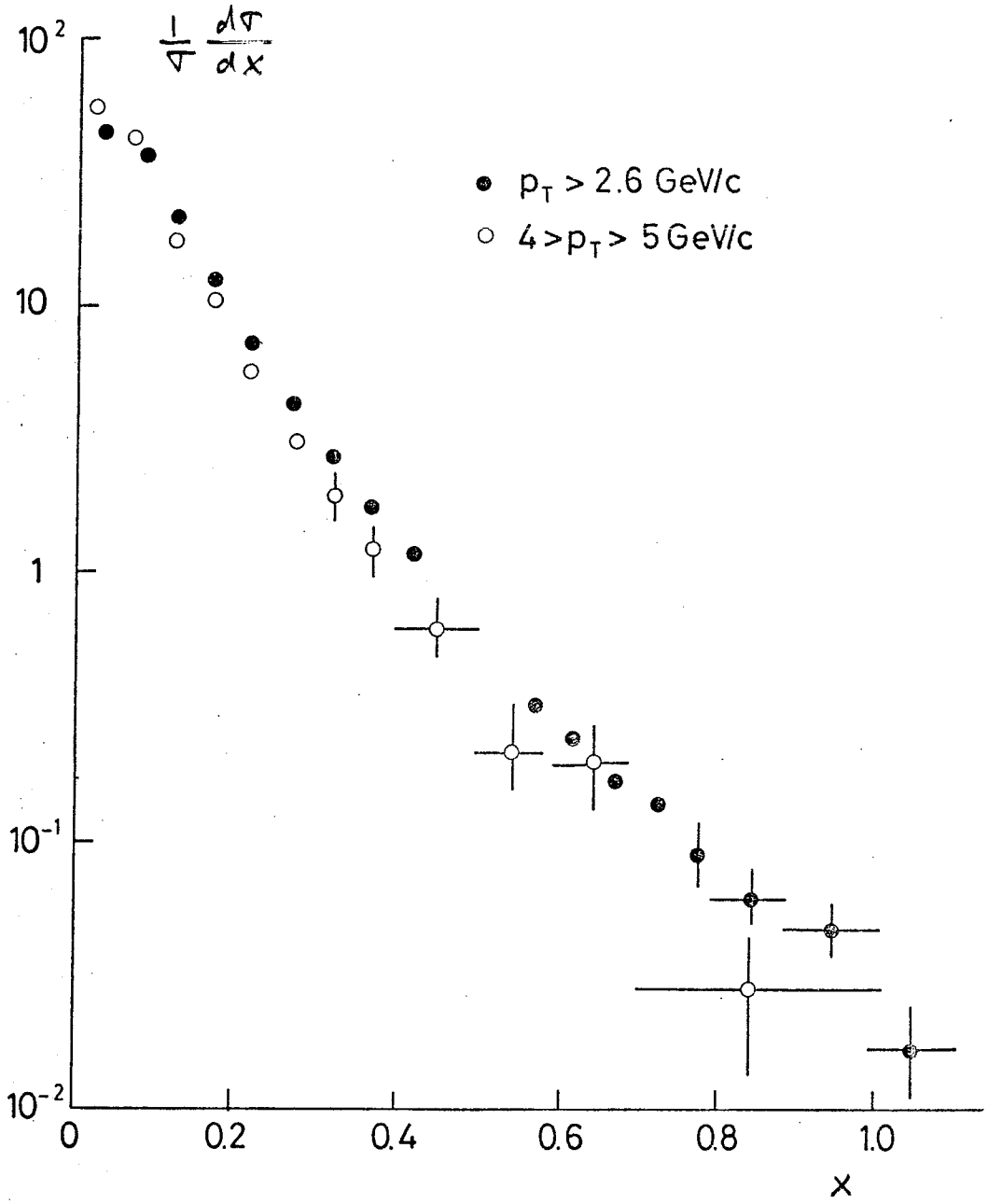

Figure 6-15-a) : Scaling as observed by the Caltech-UCLA-Fermilab-Illinois-Indiana-Max-Planck-Munich Collaboration, at Fermilab with a jet calorimeter trigger

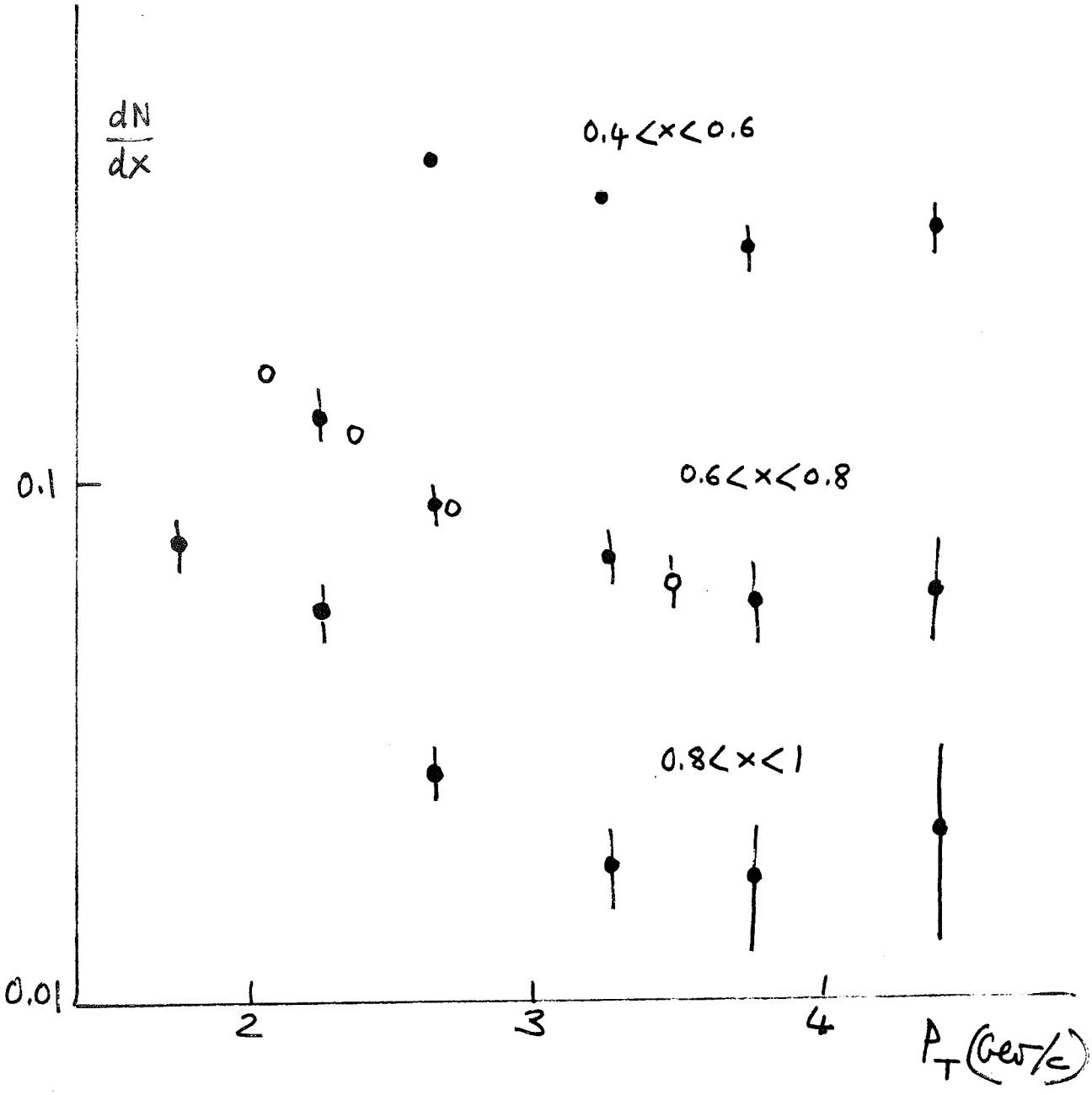

Figure 6-15-b) : Eventual scaling as observed in ISR experiments by the British-French-Scandinavian Collaboration (full dots) and CERN-Collège de France-Heidelberg-Karlsruhe Collaboration (open dots)

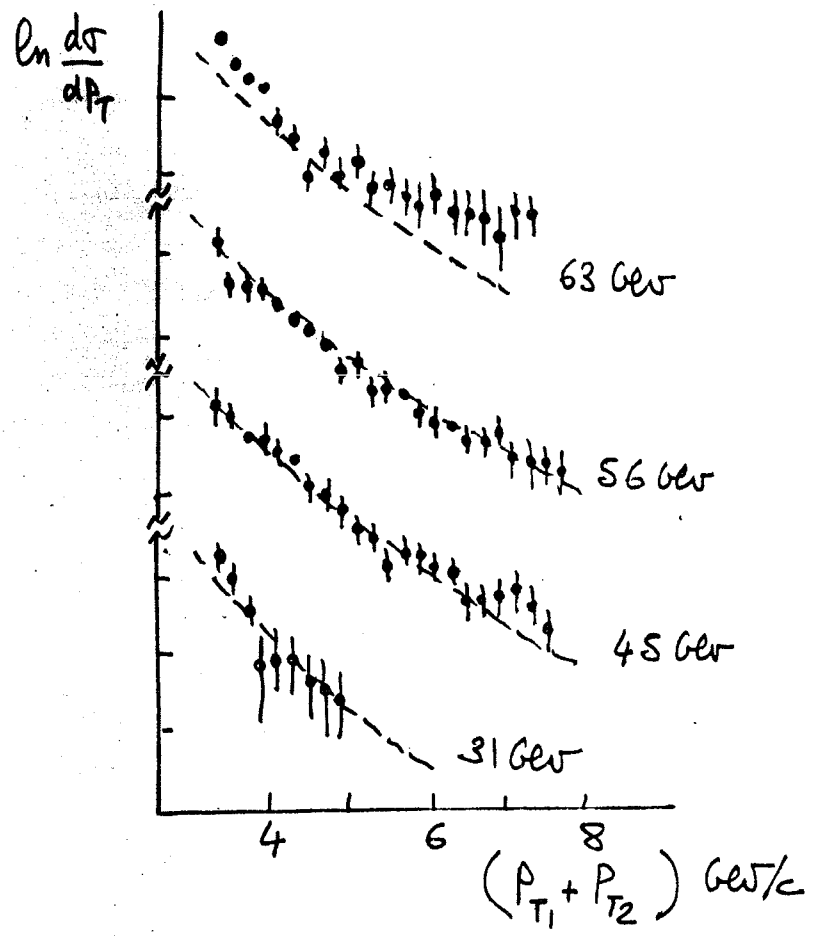

Figure 6-16 : Two π^0 distribution at large p_t and unormalized single π^0 distribution (dotted line). The p_t dependence is the same whatever one triggers upon. Data from the Aachen-CERN-Heidelberg-Munich Collaboration

As discussed in section 3, strong interactions do not become simpler at very high energies. They could become simpler at very large transverse momenta. This is a domain of research where the ISR could still have a unique role. Recent evidence for jet structure and scaling in jet fragmentation is very encouraging. Jet (calorimeter) triggering is a promising approach.

Table 6-2 lists the ISR experiments the results of which have been presented in this section.

Table 6-2

List of ISR experiments with important contributions to the study of large p_t phenomena

(i) Discovery of large p_t production

102 Saclay-Strasbourg (charged particles)

103 CERN-Columbia-Rockefeller (γ rays)

203 British-Scandinavian (charged particles)

(ii) Angular correlations with large p_t trigger

801 Pisa-Stony Brook

205 CERN-Daresbury-Liverpool-Rutherford

701 Aachen-CERN-Munich

(iii) Momentum correlations with large p_t trigger

105 CERN-Columbia-Rockefeller-Saclay

412 CERN (referred to as CERN-SFM)

407/408 CERN-Collège de France-Heidelberg-Karlsruhe

410/413 British-French-Scandinavian

The last three experiments used the Split Field Magnet facility.

(iv) Very large p_t triggers $p_t > 10$ GeV (γ rays) and correlations

702 CERN-Saclay

108 CERN-Columbia-Oxford-Rockefeller

7. Lepton and Lepton Pair Production

Hadron production eventually leads to lepton production through weak decays. The daughter lepton yield should then follow the parent hadron yield in its p_t dependence and therefore rapidly fall with p_t. Indeed when first probing large p_t production, one looked for leptons, which, no longer associated with an exponentially falling hadronic production, would have signalled some new phenomena. Electromagnetic and weak effects are expected to be power behaved at large transverse momentum and should eventually win over any large but exponentially behaved hadronic yield. As discussed in section 6, however, the main finding was that the hadronic yields themselves no longer decrease exponentially at large p_t. The relatively large amount of hadrons thus observed swamped for a while the observation of prompt leptons, not readily associated with the weak decay of the abundantly produced hadrons. Nevertheless, in 1974, prompt leptons could be ascertained at Fermilab and at the ISR[41]. The observed yields turn out to be remarkably proportional to the pion yield over a large p_t range ($1 < p_t < 3$ GeV/c) and over a huge energy range ($200 < E < 2000$ GeV). This is shown in figure 7-1 which gives the electron/π^o ratio at wide angle over the ISR energy range. Figure 7-2 gives Fermilab results for the muon/pion ratio at 300 GeV/c.

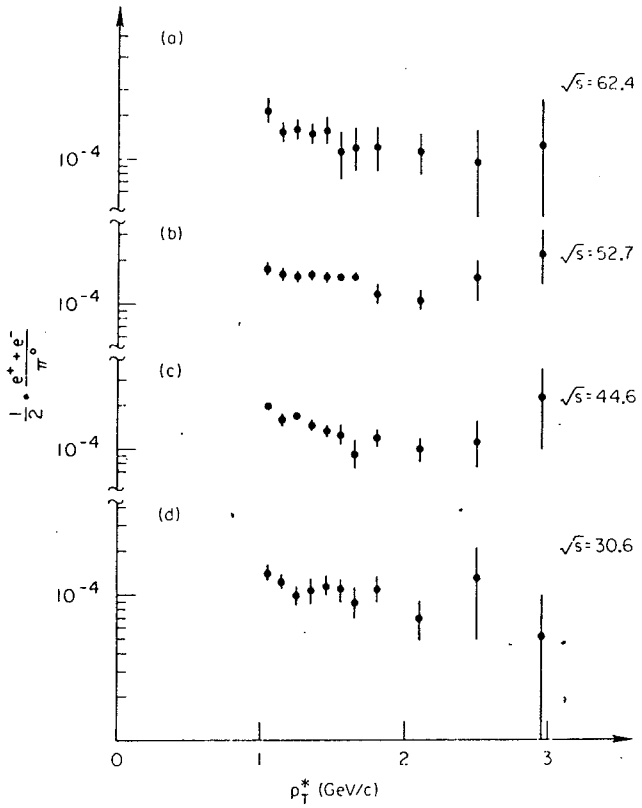

Figure 7-1 : Electron/pion ratio at the ISR. The ratio is remarkably constant as s or p_t vary

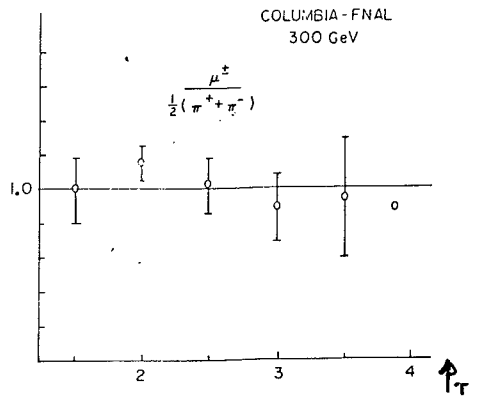

Figure 7-2 : μ/π ratio. Data from the Chicago-Princeton Collaboration at Fermilab

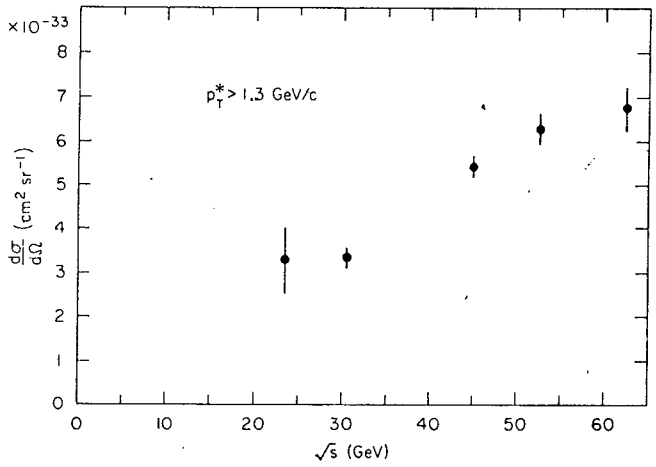

Figure 7-3 : Integrated electron yield as a function of energy. Data from the CERN-Columbia-Rockefeller-Saclay Collaboration

In the p_t range covered by these data, the pion yield increases much with energy. So does the prompt lepton yield. Figure 7-3 gives the energy dependence of the integrated yield for $p_t > 1.3$ GeV/c.

It is known that the e^+/e^- (μ^+/μ^-) ratios are compatible with one and that the e/μ ratio is also compatible with one. Such ratios are however quoted with rather large errors ($\sim$20%).

The behaviour of the e/π ratio at low p_t ($p_t < 1$ GeV/c), as observed in one experiment at the ISR, shows a sharp rise. This is seen in figure 7-5. Further checks are needed. At the same time the e/π ratio at lower energies (E < 100 GeV) is still the matter of debates. It is of course at lower p_t and at lower energies that the signal over background ratio is sharply decreasing. This makes conclusions far more difficult to reach.

We shall therefore focus on the $1 < p_t < 4$ GeV/c range where agreement now prevails among different results. The lack of energy and p_t dependence of the lepton/pion ratio makes it tempting to look for a hadronic origin. The value of the observed ratio, close to 10^{-4}, is indeed not far from α^2!

Part of the observed leptons could come from the formation and decay of vector mesons. In such a case one expects a p_t distribution which peaks at $p_t \approx \frac{M}{2}$ where M is the vector meson mass, and which eventually decreases with p_t as the vector meson production does. This is a well known Jacobian peak effect. Figure 7-4 gives for instance the yields expected from the production and decay of the J/ψ particle. The peaking gets smeared out as the p_t distribution of the parent particle widens. With ρ, ω, φ and J/ψ as possible sources, one may already reconstruct part of the inclusive distribution. Figure 7-5 shows the result of such an attempt[42]. At lower p_t there is still room for some contribution from the semi-leptonic decay of charmed particles. At larger p_t there is also room for production of large mass lepton pairs. In the latter case the cross-section can be computed in terms of quark distribution, following the calculation procedure corresponding to the impulse approximation of figure 6-3-c). This is the Drell-Yan process. It is clear from figure 7-5 that no single process stands out. Their relative weight could be obtained from the analysis of correlations (low mass lepton pairs on the same side, large mass lepton pairs on the opposite side, or absence of a visible antiparticle in the case of charmed particle decay). Indeed, if inclusive yields have initially attracted much attention as corresponding for a time to the only available data[43], the corresponding study oriented itself as quickly as possible toward the analysis of lepton pairs. Too many contributions enter the inclusive distribution for any special feature to show up. The overwhelming fraction of the produced leptons are now known to be associated with pair production (e^+e^- or $\mu^+\mu^-$). Charmed particle formation should contribute a little but no direct test is presently available. The pair production of charmed particles could be signaled by an $e^{\pm}\mu^{\mp}$ positive correlation, one particle having a semileptonic decay with $e^-\bar{\nu}$, while the other one would have a semileptonic decay with $\mu^+\nu$. Attempts at detecting such positive correlations have so far failed. Nevertheless the expected production rates and branching ratios together with the limited acceptance of the detectors could actually lead only to little hope. On the other hand, observation of large mass lepton pairs, The Drell-Yan

process notwithstanding, is an efficient way to search for new narrow vector mesons which are likely to be associated with a new quark. Indeed the J/ψ was discovered that way in 1974 and the ϒ was discovered that way in 1977. We shall therefore concentrate on the study of large mass lepton production (M > 2 GeV say). This is at present the object of an extensive effort at the ISR with the Solenoid detector (I-1), the muon pair toroid spectrometer (I-2), the lamp shade magnet (I-6), the Double Arm wide angle spectrometer (I-7) and the Argon Calorimeter (I-8)!

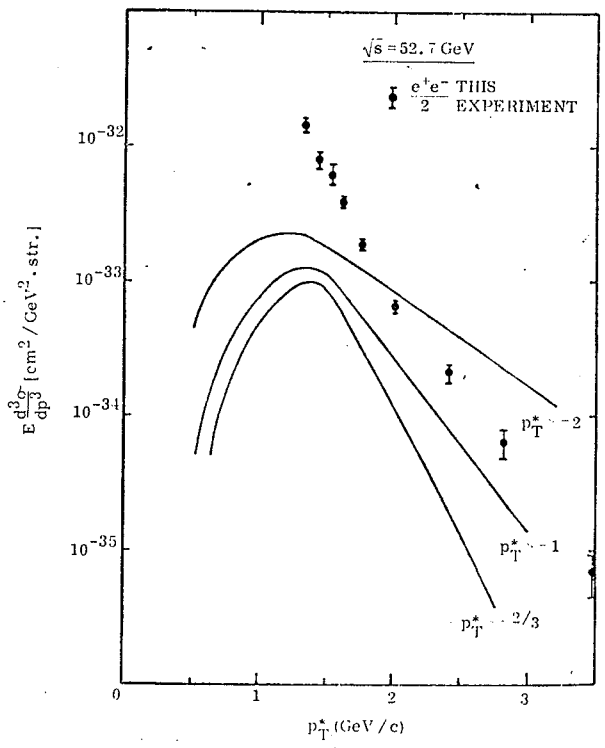

Figure 7-4 : Electron yield associated with the production of the J/ψ particle. The Jacobian peak is smeared as the p_t distribution of the J/ψ widens

We shall consider first the Drell-Yan process, corresponding to the standard electromagnetic production of a lepton pair (figure 6-3-c)). The differential cross-section is then given by

$$\frac{d^2\sigma}{dM^2 dx} = \sum_i \int F_i(x_1)\bar{F}_i(x_2)\, q_i^2\, \frac{4\pi\alpha^2}{3M^2}\, \delta(sx_1x_2 - M^2)\, \delta(x - x_1 + x_2)\, dx_1\, dx_2 \qquad (7.1)$$

M is the lepton pair mass and x the fraction of the center-of-mass longitudinal momentum which it has. $F_i(x)$ ($\bar{F}_i(x)$) are the quark (antiquark) momentum distribution in the incident hadrons. q_i is the quark charge. The sumation is also extended

to colours. One neglects at this stage the transverse momentum of the quarks which should eventually give the transverse momentum of the pair, according to the impulse approximation of figure 6-3-c).

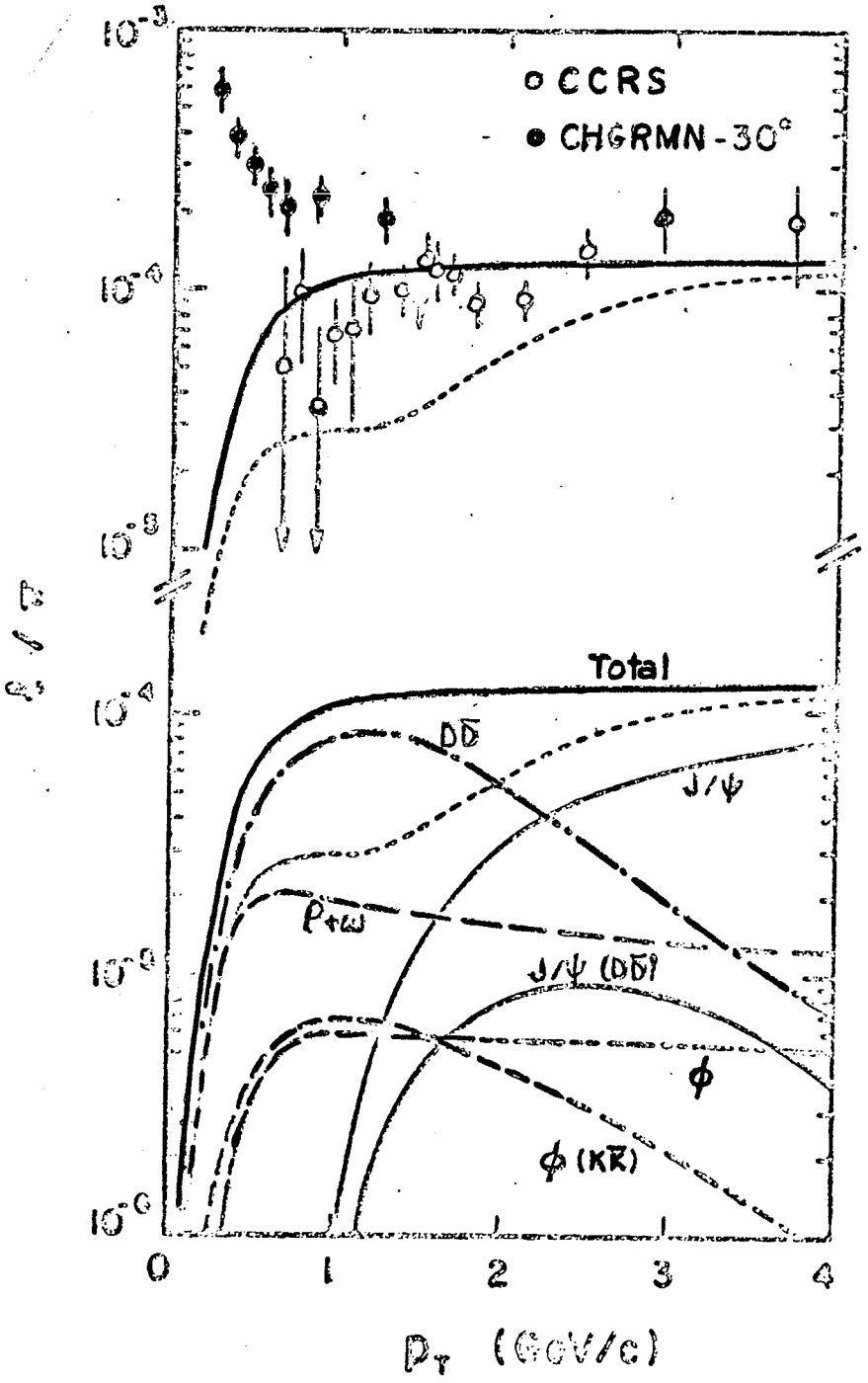

Figure 7-5 : The Bourquin-Gaillard "cocktail" model for the prompt lepton yield. Also shown are results from the CERN-Columbia-Rockefeller-Saclay Collaboration and of the CERN-Harvard-Genoa-Munich-Northwestern-Riverside Collaboration

Integrating over the variables x_1 and x_2, one gets

$$\frac{d\sigma}{dM^2 dx} = \frac{4\pi\alpha^2}{3M^4} \frac{x_1 x_2}{\sqrt{x^2 + 4\frac{M^2}{s}}} \sum_i q_i^2 F_i(x_1) \bar{F}_i(x_2) \tag{7.2}$$

with

$$x_1 = \frac{1}{2}\left(x + \sqrt{x^2 + 4M^2/s}\right) \tag{7.3}$$

$$x_2 = \frac{1}{2}\left(-x + \sqrt{x^2 + 4M^2/s}\right)$$

Keeping x fixed, the differential cross-section $\frac{d\sigma}{dM}$ once multiplied by M^3 depends only on the scaling variable M^2/s.

$$\frac{d\sigma}{dM dx} = \frac{1}{M^3} G\left(\frac{M^2}{s}\right) \tag{7.4}$$

This is a result of the parton model, which, while probably a drastic approximation, is the best present approach to available experimental results.

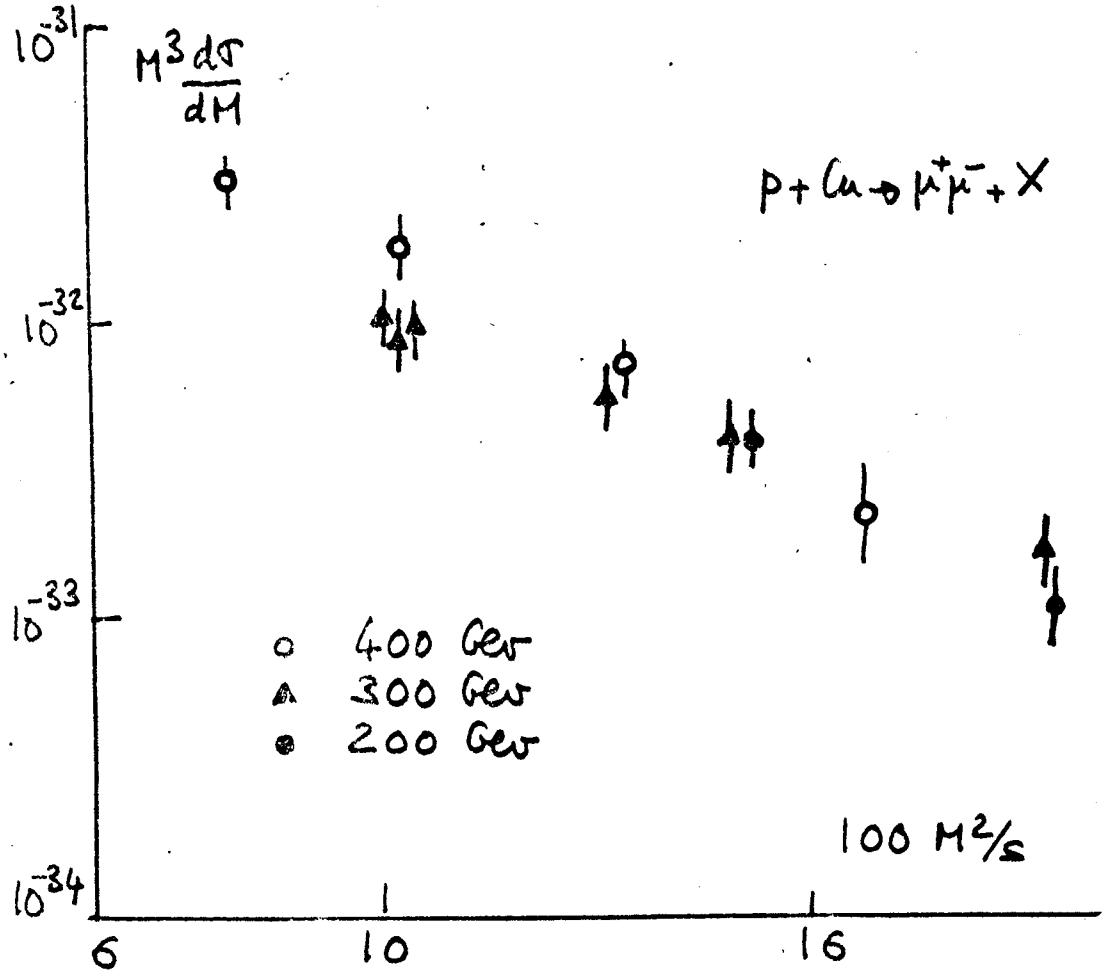

Figure 7-6-a) : Test of scaling. Results from the Chicago-Princeton Collaboration at Fermilab (Piroué et al)

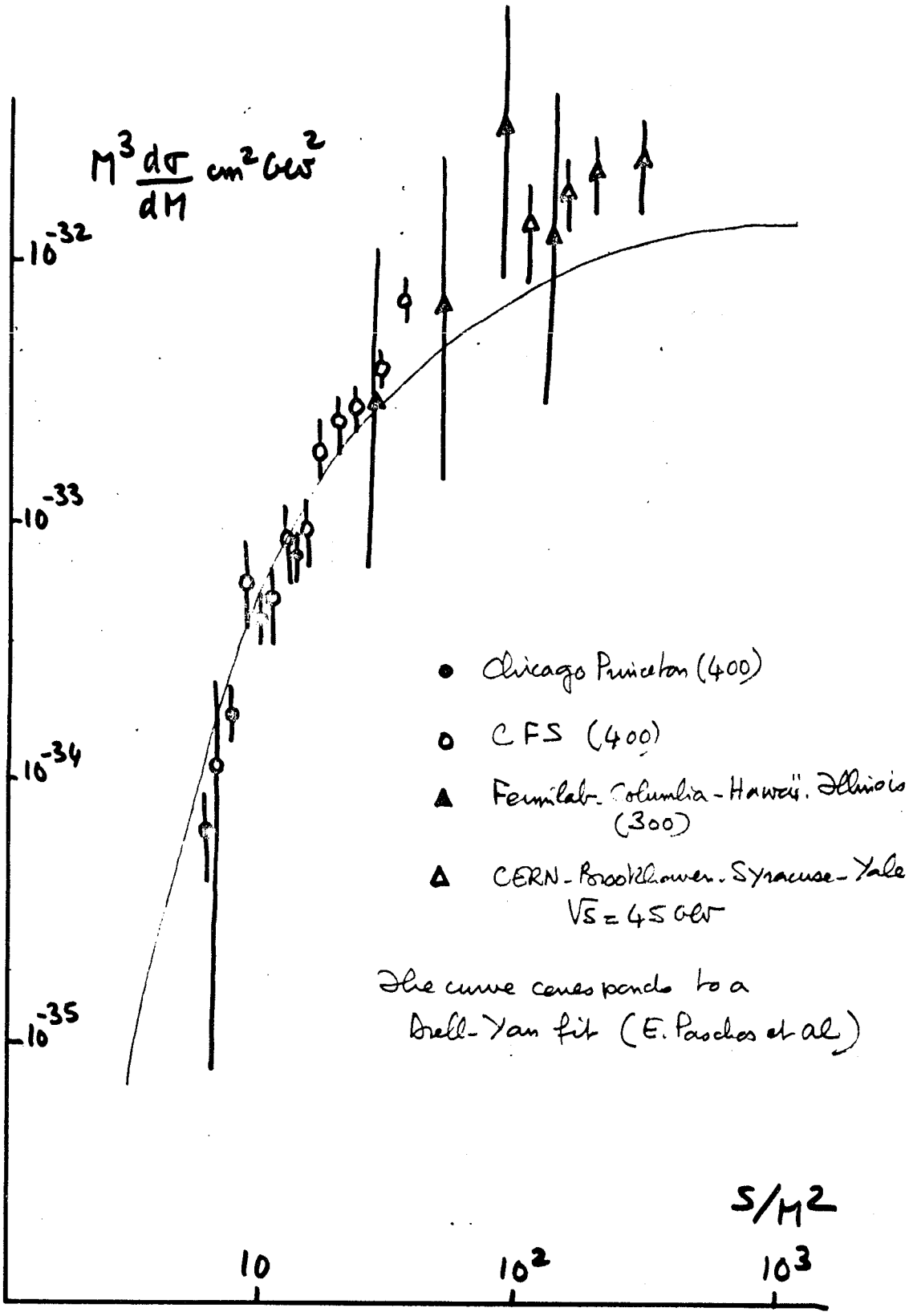

Figure 7-6-b) : General test of scaling. The ISR results should eventually be very important in such a test. They still lack statistical precision

Figure 7-6-a) shows a very good test of scaling as possible with recent Fermilab results on muon pair production. Figure 7-6-b) puts together lepton pair results at all energies (Fermilab and ISR). The solid curve corresponds to a parton calculation. The agreement is very encouraging. Figure 7-6 tests the scaling property more than the actual nature of the constituents. The fact that constituents with fractional charges are actually involved is tested to some extent by the results shown in figure 7-7. Lepton pair production in the π^+-Carbon reaction mainly go through $\bar{d}$ d annihilation, whereas $\bar{u}$ u prevails in π^--Carbon pair formation. If the Drell-Yan process dominates one should therefore expect a factor 1/4. On the other hand, lepton pair production though vector meson, as dominant at low mass (ρ, ω ...), and on the J/ψ, should follow isospin rules and give a ratio 1. The data of figure 7-7 indicate at least a trend of that type.

The question of scaling, and the study of proton structure, to which it is directly connected, presently justify much effort. As is obvious however from what precedes, fixed target machines have an edge. The relatively low luminosity available at the ISR is a serious predicament. Nevertheless, the importance of scaling tests over as wide an energy range as possible should attach much interest to forthcoming ISR results.

As previously stressed the great topical interest of lepton pair study is to search for new narrow vector mesons. One may tentatively assume for the sake of argument that they are also produced according to an impulse approximation process. In such a case, the differential cross-section reads

$$x \frac{d\sigma}{dx} = \frac{2\pi}{M^2} \sum_{ij} g_{ij}^2 F_i(x_1) \bar{F}_j(x_2) \qquad (7.5)$$

with x_1 and x_2 given by (7.3). M is the vector meson mass, g_{ij} is the coupling constant of the produced vector meson to the constituent i and $\bar{j}$ it originates from. It can be looked upon as a current coupling in a Vector Dominance approximation. The product σM^2 has now the same scaling behaviour as $M^3 d\sigma/dM$ in the case of the Drell-Yan process. One therefore expects a sharp rise as s/M^2 increases (one can then use lower x values) which is eventually followed by some saturation behaviour. This is illustrated by figure 7-8 which puts together J/ψ production cross-section at wide angle (rapidity zero). The larger the mass, the larger the cross-section increase which one may thus expect between Fermilab (SPS) and the ISR. This may <u>partly</u> compensate for the relative loss in luminosity.

Even if the cross-section increases with s/M^2 the M^{-3} dependence of the Drell-Yan process, and the M^{-2} dependence of vector meson formation, make it very difficult to go beyond rather low limits. Observing a narrow vector state is a priori much easier since one roughly gains a factor $\alpha^{-2\frac{BM}{\Delta}}$, where B is the

branching ratio and Δ the mass resolution, from what is expected of the Drell-Yan process. If lepton pair production could be studied up to 6 GeV, one could hope to reach 14 GeV say in the case of a new vector-meson. This is however very difficult.

The subject of lepton pair search looked of great promise at the ISR in view of the expected scaling properties of production cross-section with, accordingly, a sharp increase with energy of cross-sections. This motivated the effort already referred to (table 7-1). It is however obvious that Fermilab could contribute much more and that so far luminosity paid over energy. The present ISR programme may however still bring original and interesting results. It should in any case soon provide information on associated hadrons to a large mass lepton pair.

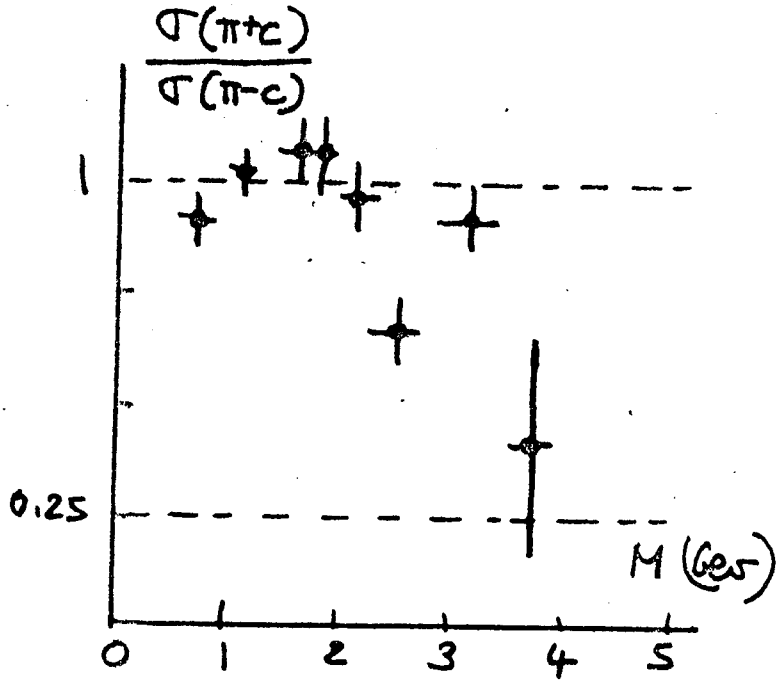

Figure 7-7 : The π^+C/π^-C lepton pair ratio. Results from the Chicago-Princeton Collaboration at Fermilab (Pilcher et al)

Table 7-1 lists the ISR experiments referred to in this section. Also listed are the newly approved experiments.

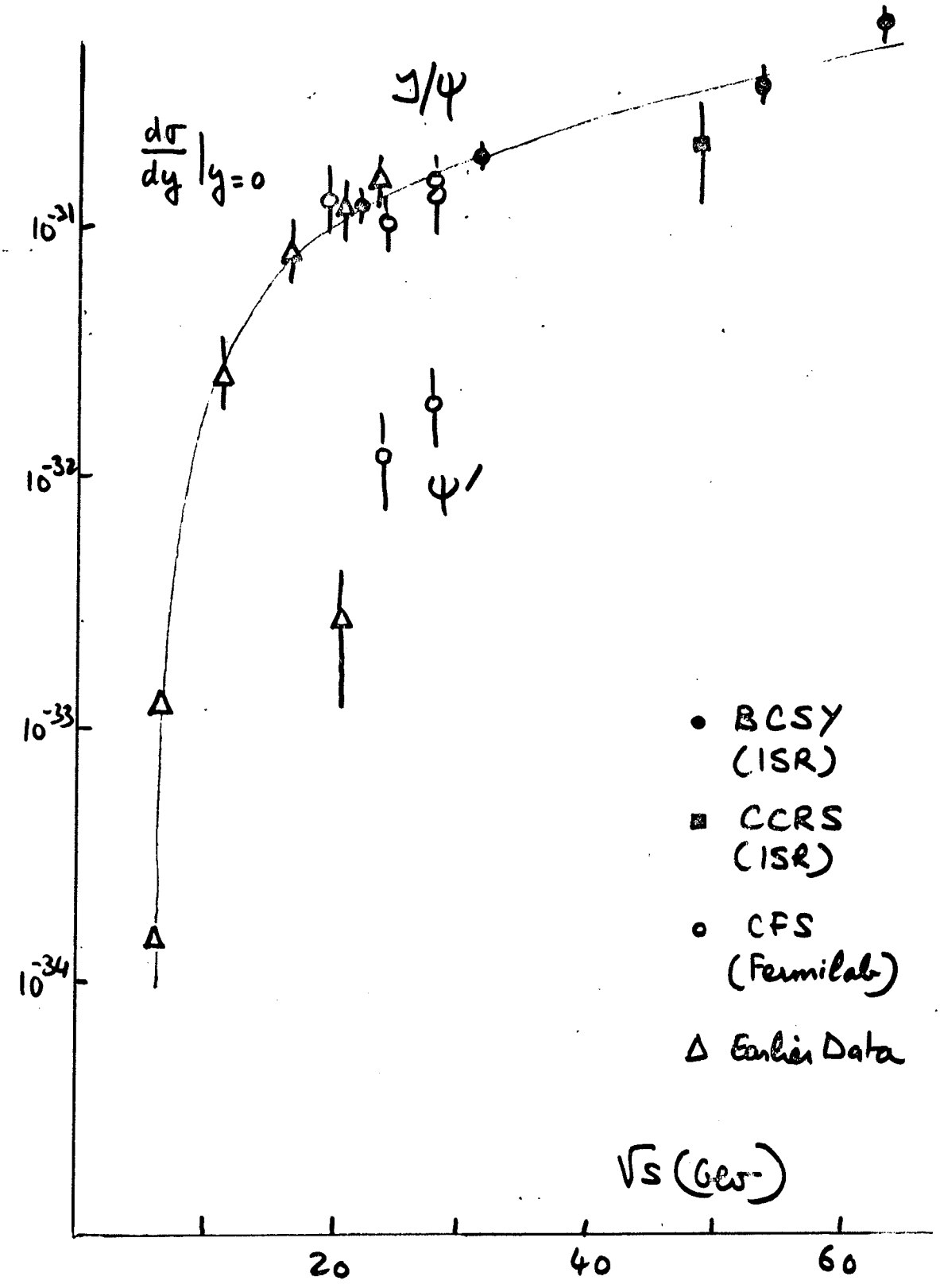

Figure 7-8 : J/ψ production cross-section. Results from Brookhaven, Fermilab and ISR

Table 7-1

ISR experiments with important results on lepton production

(i) Single electron yield and lepton pair production

103 CERN-Columbia-Rockefeller

105 CERN-Columbia-Rockefeller-Saclay

605 Aachen-CERN-Harvard-Munich-Riverside

(ii) Lepton pair production and special search for the J/ψ

702 CERN-Saclay (Double Arm spectrometer)

414 CERN-Hamburg-Heidelberg-Orsay-Vienna (SFM)

806 CERN-Brookhaven-Syracuse-Yale (Liquid Argon Calorimeter and transition radiation detector)

(iii) The new generation of lepton and lepton pair detectors

108 CERN-Columbia-Oxford-Rockefeller (Solenoid)

606 Aachen-CERN-Harvard-Munich-North Western-Riverside (Lamp Shade magnet)

804 Genoa-Harvard-MIT-Pisa (Dimuon torroid spectrometer)

415 Bologna-CERN (Upgraded SFM)

416 CERN-Collège de France-Heidelberg-Karlsruhe (Upgraded SFM)

8. Particle Search

Large p_t production of hadrons or leptons, to the extent that it signals some rare phenomena, are often favoured triggers in searching for new effects or new particles. Such searches have been extensively carried out at the ISR. It is well known that yields for heavy particle production ($\bar{p}$ and more recently J/ψ) show an important increase from PS to ISR energies (over a factor 10 for $\bar{p}$ and 100 for J/ψ). Energy could be a very important parameter. Even though low luminosity and background provide important limitations, searches will continue. Something might still be "protected" by a threshold at SPS energy and no longer at ISR energies.

Large p_t prompt γ rays may also signal something new and interesting. Such reaction mechanisms are hard to distinguish from dominant π^o production. Nevertheless, γ/π^o ratios could be obtained in some experiments. Figure 8-1 gives

such a ratio which is found to be practically p_t and energy independent over the studied range. The subject is not yet settled. It is quite topical.

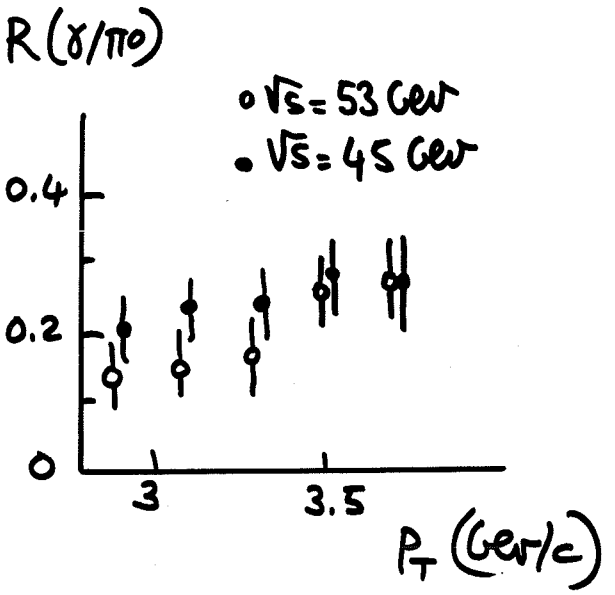

Figure 8-1 : The γ/π^o ratio. Results from the Aachen-CERN-Heidelberg-Munich Collaboration

Search for charmed particle has been much in favour but a disappointment in hadron induced reactions. A search for narrow heavy resonance in two particle distributions was attempted using the small angle spectrometer of the CHLM Collaboration and the wide angle spectrometer of the BS Collaboration. No significant result was found. The limits for cross-sections which one may consider at the ISR are of the order of 10^{-36} cm^2 (one count a day say over a 4π solid angle). Branching ratios and limited solid angles were indeed expected to contribute taxing factors to a charm search. We already mentioned the non-significant results which came out of $e\mu$ correlations.

Searches for quarks and for magnetic monopoles have been specially devised. Table 8-1 lists search experiments at the ISR.

The non-observation of the quarks at ISR energies, with 60 times the proton rest mass available in the reaction, is in itself a very important finding. Such a negative result contributed to the present revival which confinement models, built in the framework of Quantum Chromo dynamics, are bringing to Quantum field theory as applied to hadron physics. Present cross-section limits are at the level of 10^{-7} mb for quarks, usually looked for as fractionally charged particles or

heavy stable particles. Figure 8-2 shows the SFM with external detector installed for the CERN-Bologna quark search.

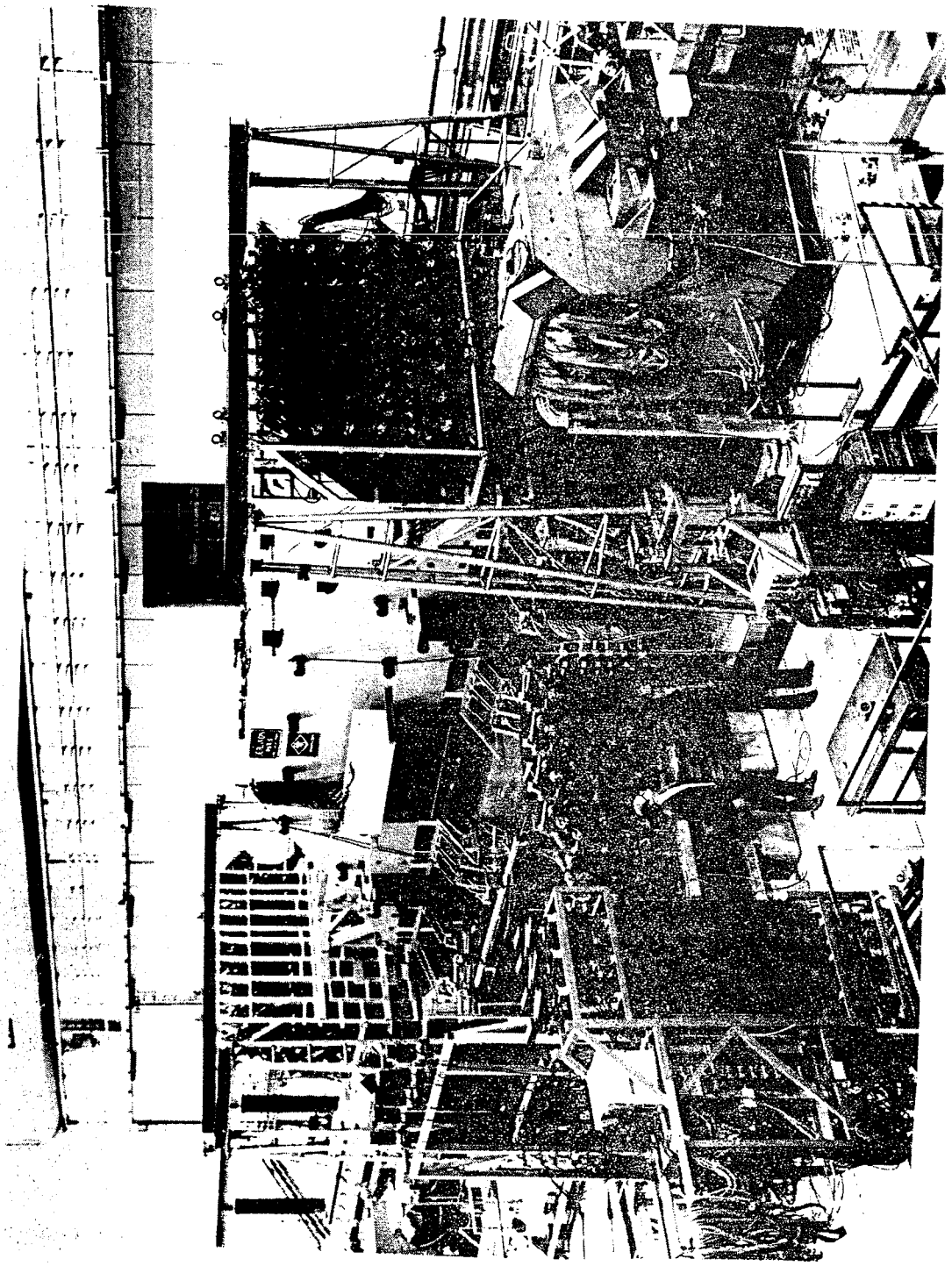

Figure 8-2 : The Split Field Magnet, referred to many times in connection with large p_t and diffractive studies, here seen with the external extensive detector used for the quark search of the CERN-Bologna Collaboration. This should eventually bring the upper limit for production cross-section to 10^{-35} to 10^{-36} cm^2

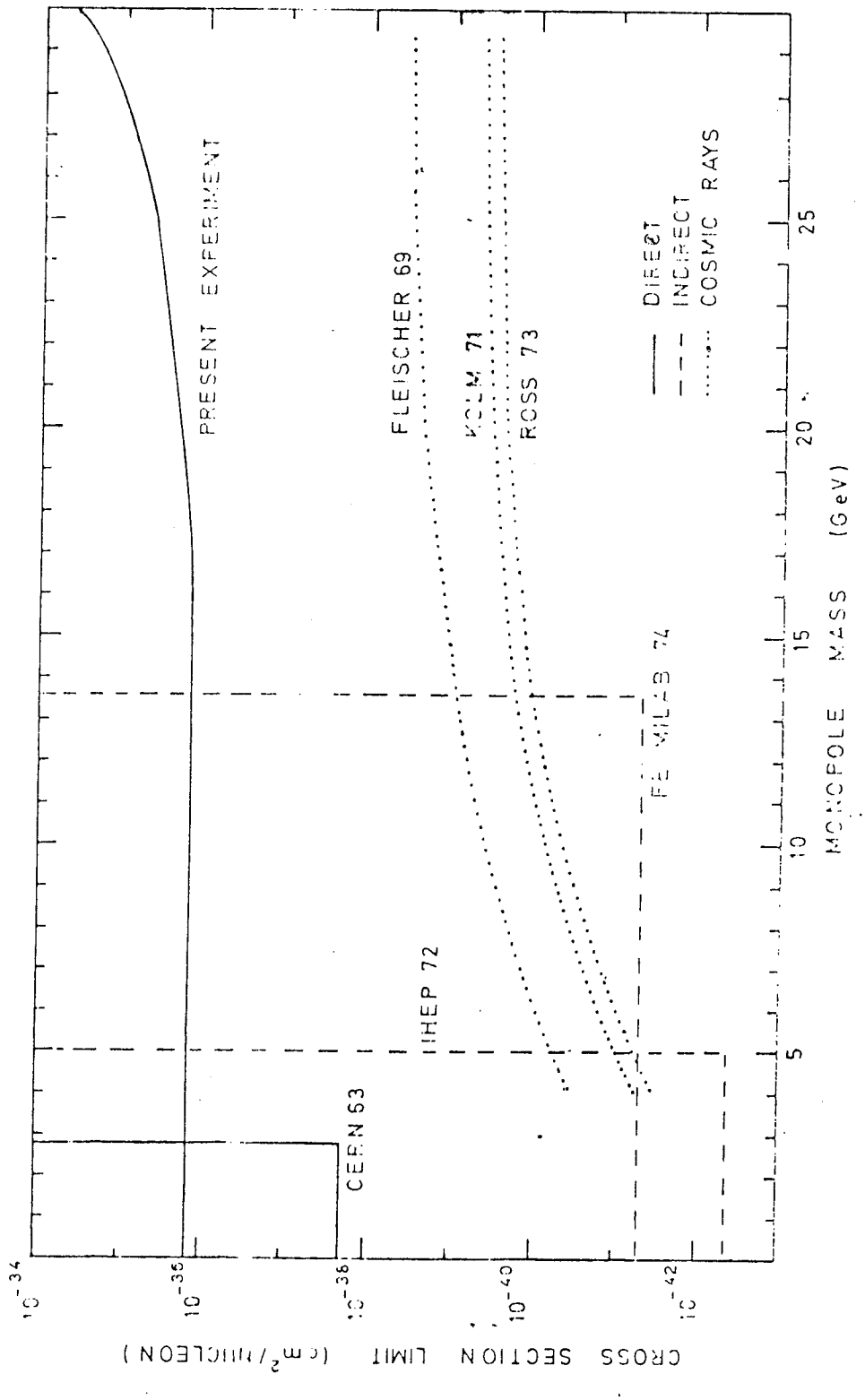

Figure 8-3 : A compilation of upper limits for monopole production

Table 8-1

ISR experiments with particle search as an important motivation.

(i) Search for magnetic monopoles through anomalous multigamma production

104 Brookhaven-Gruman-Rome

107 Adelphi-Brookhaven-Rome
through ionization and through trapping

106 Bologna-Rome

301 Bologna Fermilab

(ii) Early search for prompt leptons

204 British Universities

(iii) Specific search for quarks

203 British-Scandinavian

402 CERN-Munich ($\sigma < 2.10^{-34}$ cm^2)

406 CERN-Bologna

(iv) Search for Charm through eμ correlations

605 Aachen-CERN-Harvard-Munich-Riverside

702 CERN-Saclay

Searches for magnetic monopoles are based on possible large magnetic charges which would heavily ionize and we shall dwell a little on them as an example of particle search. Three types of monopole searches have been performed so far at the ISR. Present limits for the production cross-section are at the 10^{-9} mb level. Figure 8-3 shows a compilation of upper limits for monopole production. The Bologna-CERN Collaboration used plastic detectors to detect monopoles directly. Nitrocellulose sheets are sensitive to particles which ionize more than 0.8 GeV g^{-1} cm^2, while the threshold for marKofol-E is 3.5 GeV g^{-1} cm^2. Both were used. Because of these high threshold values, plastic detectors may be used in a large background of minimum ionizing particles, the background limit being given by nuclear fragment with $Z = 2$. In the developed plates these fragments yield a general background which shows up as randomly oriented tracks at the surfaces. Consequently, an area scan of the sheets, at their centres, has almost no background. The present upper limit is 3×10^{-36} cm^2 for monopoles with $0.5 < n < 3$ and $M < 24$ GeV. In a new experiment the Bologna Fermilab Collaboration (at the ISR) is working on an indirect search, trying to detect magnetic monopoles trapped in a vacuum chamber and in collectors around one intersection region used for beam dump. A Collector will later be placed close to the I-1 solenoid to benefit from the focalizating field. Magnetic monopoles, if produced, would be eventually extracted, accelerated to several GeV in a solenoid and detected through scintillation counters. Monopoles thus trapped should also induce a permanent transient in a superconducting solenoid. The cross-section limit could thus be brought down to 10^{-36} to 10^{-37} cm^2. Finally, two sequential experiments studied multigamma events where peculiar signals could be associated with monopoles.

9. Antiproton-proton Interactions at ISR Energies

According to prevailing theoretical ideas antiproton-proton and proton-proton interactions should eventually become identical with increasing energy. This may occur relatively fast (with an inverse power behaviour $s^{-\frac{1}{2}}$). This is expected to be the case at the total cross-section level if a behaviour of the type shown in figure 3-1 for $K^{\pm}p$, but also known to apply for the difference of the $\bar{p}p$ and pp total cross-sections at Fermilab energies, continues to hold at higher energies. This corresponds to Regge behaviour. This may occur relatively slowly. This can be the case for heavy mass lepton pair production. In such a case the relevant values of x_1 and x_2 (7.3) decrease as s/M^2 increases. At low s/M^2 production in pp collisions might be strongly quenched by the vanishing distribution of antiquarks as either x increases (the behaviour of $\bar{F}$ in (7.2)). This will not apply to production in $p\bar{p}$ collisions which can proceed from valence antiquark interactions. Figure 9-1 gives the expected ratios for $\bar{p}p$ and pp lepton

pair production rate as a function of M^2/s. This corresponds to a Drell-Yan calculation (section 7). At low enough values of M^2/s, the sea quarks are expected to take an overwhelming role (7.3) and, accordingly, pp induced reactions become practically as frequent as antiproton induced ones. If such behaviours, either rapid or slow with increasing energy, are expected, their verification is of great importance. Experimentation at Fermilab and at the ISR gave strong supporting evidence for Regge behaviour when Quantum numbers are exchanged (section 3). It would therefore be a surprise if σ_{tot}, b, ρ ..., all the parameters which define elastic scattering, would not converge when comparing pp and $\bar{p}p$ studies. How they actually do it should nevertheless be measured. Surprises may even occur. In particular, the dip structure observed in pp scattering (figure 3-6) may or may not have obviously corresponding features in $\bar{p}p$ scattering. Exploring this would provide very useful information on diffraction scattering (Pomeron exchange) at medium transfers. On the other hand, experimentation at the ISR and at Fermilab gave strong supporting evidence for incoherent hard scattering effects among proton constituents (sections 6 and 7). The quark parton model provides some understanding for the observed phenomena and at the same time makes unescapable prediction for what should be observed in $\bar{p}p$ collisions. Verifying such predictions would be a great asset for the model and give confidence for its extension to much higher energies (section 10) and its prediction of production cross-sections for the Weak bosons. Figure 9-2 gives the presently predicted rate for W^+ production in pp and $\bar{p}p$ scattering. The W is so heavy (65 GeV say) that even at very high energies ($\sqrt{s} \sim 10$ Mw) there is still a sizeable difference between $\bar{p}p$ and pp induced yields even though not a very large one. They are the same within an order of magnitude. Such predictions are again based on the Drell-Yan approach (7.5), with $g^2/M_W^2 \sim G/\sqrt{2}$. In this particular case the cross-section does not a priori go down as M^{-2} since the coupling constant has now to increase as M, the ratio of g^2 and M^2_W being fixed by the Fermi constant. Observing predicted features in $\bar{p}p$ induced lepton pair production would tremendously enhance the confidence which one can presently attach to such calculations and promote hints for expected at least logarithmic corrections.

For all these reasons the possibility of stacking $\bar{p}$ in the ISR and studying $\bar{p}p$ interactions at very high energies has always been extremely tempting. Nevertheless, the luminosities which could be contemplated with $\bar{p}$ normally extracted from the SPS, looked very small (in the order of 10^{25}). Hardly any experiment could have then been thought of. It turns out though that recent developments in cooling techniques could eventually provide intense sources of $\bar{p}$. One may now envisage with confidence luminosities of the order of 10^{29}, and even higher. A wide range of experiments then becomes possible and they are the all the more interesting that sophisticated equipment is now already available around

the ring. One may even say that, looking for an interesting experimental programme over the 5 coming years, the availability of antiprotons appears as a must.

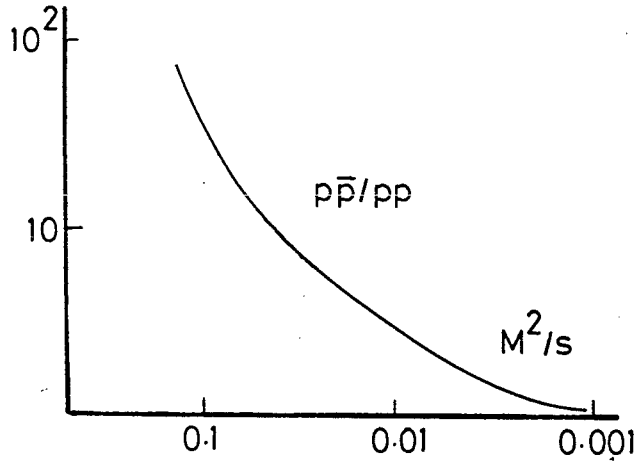

Figure 9-1 : Lepton pair production ratio in pp and $p\bar{p}$ reaction as a function M^2/s

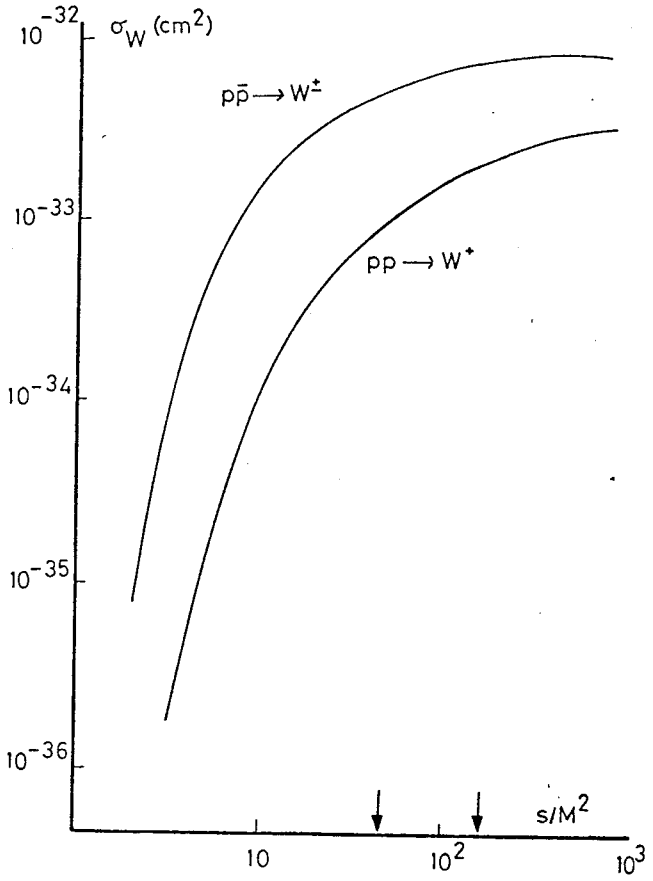

Figure 9-2 : Excitation curves for W production in pp and $\bar{p}p$ collisions. The Z^o cross-section is expected to be slightly lower

At CERN it is certainly very tempting to inject these antiprotons into the SPS and use the synchrotron as a collider (section 10). One may thus hope to reach the weak bosons[44]. Nevertheless the SPS will have to also run with its normal mode of operation a large fraction of the time and the intense $\bar{p}$ source as obtained from the PS and the cooling ring should accordingly often be available for injection into the ISR. Actually $\bar{p}$ in the SPS are a priori much more interesting because of their allowing the SPS to be used as a collider, with p and $\bar{p}$ circulating with opposite momenta in the same ring, rather because they are $\bar{p}$ as opposed to p. At such energies, any big surprises notwithstanding, one expects pp and $\bar{p}p$ interactions to be very much the same. Even for W production, the difference is not very large (figure 9-2). It is at lower energies (and the ISR energy range looks particularly interesting) that one may expect still sizeable differences about which predictions exist but which it would be most interesting to test.

We can consider in turn the different domains previously itemized. With $\ell n\ s$ physics the most interesting topic appears to be that of elastic scattering and total cross-sections. Expected are behaviours merging into these known for pp scattering (section 3) but the ISR energy range is such that differences are still sizeable (figure 2-7). This is where to check for the approach to a common behaviour for $\bar{p}p$ and pp scattering. For the general features of particle production (section 4) no very important differences are expected, except for obvious charge symmetry effect in the fragmentation region. To the extent that the π^+ and π^- yields in pp collisions are practically equal in the central region (figure 4-4) and that the annihilation cross-sections are small, nothing should be prominent at low x. Nevertheless some differences exist and could be large enough to be studied. Figure 9-3 gives the $\pi^\pm$ yields in pp and $\bar{p}p$ collisions at 100 GeV at Fermilab. There is still some noticeable difference among slow center-of-mass particles. They are probably largely due to the annihilation channels. Such an effect is expected to gradually disappear as one covers the ISR energy range. How this occurs (simple Regge behaviour?) is however interesting to know. Diffractive effects (section 5) are by definition expected to show no change between p and $\bar{p}$ induced reaction except for obvious charge symmetry effects. Diffraction proper would then be tested.

With large p_t phenomena (section 6) one may expect now important charge effects as the relevant constituents are changed into their antiparticles. Nevertheless, if large charge differences eventually occur (figure 6-5-c)) it is at larger p_t than those usually reached so far in correlation experiments at the ISR. Differences between pp and $\bar{p}p$ induced reactions should be very pronounced only when using very large p_t trigger ($p_t \gtrsim 5$ GeV/c say). With progress in detectors now motivated by the interest in large p_t processes, this may eventually

be possible, even with luminosities at the 10^{29} level. Comparison between pp and $\bar{p}p$ reactions may then bring very useful information on the nature of the constituents involved in the process of figure 6-3-d). The question of the important baryon yield may then be clarified.

As previously emphasized it is perhaps in the study of lepton pair formation that most information is expected in a domain directly connected with hadron structure. For mere counting rate limitations it may be difficult to reach very high masses ($M \gtrsim 4$ GeV say). Nevertheless, at this level one still expects important differences which are worth checking (figure 9-1). The signal over background ratio in the production of the J/ψ will also be of great interest. This is a very sensitive parameter in models for the new particle excitation[45]. For instance if charmed quark are mainly responsible for J/ψ excitation at very high energy one expects the $\bar{p}p$ and pp induced yields to eventually become equal. The Drell-Yan lepton pair backgrounds should also merge but more slowly with energy. This approach to J/ψ production got some support from a recent SPS experiment[46]. Tests at much higher energies would be very useful.

With an intense source of $\bar{p}$ as those which can now be expected from cooling techniques, one may rightfully consider 2 years of exciting experimental activity at the ISR. In short experimentation with $\bar{p}p$ is a very efficient way to put to a test all present understanding of hadron physics at ISR energies.

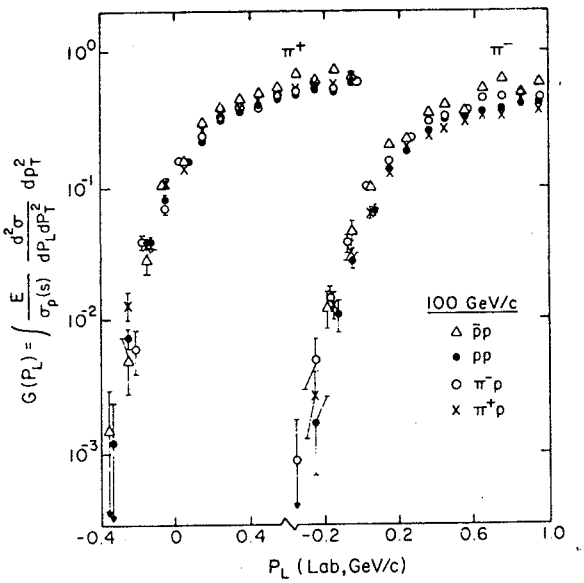

Figure 9-3 : Inclusive $\pi^{\pm}$ yield for pp and $\bar{p}p$ collision. Track chamber results from Fermilab

At present there is also much interest in low energy $\bar{p}p$ interactions where narrow resonance states have been reported (baryonium states). One could explore this at the ISR having p and $\bar{p}$ circulating in the same direction (ortho ISR scheme) low center-of-mass energy reactions would then occur among very high energy particles (the energy definition could be precise). With strongly collimated final system one could a priori easily analyze reaction products through forward spectrometers. This is also an interesting possibility for future developments.

10. Physics at Collider Energies

In the near future, colliding beam proton machines could reach energies of the order of 400 to 1000 GeV in the center-of-mass system. This may involve two rings. This may involve a single ring with circulating protons and antiprotons. This new energy domain should be rich in surprises. Yet the key present motivation for such an endeavour is the search for the $W^{\pm}$ (Z^{o}) weak bosons.

At present, the best potential machine for the study of the connection between weak and electromagnetic phenomena, considered as two facets of the same basic interaction, appears to be an electron-positron ring facility. Yet, while the major successes of Gauge theories with, within three years, the discovery of weak neutral currents, that of the new particles, with their hidden charm nature now ascertained, and then that of charmed particle proper, brings much currency to the presence of weak bosons, the expected masses are in the 60 - 80 GeV range. As a result, 200 GeV in the center-of-mass looks as a minimum for optimized research. Synchrotron radiation is such that at these energies, the optimal choice for the radius gives $R \sim s$ as opposed to $R \sim \sqrt{s}$ for a proton machine[47]. A typical normalization value is R = 6 km for $\sqrt{s}$ = 200 GeV. The relation between R and $\sqrt{s}$ for an $e^{+}e^{-}$ machine, a pp machine and a fixed target accelerator is shown in figure 10-1 (lines B and C1 respectively). Costs and site problems increasing with the radius, reaching very high energies, typically one order of magnitude higher than those obtained at the CERN-ISR, appears as a priori much easier with protons than with electrons. While from what is discussed in sections 3 to 7, protons are very complicated probes, they are relatively easy to accelerate.

One can indeed use the fact that, when it comes to electromagnetic interactions, the proton does not behave as a whole but rather as a set of point-like constituents (section 7) to estimate from the nominal center-of-mass energy, the energy which is actually relevant at the constituent level. Since $\bar{s} = sx_1x_2$ with $x \simeq 0.1$, this shifts the proton line C1 left by one order of magnitude on the graph of figure 10-1 to C2. When it comes to large mass particle production

such as that of the W one has in present models to consider indeed the center-of-mass energy which is available at the constituent level. This reduces what could a priori be expected from the line C1. However, since there are no major problems coming from synchrotron radiation, one can in principle use a superconducting ring and thus gain back a factor 3 in energy at fixed radius. One thus reaches the line C3 on figure 10-1. The lines B and C3 should correspond to a fair comparison. To the extent that the radius is a major element in cost and site problems, one sees that, when it comes to energies greater than $\sqrt{s} \sim 100$ GeV, a proton-proton colliding ring appears as a more reasonable project even if one considers the energy available at the constituent level only. For these reasons, it seems likely that the discovery of the weak boson(s) will be put to the credit of a proton collider, expected to come ahead in time from a probably more efficient, but far more expensive, electron-positron storage ring facility.

We have used the generic name "collider" rather than proton ISR since intersecting storage rings are only one of the types of facility presently being considered or developed. Table 10-1 shows the different types of machines which are talked about at present. The Fermilab Doubler/Saver, used together with the accelerator main ring as a collider is being developed as the Tevatron system. Reviewing the different projects, there are obviously two key parameters to consider, the center-of-mass energy and the luminosity, respectively. Present estimates for the W(Ƶ) production cross-section put it at the level of 10^{-32} - 10^{-33} cm^2 for $\sqrt{s} \gg M_W$ (section 9). The condition $\sqrt{s} \gg M_W$ should be well satisfied at 800 GeV. At $\sqrt{s} \approx 200$ GeV the cross-section should be lower by an order of magnitude from the 800 GeV estimate (figure 9-2). It follows that a luminosity of 10^{30} cm^{-2} sec^{-1} and an energy of 200 GeV appear as very minimal requirements. All projects accordingly meet these conditions (table 10-1). Some of these projects come as developpements on existing machines. The Fermilab Tevatron project should in particular give a center-of-mass energy of 1000 GeV (the Doubler beam at 1000 GeV intersecting with the main ring beam at 250 GeV) with a luminosity of the order of 10^{30}. With an intense source of $\bar{p}$ available with cooling (10^{12} $\bar{p}$ say injected into the SPS), the use of the SPS as a collider, accelerating p and $\bar{p}$ at the same time, and holding the bunched beams as in a storage ring, would give a center-of-mass energy of 540 GeV (possibly 800 GeV) and a luminosity of the order of 10^{30}. These two projects are likely to lead to the first actual attempts at the W(Ƶ^o). A very high energy collider built as such, such as Isabelle, could have a luminosity of the order of 10^{33}. In view of the estimates for the W(Ƶ) cross-section, this is a very meaningful gain. To put it in a nutshell, one may say that if ingenuity (and some money) buys the energy, money buys the luminosity (and experimental versatility).

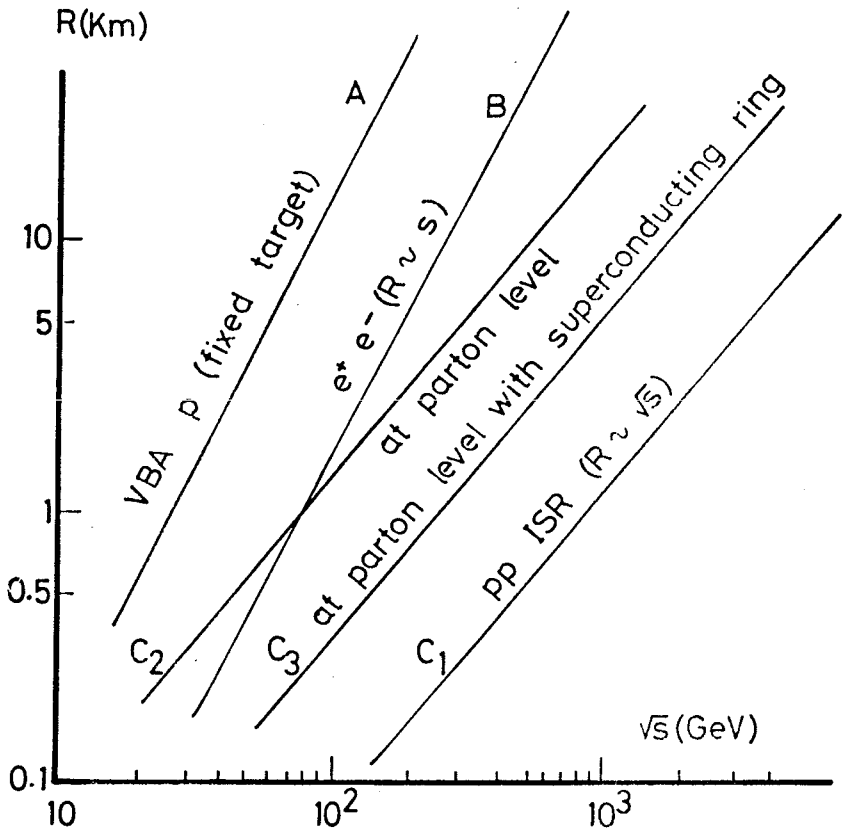

Figure 10-1 : The available center-of-mass energy $\sqrt{s}$ as a function of the machine radius R for different types of machines. In the proton-proton (or $\bar{p}p$) case one distinguishes the pp c.m. energy from the 'effective' energy available at the constituent level (C_1 and C_2 respectively). With superconducting magnets one may gain a factor 3 in energy at fixed radius

$\sqrt{s} \sim 200$ GeV	$L \sim 10^{30}$ SSR	$L \sim 10^{33}$ Superconducting ISR
$\sqrt{s} > > 200$ GeV	Doubler-Saver as a Collider SPS ($\bar{p}$) D/S ($\bar{p}$)	ISA Large Storage Rings Projects LSR, POPAE

Table 10-1 : The present proton-proton (proton-antiproton) projects, which are talked about are classified according to the center-of-mass energy $\sqrt{s}$ and the luminosity L. The left-hand column corresponds to so-called developments from present accelerators. The lower box in the right-hand side column corresponds to entirely new machines

Physics at Collider energies has already been discussed extensively in connection with the Isabelle project [8], the Fermilab project[48] and the CERN $\bar{p}p$ project[49]. We shall therefore limit ourselves to a quick overview.

We shall first discuss large cross-sections. While protons are relatively easy to accelerate and while proton-proton interactions may be the quickest way to produce the $W(Z^o)$, it is clear that one is trading the relevant advantages for a huge background. This background, which has then to be understood, is however interesting in itself as the first look at hadronic phenomena in a completely new energy domain. One has found that over the ISR energy range large cross-sections do not vary much (section 2). Nevertheless, extrapolating $\ell n\ s$ physics to collider energies leads one to expect important changes. The rapidity range increases from 8 to 14! The mere extrapolation of present trends should produce important variations. As an example figure 10-2 gives the pp total cross-section on a graph where the straight line stands at $\sqrt{s}$ = 800 GeV, a typical collider energy. Extrapolating even a bashful logarithmic rise (section 3) leads to expect important changes. Actually, the analysis of the behaviour of the real part of the forward amplitude (section 3) allows to infer that the total cross-section has to rise over a large energy range (up to $\sqrt{s}$ = 300 GeV say).

While asymptopia may lose part of its presently elusive character, the second key point of $\ell n\ s$ physics, namely the impressive stability of densities in longitudinal phase space would be the reference behaviour from which to analyze deviations. Such deviations exist (figure 4-7). Probing them over a far wider energy range could reveal their dynamic origin. While the mere extrapolation of ISR results would give an almost constant density with relatively small short range correlations, new features would be associated with large fluctuations in phase space density.

The extrapolation of the logarithmic behaviour discovered at the ISR is however likely to fail when the energy becomes large enough. Many hints from Cosmic-ray results indicate that hadronic phenomena show important changes as one goes beyond 10^5 GeV, an energy which is lower than the equivalent laboratory energy for a collider with $\sqrt{s}$ = 800 GeV. The important question with large cross-sections is therefore to analyze how $\ell n\ s$ physics fails to extrapolate in a simple way. Evidence from cosmic rays may not be piecewise compelling. Yet there is an array of results showing that important changes occur between 10^4 and 10^5 GeV[2]. One may mention that beyond 10^5 GeV (which corresponds to very low fluxes and therefore to relatively large cross-sections to the extent that anything is observed) there is apparently (i) a supplementary increase of σK, the product of the total cross-section by the inelasticity factor, from the general trend observed at lower energies, (ii) a large amount of muons, (iii) production of

heavy clusters of particles, (iv) a pronounced increase in the mean multiplicity, (v) an increase of the absorption length for the core of extensive air showers (the Tien-Shan effect), (vi) peculiar events such as Centauro, Andromeda ... None of these features is extremely solid by accelerator physics standards. Nevertheless, they all concur to indicate that at collider energies one should expect something different from the mere extrapolation of ℓn s physics. One should see large deviations from a typically uniform rapidity distribution, which now appears as the obvious reference pattern.

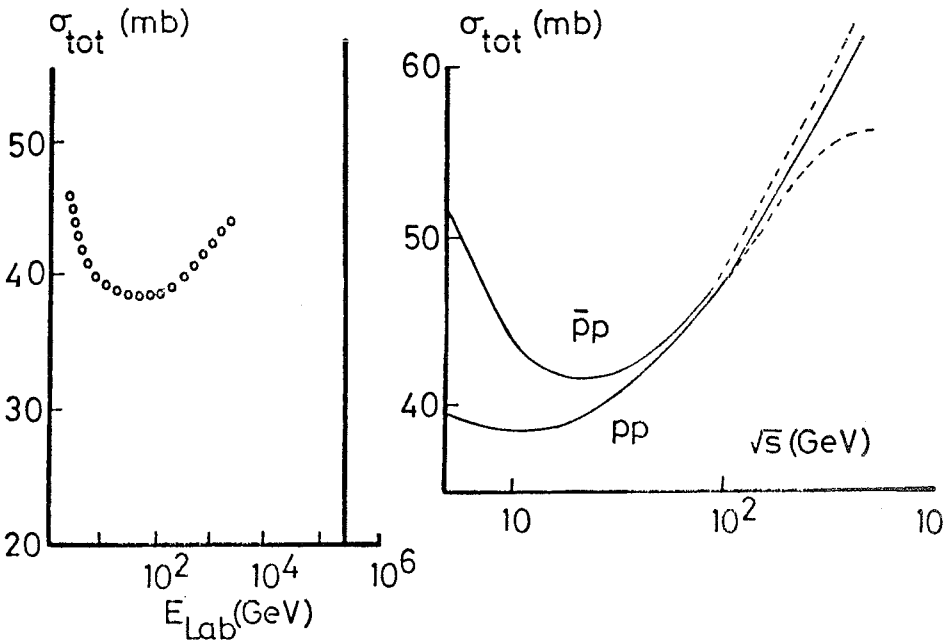

Figure 10-2 : The pp total cross-section as a function of energy. The vertical line on the left-hand side corresponds to a center-of-mass energy of 800 GeV. The dashed curves on the right-hand side correspond to limits given by the measurement of ρ at ISR energies using dispersion relations

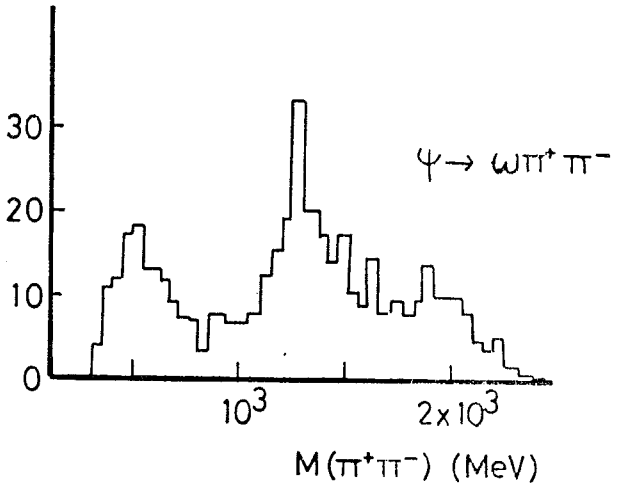

Figure 10-3 : $\pi\pi$ mass spectrum in $\psi \rightarrow \omega\pi^+\pi^-$ at SPEAR

Concluding at this stage our discussion of large cross-sections one may say that (i) Even though ℓn s is what sets the pace for change, a change in ℓn s by 5 to 6 units, as available going from ISR energies to Collider energies, is very valuable, (ii) While a refined knowledge of present hadronic phenomena should result from such studies over a large ℓn s domain, the most spectacular things should correspond to the observation of a large amount of very peculiar effects hinted at by Cosmic Rays. If actual ones they stand for a completely key kind of dynamics.

At a more modest level one should say that extending significantly the rapidity range should greatly help the analysis of multipomeron exchange processes (figure 5-6). The rapidity interval available at the ISR is barely enough for evidence for such a process (figure 5-7). With 5 to 6 extra units one could study triple Pomeron exchange and much better study the hadronic excitation of the vacuum already observed in Double Pomeron exchange. The spectrum of states is likely to be different from what is observed in meson-meson scattering even when selecting the isospin 0, even C component. It may be closer to what is observed at SPEAR in ψ decay into ωX or ϕX (X being any hadronic system). Data on $\psi\ \omega\ \pi\ \pi$ decay are shown in figure 10-3. In both cases one has to consider disconnected duality graphs[50]. The subject is still to be explored. This is also related to the SU3 properties of the Pomeron, as discussed in section 5.

We now turn to hard scattering as discussed in sections 6 and 7. As previously emphasized, some low cross-section phenomena are likely to show important variation with energy as one goes beyond the present ISR range. Large p_t phenomena as discussed in section 6 correspond to still rather low energies at the constituent level. A 30 GeV proton has quark constituents of 4 GeV average momentum only. At the constituent level ISR energies compare then to SPEAR energies for point-like electron. The resulting hadron jet configurations are therefore, not surprisingly, much similar. At Collider energies one should be able to study constituent-constituent interactions at much higher energies. The p_t^{-4} dependence of inclusive cross-sections expected from a scaling behaviour could eventually appear. Figure 10-4 gives jet cross-sections which can be expected at $\sqrt{s}$ = 400 GeV (Isabelle study) with, in particular, the extrapolation of the p_t^{-8} belated scaling behaviour, which applies to ISR results below 10 GeV, and what could be the p_t^{-4} behaviour associated with Quantum chronodynamics, applying for $p_t > 10$ GeV/c. It is possible that marginal evidence for such a behaviour could soon come from experimentation at the ISR. Experimentation at a Collider should fully settle the issue and make it relatively easy to separate different behaviours. If the p_t^{-8} hadronic behaviour continues it should eventually compare with jets obtained from electromagnetic and weak interactions for $p_t \sim 50$ GeV/c, a value at which the cross-section may however be hardly large enough for investigation with a luminosity of 10^{30}.

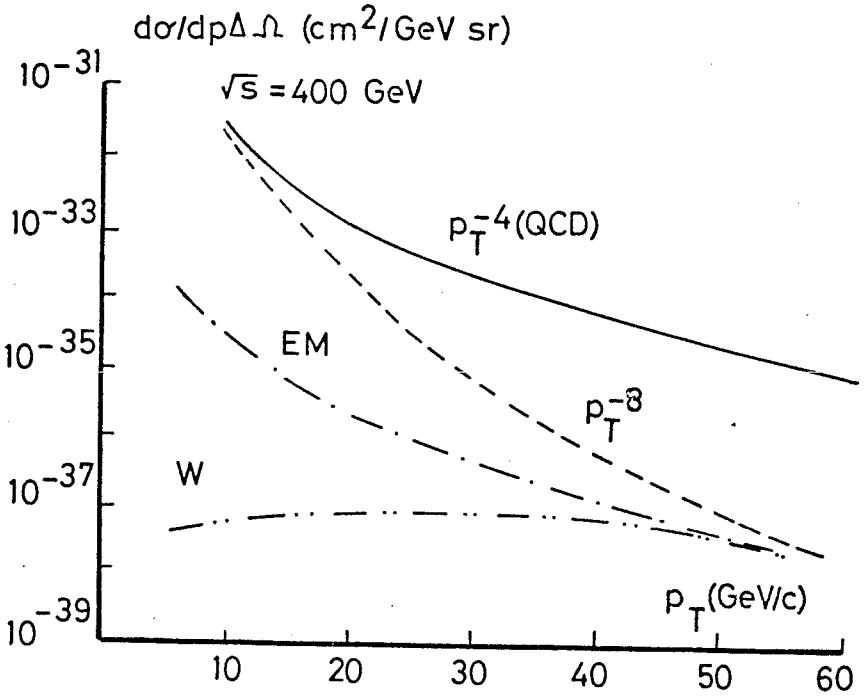

Figure 10-4 : Production cross-section for large p_t jets with different origins (R. Pierls et al., BNL report on W production)

Jet studies can be looked at as very promising. Jets provide in any case an important background against the Weak boson search and let alone for that reason have to be properly understood. Figure 10-5 gives the inclusive yield for positron expected from W decay with the Jacobian peak slightly smeared by the p_t distribution of the W. Also plotted are "background" distributions for π^+ according to the two hadronic behaviours considered in figure 10-4. Using the leptonic mode of the W should provide good enough a signal over background ratio in both cases. However this is likely to correspond to a minority mode (10% say). Looking for a dominant jet mode, one would have to face a sizeable background in the p_t^{-8} case and an overwhelming one in the p_t^{-4} one. When looking for a large p_t positron one should also have to check for the absence of a jet on the other side. W searches and jet studies are closely correlated.

Decay of meson into lepton pairs provides a much better signal over background ratio. The Z^o is probably the easiest of the weak bosons to ascertain provided production cross-sections are large enough. They are expected to be lower by typically an order of magnitude than that for the W. At lower vector meson masses, one may a priori expect that the large gain in energy allowed by the collider could bring many new states into focus. Indeed, cross-sections are expected to rise with energy the more so the larger the mass is (figure 7-8). Nevertheless, when the condition $\sqrt{s} \gg M$ is satisfied, they still go down like M^{-2}

(7.5). It therefore may be difficult to reach large masses (and 10 GeV say for the Drell-Yan continuum). This is a domain where luminosity matters as much as energy.

The question of the production of Weak bosons and vector mesons in general has been extensively debated already[51]. We shall not discuss it further. One may reasonably hope that the Colliders being presently developed will be able to provide first evidence for the Z^0 first and then perhaps for many still unexpected features. The experimental situation with respect to the Drell-Yan process, which is the present guide for estimates is certainly much better now than it was only one year ago (section 7).

Looking back at ISR physics over the past 6 years, one realizes that most of the key findings, as itemized in section 2, were actually gathered in a relatively short amount of time. In particular '73 was a really fruitful year, with evidence for rising total cross-section, good evidence on short range order, good evidence for high mass diffraction, and correlation data in large p_t phenomena hinting at a jet structure. Important progress has been followed, with in particular, evidence for a jet structure in reactions with a large p_t secondary in '75. Nevertheless, this has required a lot of effort. In the case of lepton pairs, despite great effort and much enthusiasm, the outcome has so far been a little disappointing. Most of the difficulties met can be traced to the fact that when correlations among identified and analyzed particles are needed, as is the case when one tries to study in more detail any reaction process, large detectors are required. Many of the interesting phenomena occur at relatively wide angles and involve relatively slow particles. The solid angle spanned in the laboratory has to be practically as large as the one thus covered in the center-of-mass system. This is of a great help when collecting first information (angular distribution). This however implies extensive detectors when one tries to go further.

The same should probably apply at Collider energies. It may be relatively easy to get evidence for the Z^0 and for some key features of hadronic interactions beyond 10^5 GeV. Further exploration however may be very difficult and the more so when considering the first generation of colliders with luminosities at the 10^{30} level. When estimating Z^0 production according to prevailing models one has to expect a relatively wide x distribution and therefore a relatively wide angular distribution for the decay leptons with practically no angular correlation. Covering a large solid angle with the detector is therefore a must. When considering hadron phenomena, large cross-sections or jet studies, the key point is to look for important fluctuations from a reference uniform rapidity distribution. Here also a detector covering a large solid angle is a

must. If one may tentatively use past experience, one is therefore led to advocate a wide solid angle coverage, even if it is at the expense of sophistication. A large amount of new features may be collected in a short amount of time. Going any further may require very large efforts. In any case the present Collider developments open extraordinary perspectives for particle physics.

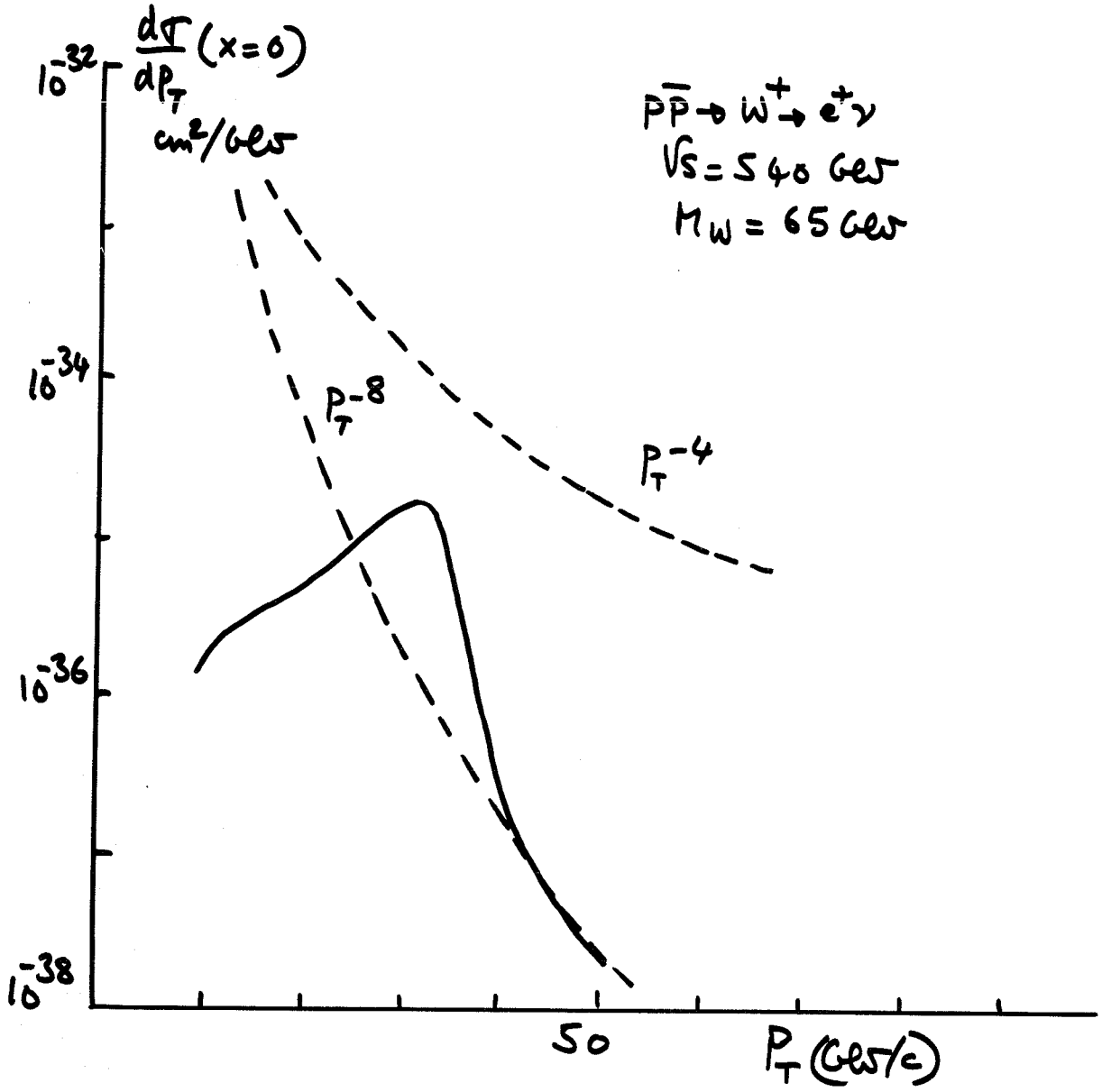

Figure 10-5 : Inclusive production of e^+ from W decay and large p_t (background) production of π^+ for two different types of behaviour of $d\sigma/dp_t^2$

Acknowledgements

I would like to thank the University of California, Riverside, and in particular the Physics Department for its warm hospitality in the spring of 1976 as I was giving the course summarized in sections 2 to 7 of this report. Sections 9 and 10 borrow much from my participation in the Fermilab Workshop in Aspen and the CERN ISR Workshop, in the summer and fall of 1976 respectively.

I would like to thank Christine Redman for her kind and efficient help in the preparation of these notes.

References and Footnotes

1) For a detailed review of the features and performances of the machine, see K. Johnsen, Nuclear Instruments and Methods, 108, 205 (1973). For a review of the latest performance of the CERN-ISR, see K. Potter, Contribution to the ISR Workshop, 1977

2) For a review of present information from Cosmic Rays, see, E. Feinberg, Phys. Rep. 5, 237 (1972) and C. McCusker, Phys. Rep. 20, 229 (1975). One should also consult J. Björken, Proceedings of the Hamburg Conference (1977)

3) Charm particle search in hadron-induced reactions has so far been unsuccessful. The production cross-sections turn out to be very small. Three years after the discovery of the J/ψ, the numbers of collected events at the ISR are still in the hundreds only in the different experiments

4) All new features found so far at the ISR ((i) to (v)) have since been seen at Fermilab. The ISR had an early and efficient start and could thus secure priority on many important issues. However it has not been protected by a threshold

5) The rapidity of a particle of energy E and longitudinal momentum p_L is defined as $y = \frac{1}{2} \ln (E + p_L)/(E - p_L)$. The rapidity range allowed for secondary particles increases therefore as $\ln s$. For a detailed presentation of the key variables for particle production, see, L. Van Hove, Phys. Rep. 1, 347 (1971)

6) For a review of ISR physics as of 1973, see, M. Jacob, CERN School of Physics, Ebeltoft, CERN-73-12. For a review of ISR physics as of 1974, see, M. Jacob, Proceedings of the Bonn Summer Institute of Theoretical Physics (1974)

7) Several detailed reviews are already available. For total cross-sections and elastic scattering one should consult G. Giacomelli, Phys. Rep. 23, 123 (1976). For particle production pre ISR (and Fermilab) results are presented in L. Van Hove, Op. Cit, Ref. 5, W. Frazer et al., Rev. Mod. Phys. 44, 284 (1972), D. Horn, Phys. Rep. 4, 1 (1972). Post ISR (and Fermilab) results are reviewed in L. Foa 22, 1 (1975), R. Slansky, Phys. Rep. 11, 99 (1974) and in the two review papers on track chamber results by J. Whitmore, Phys. Rep. 10, 273 (1974) and 27, 187 (1976). For diffraction phenomena one may consult the papers on particle production listed above and U. Amaldi et al., Annual Review of Nuclear Science 26, 385 (1976). For large transverse momentum phenomena, one may consult D. Sivers et al., Phys. Rep. 23, 1 (1976), J. Björken, SLAC Summer School lecture notes (1976). For prompt lepton production, one may consult L. Lederman, Phys. Rep. 26, 149 (1976),

J. Cronin, Erice lecture notes (1976). This list is far from exhaustive. Recent developments in hadron physics have been covered in many Rapporteur talks (the P. Darriulat rapporteur talks at the Palermo Conference (75) and Tbilisi Conference (76) for large p_t phenomena) and summer school courses

8) A proton-proton colliding beam facility BNL 50648 (1977)

9) The CERN Grey books should, whenever needed, provide access to extra information about the ISR experiments referred to here by their number

10) See for instance, M. Jacob, Comments 5, 171 (1972) and 7, 133 (1976)

11) The Pseudo rapidity is defined as $\eta = \frac{1}{2} \ln \frac{P + P_L}{P - P_L} = - \ln \operatorname{tg} \frac{\theta}{2}$, where θ is the production angle in the center of mass system. An angular distribution may thus already give a rather faithful rapidity distribution

12) The discovery of rising cross-sections is reported in U. Amaldi et al., Phys. Letters 43 B, 231 (1973), 44 B, 1112 (1973) and S. Amendolia et al., Phys. Letters 44 B, 119 (1973)

13) This is the elusive asymptopia, as discussed for instance in M. Jacob, Comments 6, 31 (1974). Rising cross-sections were indeed predicted in some models : H. Cheng and T.T. Wu, Phys. Rev. Letters 24, 1456 (1970). What is observed does not correspond however to a maximum opacity and a saturation of the Froissart bound. For a review on bounds see S.M. Roy, Phys. Rep. 5, 125 (1972)

14) First evidence for high mass diffraction is reported in M. Albrow et al., Phys. Letters 40 B, 136 (1972), 42 B, 279 (1972 and 44 B, 207 (1973)

15) Evidence for an anomalously large production at high p_t is reported in M. Banner et al., Phys. Letters 41 B, 547 (1972), 44 B, 537 (1973) and B. Alper et al., Phys. Letters 44 B, 527 (1973), for charged particles. It is reported by F. Büsser et al., Phys. Letters 46 B, 471 (1973) for neutral particles

16) F. Büsser et al., Phys. Letters 48 B, 371 (1974), 56 B, 482 (1975). For a review of prompt lepton production see L. Lederman Op. Cit., Ref., 7

17) L. Lederman, Proceedings of the Budapest and Hamburg Conferences (1977)

18) A. Bohm et al., Phys. Letters 49 B, 491 (1974)

19) The MacDowell-Martin bound gives $\frac{\sigma_{tot}^2}{18 \pi \sigma_{el}} \leq 2 \frac{d}{dt} \ln \operatorname{Im} F(t) \big| t = 0$
It is almost satisfied. The slope is almost as small as it can be. The proton has almost as large a size for its absorbing power. It remains rather transparent

20) The proton shape is often parameterized in terms of the inelastic cross-section as function of impact parameter
$\frac{1}{2\pi r} \frac{d\sigma \text{ in } (r)}{dr} = 4 \, |f(r)| \, (1 - |f(r)|)$. Full absorption corresponds to $f(r) = \frac{i}{2}$. The departure from full absorption seen in figure 3-8 is not as large an effect as for $\sigma_{in}(o)$. Yet the approximately Gaussian shape corresponds to a rather transparent proton

21) For a review of recent approaches to diffraction scattering see, H. Abarbanel et al., Phys. Rep. 21, 119 (1975) and Moshe Moshe, Phys. Rep. to be published (1978)

22) For a discussion of large angle scattering at high energy see D. Sivers et al., Op. Cit. Ref. 7. For a discussion of the SU(3) properties of the Pomeron as obtained from recent Fermilab results, see Ch. Quigg et al., Fermilab report (1974)

23) For a review of standard theoretical approaches to diffraction scattering, see, F. Zachariasen, Phys. Rep. 2, 1 (1971). For a review of recent Reggeon calculus approaches see H. Abarbanel, Op. Cit. Ref. 21. A detailed review of Reggeon Calculus is available in M. Baker et al., Phys. Rep. 28, 1 (1976). For a discussion of the Optical and Regge approaches to diffraction see U. Amaldi et al., Op. Cit. Ref. 7

24) The idea of scaling is developed in J. Benecke et al., Phys. Rev. 188, 2159 (1969), C.N. Yang, High Energy Collisions, Gordon and Breach (1969), R. Feynman, Phys. Rev. Letters 23, 1415 (1969). For a detailed discussion of recent tests of scaling see R. Slansky, L. Foā and J. Whitmore Op. Cit. Ref. 7

25) Such a distribution was considered long ago by K. Wilson, Acta Physica Austiaca 17, 37 (1963). The rapidity plateau is a consequence of the multiperipheral model as discussed in S. Fubini, Scottish Universities Summer School (1963). The rapidity plateau is not a specific property of multiperipheral production. Short range order is much more specific. See D. Horn Op. Cit. Ref. 7

26) A. Mueller Phys. Rev. D2, 2963 (1970)

27) For a detailed review see Z. Koba, CERN School of Physics, Ebeltoft, 1973

28) CERN-Columbia-Rockefeller-Saclay Collaboration, Nuclear Physics, to be published. M. Banner, private communication

29) For a general review see U. Amaldi et al., Op. Cit. Ref. 7. For recent reviews of the Double Pomeron process, see ISR summary 18 and 22, CERN reports and CERN-Collège de France-Heidelberg-Karlsruhe, Nuclear Physics B, to be published. A. Putzer, private communication

30) The exchange approach to diffraction implies factorization properties relating elastic scattering, single diffractive excitation and double diffractive excitation. For recent tests see results from the Aachen-CERN-UCLA-Harvard Collaboration and results from the Princeton-Pavia Collaboration. Applying factorization to the Pomeron proton elastic amplitude (involved through the optical theorem in the calculation of the single diffractive cross-section) one can obtain a triple Pomeron coupling and use it for the estimate of the Pomeron-Pomeron total cross-section

31) This corresponds to a Regge approximation for a Reggeon-hadron amplitude. For a review see M. Jacob, Rapporteur talk, Batavia Conference (1972)

32) For a detailed review of expected properties and estimates for the Double Pomeron process see A. Kaidalov, Phys. Rep., to be published. For recent results see Ref. 29

33) First evidence for large p_t is referred to in Ref. 15. For a recent account see L. Lederman, Comments 6, 41 (1974) and S. Ellis et al., SLAC Summer School (1977)

34) S. Berman et al., Phys. Rev. Letters 25, 1683 (1970), S. Berman et al., Phys. Rev. D4, 388 (1971)

35) The identification between partons and quarks came from the analysis of deep inelastic scattering. For a review of the parton model see R. Feynman, Photon-hadron interactions, Benjamin (1972) and J. Kogut et al., Phys. Rep. 8, 75 (1973). For a review of Asymptotic freedom which may provide the proper theoretical framework for quark model calculations see H. Politzer, Phys. Rep. 14, 129 (1974)

36) For a review see L. Voyvodic, Phys. Rep. to be published (1978)

37) Jet fragmentation has recently been discussed in R. Field and R. Feynman, Phys. Rev. D15, 2590 (1977), R. Feynman, Orbis Scientiae, Coral Gables (1977), S. Ellis et al., Nucl. Phys. B108, 93 (1976), M. Jacob et al., Nucl. Phys. B113, 395 (1976). We choose to use a value of n one unit higher than the asymptotic one in order to absorb X_T dependence over the limited p_t ranges of present ISR experiments. This simplifies the argument. The connection between forward jets and jets in deep inelastic scattering is discussed in L. Van Hove et al., Nucl. Phys. B243 (1975)

38) Recent results from Experiment 260 at Fermilab, E. Malamud, Kaysersberg Conference (1977)

39) R. Feynman and R. Field Op. Cit. Ref. 37. G. Fox, R. Field and R. Feynman, Caltech preprint (1977), R. Baier et al., Nucl. Phys. B118, 139 (1977). For a general discussion see M. Jacob, Rencontres de Monriond (1977)

40) The constituent interchange model is presented in detail in D. Sivers et al., Op. Cit. Ref. 7. A recent discussion to be found in the Monriond report (1977) Op. Cit. Ref. 39

41) J. Cronin et al., Phys. Ref. D11, 3105 (1975)

42) M. Bourquin and J.M. Gaillard, Proceedings of the Stanford Conference (1975)

43) For a detailed review see L. Lederman, Op. Cit. Ref. 7 and J. Cronin, Proceedings of the Hamburg Conference (1977)

44) Ch. Quigg, Fermilab Report (1977), Rev. Mod. Phys. 49, 297 (1977), L. Trueman et al., Brookhaven Report (1977)

45) D. Green et al., Nuovo Cimento 29, 123 (1975), A. Donnachie et al., Nucl. Phys. B112, 233 (1976)

46) Experiment WA12 at the SPS (1977)

47) J. Richter, Nucl. Instr. and Methods 136, 47 (1976)

48) The Fermilab Tevatron project, Fermilab Report (1977)

49) CERN $\bar{p}p$ study week's reports (1977)

50) For a review of duality rules see K. Igi et al., Phys. Rep. 31, 238 (1977)